JOC The Journal of Organic Chemistry

Article

pubs.acs.org/joc

Selective G-quadruplex DNA Stabilizing Agents Based on Bisquinolinium and Bispyridinium Derivatives of 1,8-Naphthyridine

V. Dhamodharan, S. Harikrishna, C. Jagadeeswaran,[§] K. Halder,[‡] and P. I. Pradeepkumar*

Department of Chemistry, Indian Institute of Technology Bombay, Mumbai 400076, India

Supporting Information

ABSTRACT: Various biologically relevant G-quadruplex DNA structures offer a platform for therapeutic intervention for altering the gene expression or by halting the function of proteins associated with telomeres. One of the prominent strategies to explore the therapeutic potential of quadruplex DNA structures is by stabilizing them with small molecule ligands. Here we report the synthesis of bisquinolinium and bispyridinium derivatives of 1,8-naphthyridine and their interaction with human telomeric DNA and promoter G-quadruplex forming DNAs. The interactions of ligands with quadruplex forming DNAs were studied by various biophysical, biochemical, and computational methods. Results indicated that bisquinolinium ligands bind tightly and selectively to quadruplex DNAs at low ligand concentration (~0.2−0.4 μM). Furthermore, thermal melting studies revealed that ligands imparted higher stabilization for quadruplex DNA (an increase in the T_m of up to 21 °C for human telomeric G-quadruplex DNA and >25 °C for promoter G-quadruplex DNAs) than duplex DNA ($\Delta T_m \leq 1.6$ °C). Molecular dynamics simulations revealed that the end-stacking binding mode was favored for ligands with low binding free energy. Taken together, the results indicate that the naphthyridine-based ligands with quinolinium and pyridinium side chains form a promising class of quadruplex DNA stabilizing agents having high selectivity for quadruplex DNA structures over duplex DNA structures.

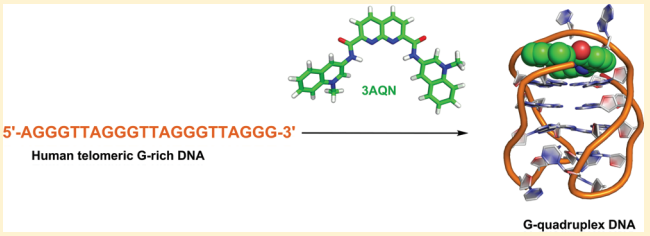

INTRODUCTION

G-quadruplexes are tertiary nucleic acid structures made up of multiple Hoogsteen base paired G-quartets stacked on top of each other (Figure 1).[1,2] Putative G-quadruplex forming sequences are found at the end of eukaryotic chromosomes (telomeres),[3] in promoter regions[4] of important proto-oncogenes such as *c-kit*[5] and *c-myc*,[6,7] in introns,[8] and in the untranslated regions (UTRs) of mRNAs.[9] G-quadruplex structures are considered to play important roles in the regulation of gene expression and the maintenance of telomere length. For example, formation of a quadruplex at the telomeric end can halt the function of the telomerase enzyme.[10] Formation of quadruplex structures at the promoter regions can regulate gene expression at the transcriptional level,[7] and induction of quadruplexes at the UTRs can modulate gene expression at the translational level.[11−13] The discovery that telomeric DNA is get transcribed into noncoding telomeric RNA (TERRA) adds further structural and functional complexities of potential quadruplex structures in biological systems.[14] Notably, a recent study in yeast has provided evidence for the existence of quadruplex structures *in vivo* and their effects on DNA replication.[15−18]

G-quadruplexes are structurally diverse due to their strand direction, sequence, loop orientation, and the nature of metal cation stabilizing the quadruplexes.[2,19,20] G-quadruplex structures can be intermolecular (bi- and tetramolecular) or intramolecular (unimolecular) in nature.[21] The orientation of the strands in the quadruplex can be parallel or antiparallel in direction.[21] The length and sequence of intertwining loops are important for the formation and the stability of quadruplex structures.[22−24] Even though G-quadruplexes can adopt different conformations, they still typically share a common planar quartet structural feature,[7] which offers a platform to induce and stabilize the quadruplexes by means of small organic molecules that stack on top of quartets. However, this common structural feature poses challenges for the design of ligands with considerable selectivity toward one type of quadruplex over other G-quadruplex structures. Since the loop sizes vary from one type of quadruplex form to the other, it is important to consider ligand interactions with different types of loops and grooves. Such interactions, coupled with end stacking, can be used to achieve better selectivity and discrimination among various quadruplex topologies.[25−27]

G-quadruplex nucleic acids are potential therapeutic targets for anticancer therapy.[7,28,29] Ever since the ligand 2,6-diamidoanthraquinone mediated quadruplex stabilization was shown to inhibit telomerase activity,[30] many classes of ligands have been studied as G-quadruplex stabilizing agents.[31−33] For example, acridine-based ligand (BRACO-19),[34] pentacyclic acridinium ligand (RHPS4),[35] bisquinolinium compounds (360A),[36] cationic porphyrin (TMPyP4),[37] macrocyclic natural product (telomestatin),[38] and their analogues have been investigated in both *in vitro* and *in vivo* settings. Though

Received: September 2, 2011
Published: November 29, 2011

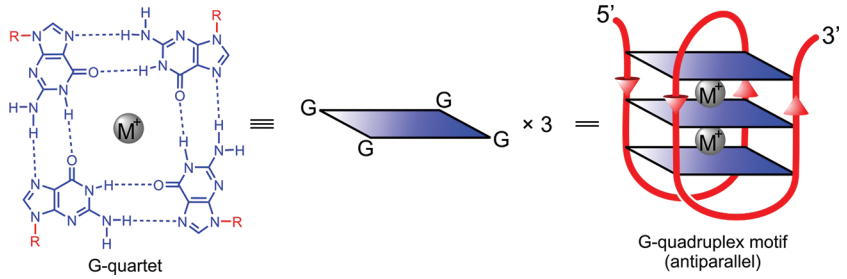

Figure 1. Structure of a G-quartet and a G-quadruplex. G-quartet is formed by the planar arrangement of four guanines connected by eight Hoogsteen hydrogen bonds shown in dotted lines. The metal ion coordinates to O6-atoms of guanines in the quartet. The G-quartets are stacked on top of each other to form a G-quadruplex; the conformer shown is the antiparallel basket-type structure.

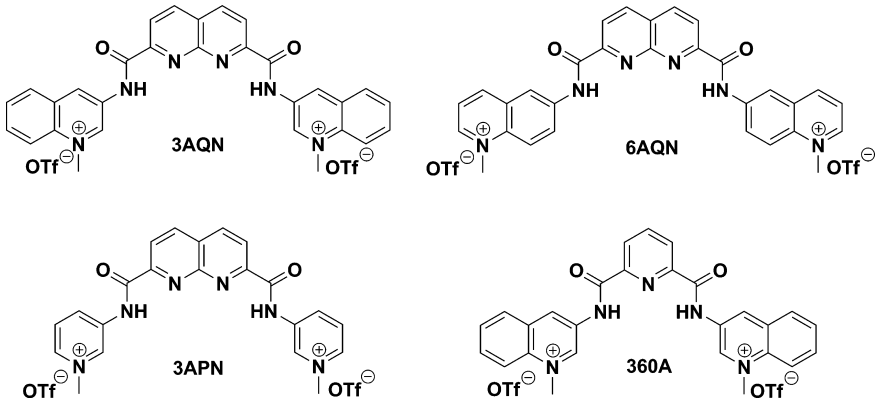

Figure 2. Structures of G-quadruplex DNA stabilizing ligands. Ligands **3AQN** and **6AQN** contain a naphthyridine central core with quinolinium side chains; the ligand **3APN** contains a 1,8-naphthyridine central core with pyridinium side chains, and the reference compound **360A** contains a pyridine central core with quinolinium side chains.

numerous types of ligands have been reported as potential G-quadruplex interacting/stabilizing agents, few have shown specificity toward the targeted quadruplex structure over other quadruplex topologies.[39,40] Moreover, the mechanism of anticancer action of many of the quadruplex targeting ligands is not well understood. It has been shown that many of the ligands reported in the literature may not be the direct inhibitors of telomerase. Instead they compete with or displace the telomere binding proteins such as hPOT1 and thereby induce a DNA damage response.[28,29] It has also been proposed that formation of quadruplex structures at telomere ends may lead to DNA strand breakage and thereby impart anticancer activity.[28,29,41]

In addition to the potential therapeutic applications, strong and selective quadruplex binding agents can be used to probe the presence of quadruplexes *in vivo*.[42] Therefore, the search for novel, selective G-quadruplex stabilizing agents has been extensively pursued. Along these lines, here we report the synthesis of bisquinolinium and bispyridinium derivatives of 1,8-naphthyridine (Figure 2) and characterization of their interactions with quadruplex DNA. The potent G-quadruplex stabilizing agent **360A**[36] is used as a reference compound in our studies. Binding efficacy of ligands has been tested with human telomeric DNA as well as promoter DNAs such as *c-kit1*, *c-kit2*, and *c-myc*. The discriminatory ability of the ligands to target quadruplex DNA over duplex DNA was also investigated. We employed various biophysical [fluorescence intercalator displacement (FID) assay, CD titration, and CD melting] and biochemical techniques (*Taq* polymerase stop assay and nondenaturing gel electrophoresis), as well as molecular dynamics (MD) simulations, to study the interaction of ligands with quadruplex DNA. All ligands were found to have strong selectivity toward quadruplex DNA over duplex DNA. The results presented here suggest that in addition to the structural features of the central core of the ligand, the side chains also play critical roles in achieving selective quadruplex DNA stabilization.

RESULTS AND DISCUSSION

Ligand Design and Synthesis. Bicyclic heteroaromatic compounds such as 1,8-naphthyridine can be utilized to assemble potential G-quadruplex stabilizing ligands. Though a dimeric form of 1,8-naphthyridine has been used to inhibit the function of telomerase, its mode of action stems from an interaction with a nonquadruplex structure at the telomere end.[43] Moreover, to the best of our knowledge, naphthyridine based ligands have not been explored as G-quadruplex DNA stabilizing agents. Therefore, herein, three representatives of a new class of 1,8-naphthyridine based ligands (**3AQN**, **6AQN**, and **3APN**) were designed and synthesized to achieve specific quadruplex stabilization (Figure 2). The potent G-quadruplex stabilizing agent **360A**, which has a pyridinium central core and two quinolinium side chains, was prepared and used as reference compound.[36] The rationale for the design of our ligands is that the internal H-bonds between the NH of amide bond and the naphthyridine- N atom can lock the ligand conformation into a planar crescent-shaped form.[44] Additionally, the large aromatic core of the naphthyridine ring potentially offers better stacking on G quartets, and the cationic side chains can interact with the negatively charged phosphate backbone of loops of the quadruplex via electrostatic interactions.[45] The side chains of the ligands may also improve

dx.doi.org/10.1021/jo201816g | J. Org. Chem. 2012, 77, 229–242

Scheme 1. Synthesis of G-quadruplex DNA Stabilizing Agents[a]

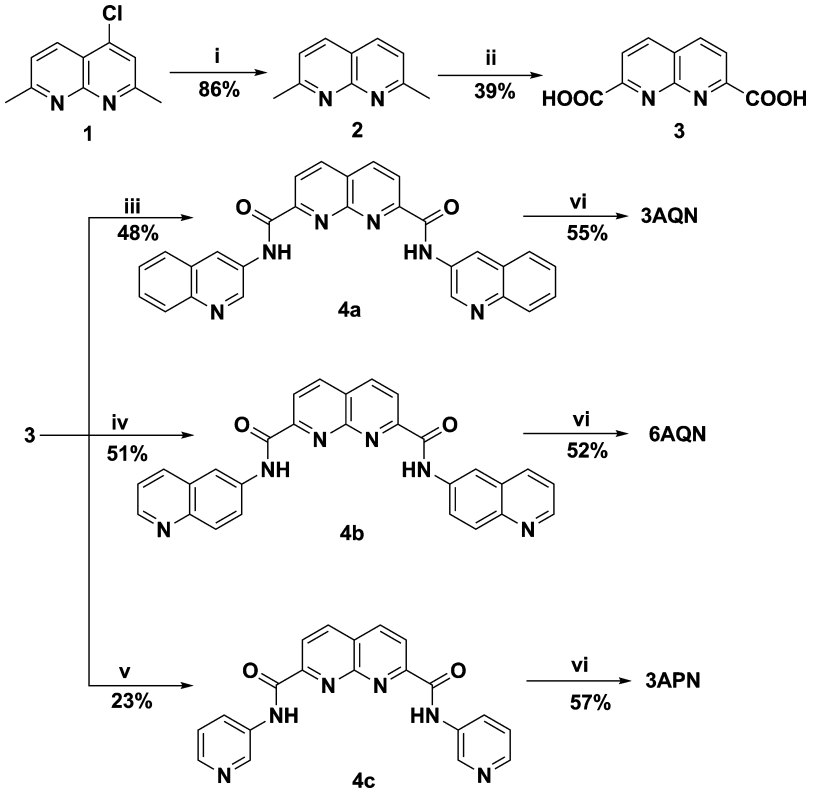

[a]Reagents and conditions: (i) ammonium formate, Pd (10%)/C, MeOH, 6 h, rt; (ii) (a) SeO_2, 1, 4-dioxane, 12 h, rt, (b) conc HNO_3 3 h, 80 °C; (iii) 3-aminoquinoline, EDC·HCl, HOBt, DMAP, DMF, 24 h, rt; (iv) 6-aminoquinoline, EDC·HCl, HOBt, DMAP, DMF, 24 h, rt; (v) 3-aminopyridine, EDC·HCl, HOBt, DMAP, DMF, 24 h, rt; (vi) MeOTf, DMF, 80 °C for 4 d.

the selectivity for quadruplex DNA over duplex DNA. The quinolinium side chains, previously identified through a screening assay,[46] were chosen for our ligands because of their presence in several potent quadruplex stabilizing ligands such as triazine derivative (**12459**),[46] pyridine-dicarboxamide (**360A**, **307A**),[47] phenanthroline-dicarboxamide (**Phen-DC$_3$** and **Phen-DC$_6$**),[48] and bis(2-quinolinyl)pyridine-dicarboxamide (**RR 82**, **RR 110**).[42,49,50] Since the position of the positive charges on the side chain varies in the 3-aminoquinolinium (**3AQN**) and 6-aminoquinolinium (**6AQN**) compounds, these new molecules offer an opportunity to compare the efficiency of the side chain interactions with the loops and grooves of the quadruplex structures. The pyridinium side chain was selected to probe the structural differences in the side chains, which affect the quadruplex recognition.

The synthetic strategy used to assemble the naphthyridine ligands is shown in Scheme 1. The key intermediate, 2,7-naphthyridinedicarboxylic acid **3**, was prepared in six steps using reported procedures[51−54] with slight modifications. Compound **1** was prepared as previously described,[51] and the subsequent dechlorination using Pd(5%)/$CaCO_3$ at 4 atm of H_2 was found to be low-yielding in our hands.[52] However, dechlorination by ammonium formate[55] and Pd(10%)/C yielded compound **2** in 86% yield. Oxidation of compound **2** by SeO_2 followed by HNO_3 treatment furnished **3** in 39% yield.[53,54] The direct coupling of **3** with 3-aminoquinoline by using EDC·HCl, HOBt, and DMAP produced the amide **4a** in 48% yield. Employing similar reagents and conditions with 6-aminoquinoline and 3-aminopyridine, the amides **4b** and **4c** were synthesized in 51% and 23% yield, respectively. Methylation of compounds **4a**, **4b** and **4c** by methyl triflate gave the final product **3AQN** in 55%, **6AQN** in 52%, and **3APN** in 57% yield, respectively. All ligands contain triflate counterions, which increase ligand solubility in water unlike widely used iodide counterions. All compounds were fully characterized by ^{1}H NMR, ^{13}C NMR, and HRMS.

Fluorescence Intercalator Displacement (FID) Assay. Ligand binding affinity and selectivity toward quadruplex DNAs were determined by the FID assay.[56] This assay is based on the decrease in the fluorescence intensity due the displacement of thiazole orange (TO) dye from the quadruplex structures upon titration of quadruplex stabilizing ligands.[56] FID curves (Figure

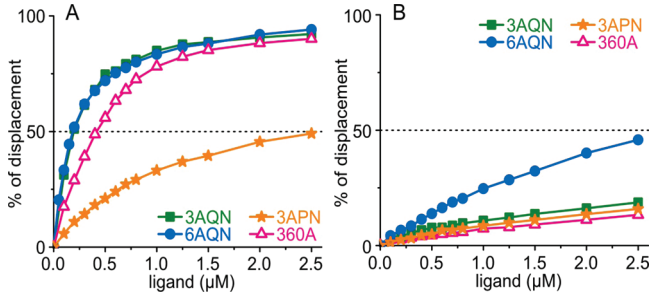

Figure 3. FID assays of ligands with telomeric G-quadruplex DNA and duplex DNA in the presence of 100 mM NaCl, 10 mM sodium cacodylate buffer, pH 7.2, and 0.5 or 0.75 μM thiazole orange. (A) Prefolded telomeric quadruplex (0.25 μM) with ligands (0 to 10 molar equiv). (B) Duplex DNA (0.25 μM) with ligands (0 to 10 molar equiv).

dx.doi.org/10.1021/jo201816g | J. Org. Chem. 2012, 77, 229−242

3A and Figure S1, Supporting Information) were obtained by plotting percentage of displacement of thiazole orange versus concentration of ligand. The displacement concentration ($^{G4}DC_{50}$, concentration of ligand to displace 50% thiazole orange from G-quadruplex DNA) values are reported in Table

Table 1. Binding Affinities of Ligands to Various Quadruplex and Duplex DNA Measured from Fluorescence Intercalator Displacement (FID) assay

	$^{G4}DC_{50}$ (μM)[a]					
ligands	telomeric	*c-kit1*	*c-kit2*	*c-myc*	$^{ds}DC_{50}$ (μM) duplex (ds26)	selectivity[b] for human telomeric DNA over duplex
3AQN	0.20	0.49	0.50	0.47	>2.5	33
6AQN	0.19	0.35	0.25	0.46	>2.5	16
3APN	>2.5	>2.5	1.95	1.47	>2.5	
360A	0.41 (*0.29*[c])	0.40	0.31	0.44	>2.5	33 (42[c])

[a] DC_{50} is the concentration of ligand needed to displace 50% of thiazole orange (TO). Experiments were duplicated and estimated error values are within ±5%. [b] The selectivity of the ligands was estimated using the formula 2.5/^{G4}C. (^{G4}C was calculated as follows: at 2.5 μM ligand concentration, the percentage of TO displacement from the duplex DNA was calculated. The concentration of ligand to achieve this much displacement from the telomeric quadruplex is known as ^{G4}C.) [c] Reported in the literature.[56]

1. For human telomeric DNA, Na^+ (100 mM) salt was used rather than K^+ salt, since under Na^+ salt conditions the sequence forms the antiparallel quadruplex exclusively.[57] Moreover in the presence of K^+ ions, time-dependent increase in fluorescence intensity was observed with thiazole orange, and this hampers the accurate measurement of ligand binding efficiency. For the telomeric sequence, low concentration (0.2 μM) of **3AQN** and **6AQN** was required to displace 50% thiazole orange, suggesting higher binding affinity of these ligands for the quadruplex. These values are quite comparable with that of reference compound **360A** ($^{G4}DC_{50}$ = 0.41 μM). However, the ligand **3APN**, which has pyridinium side chains, showed very weak binding to the quadruplex DNA ($^{G4}DC_{50}$ > 2.5 μM). The large aromatic core of naphthyridine, together with bisquinolinium side chains, (**3AQN** and **6AQN**) offer better affinity for the quadruplex.

To determine the selectivity of the ligands toward quadruplex DNA over duplex DNA, self-complementary duplex DNA (ds26) was used in FID assays. All ligands showed $^{ds}DC_{50}$ values of >2.5 μM (>10 molar equiv), indicating ligands are highly selective toward quadruplex DNA over duplex DNA (Figure 3B and Table 1). The estimated selectivity toward quadruplex over duplex DNA of **3AQN** and **6AQN** were found to be 33- and 16-fold, respectively. Further, to determine the affinity of ligands toward other quadruplex DNA structures, the promoter sequences such as *c-kit1*, *c-kit2*, and *c-myc* were also utilized. The reference compound **360A** binds to all promoter G-quadruplex DNAs with similar affinity (Table 1). However, **3AQN** binds 2-fold more strongly to telomeric DNA over promoter DNAs ($^{G4}DC_{50}$ > 0.4 μM). Similarly, **6AQN** shows 2-fold preference for telomeric DNA over *c-myc* DNA ($^{G4}DC_{50}$ > 0.4 μM). Ligand **3APN**, which has pyridine chains, exhibited binding only to the promoter sequences such as *c-myc* and *c-kit2* (Table 1). Though the exact reason for this preference of **3APN** toward promoter sequences is not clear, it can perhaps be attributed to the different preferred topologies of promoter quadruplexes compared to the telomeric quadruplex.

Circular Dichroism Studies. CD studies were performed to explore the potential of new ligands to induce quadruplex formation in different DNAs. In the absence of monovalent metal cations, ligand may induce a particular quadruplex structure. However, in presence of metal cations, ligand may selectively bind to one kind of quadruplex. Interpretation of CD spectra requires spectra of well characterized quadruplex structures for comparison.[58] For example, the CD spectra of human telomeric quadruplex DNA under Na^+ conditions shows a positive peak around 292 nm and a negative peak around 262 nm. These peaks have been assigned as characteristics of unimolecular antiparallel quadruplex topology, and this

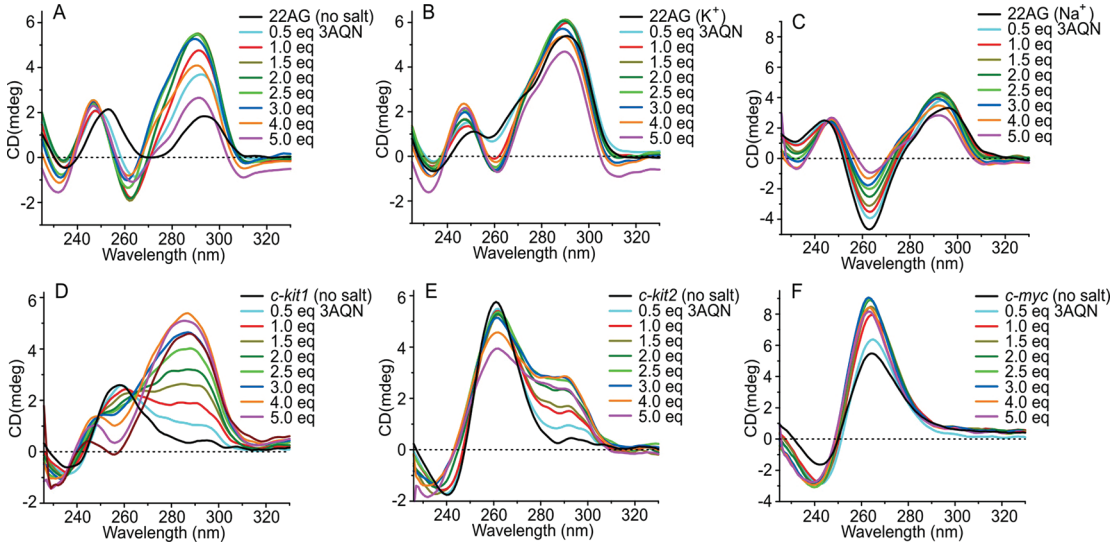

Figure 4. CD titration spectra of ligand **3AQN** (0–5 molar equiv) to quadruplex DNA (12.5 μM) in Tris buffer (50 mM, pH 7.2) in the presence and in the absence of monovalent cations at 25 °C. (A) Telomeric DNA in the absence of monovalent cations. (B) Telomeric DNA in the presence of K^+ (100 mM). (C) Telomeric DNA in the presence of Na^+ (100 mM). (D) *c-kit1* DNA in the absence of monovalent cations. (E) *c-kit2* DNA in the absence of monovalent cations. (F) *c-myc* DNA in the absence of monovalent cations.

dx.doi.org/10.1021/jo201816g | *J. Org. Chem.* 2012, 77, 229–242

structure was supported by NMR studies.[59] It should be noted that although CD is useful in assigning topology of ligand-induced quadruplex structures, this assignment needs to be further supported by NMR studies[60] or ^{125}I-radioprobing experiments.[61]

Human telomeric DNA and promoter DNAs were studied in presence and absence of Na^+ and K^+ ions. Telomeric DNA, in the absence of any added monovalent cations, shows positive peak around 290 and 252 nm and a small negative peak at 235 nm (Figure 4A). Upon addition of ligands (**3AQN**, **6AQN**, and **3APN**) at 0.5−3 equiv relative to the DNA, a negative peak at 262 nm, a positive peak at 292 nm, and a minor positive peak at 245 nm appeared (Figure 4A, Figure S2A and B, Supporting Information). As mentioned earlier, these are characteristic peaks for antiparallel quadruplex structure reported in the literature.[59,62] These results clearly suggest that ligands **3AQN**, **6AQN**, and **3APN** induce antiparallel quadruplex structures, producing an effect similar to that of reference compound **360A** (Figure S2C, Supporting Information). Although a slight decrease in the ellipticity was observed at higher concentration of of ligands (4−5 equiv), the characteristic peaks for antiparallel topology were retained.

In the presence of 100 mM KCl, telomeric DNA exhibits a mixture of parallel and antiparallel structures, which have a characteristic positive peak at 290 nm with a shoulder peak at 270 nm, a small positive peak at 250 nm, and a small negative peak at 234 nm (Figure 4B).[62] Upon addition of ligands **3AQN** and **6AQN**, a negative peak appeared at 260 nm and the positive peak at 290 nm was retained, suggesting the induction of antiparallel quadruplex structure (Figure 4B and Figure S3A, Supporting Information). However, the ligand **3APN** did not induce the antiparallel form (Figure S3B, Supporting Information). Like **3AQN** and **6AQN**, the reference compound **360A** also induced similar antiparallel quadruplex topology (Figure S3C, Supporting Information). In the presence of Na^+ ions, telomeric DNA exists in an antiparallel basket-type conformation (Figure 4C).[59,62] Upon addition of ligands, this antiparallel structure was retained (Figure S3D and E, Supporting Information). Overall, these results indicate that irrespective of the nature of metal ions, all ligands selectively induce or stabilize the antiparallel quadruplex form of telomeric DNA.

The promoter DNA sequence *c-kit1*, in the absence of any monovalent ions, exhibits a small positive peak at 260 nm indicative of a parallel quadruplex structure (Figure 4D).[40] Interestingly, addition of **3AQN** resulted in a negative peak at 260 nm and a positive peak at 290 nm. This is a clear indication of an antiparallel conformation being induced by ligand **3AQN** (Figure 4D). However, in the presence ligand **6AQN**, induction of both parallel and antiparallel structures was observed (Figure S4A, Supporting Information). Similar to **3AQN**, both **3APN** and reference compound **360A** stabilize the same topology (Figure S4B and C, Supporting Information). Moreover, *c-kit1* in the presence of K^+ ions exists as a parallel structure, which has a characteristic positive peak centered around 260 nm and a negative peak at 240 nm (Figure S5, Supporting Information).[38] As it was already well stabilized by K^+ metal ions, no increase in CD ellipticity upon addition of ligands was observed, and the parallel structure was retained.

In the absence of monovalent ions, *c-kit2* exists predominantly as a parallel structure as evidenced by the major positive peak at 260 nm and minor negative peak at 240 nm (Figure 4E).[40] Increasing the concentrations of **3AQN**, **6AQN**, and **3APN** led to formation of a peak around 290 nm and decrease in the ellipticity at 260 nm (Figure 4E and Figure S6, Supporting Information). The reference compound **360A** also induced the similar quadruplex topology (Figure S6C, Supporting Information). These results indicate that parallel quadruplex structures were induced to form a mixture of parallel and antiparallel structures. In the presence of K^+ ions, *c-kit2* exhibited a positive peak at 260 nm and a negative peak at 240 nm indicating the parallel structure (Figure S7, Supporting Information).[40] In general, in the presence of K^+ ions, addition of ligands did not affect the peaks at 260 and 240 nm, suggesting the quadruplex structure retains the parallel topology (Figure S7, Supporting Information).

In the absence of any added monovalent metal cations or ligands, the *c-myc* DNA exists in a parallel topology (Figure 4F).[40] When **3AQN**, **6AQN**, and **3APN** were added to the *c-myc* DNA, parallel structure was further stabilized as evidenced by the increase in ellipticity at 263 nm. Similar quadruplex stabilization was observed with **360A** as well (Figure S8, Supporting Information). In the presence K^+ ions, *c-myc* DNA shows a positive peak around 263 nm and a negative peak at 243 nm, which are characteristic peaks for parallel quadruplex structure.[40] Addition of ligands **3AQN** and **6AQN** to *c-myc* DNA did not perturb the quadruplex structure, which was already induced and stabilized by K^+ ions (Figure S9, Supporting Information).

CD Melting Studies. Thermal stabilization of various quadruplex DNA and duplex DNA in the presence of ligands was studied using the CD melting experiment. Thermal denaturation of antiparallel telomeric quadruplex DNA in presence of Na^+ was monitored at 295 nm. Monovalent metal cation concentration (LiCl and NaCl) was adjusted to 100 mM so as to obtain a T_m value around 50 °C in the absence of ligands.[63] This was expected to provide a large T_m window to analyze the ligand stabilizing effects. All ligands increased the stability of quadruplex DNAs (Figure 5). We observed that

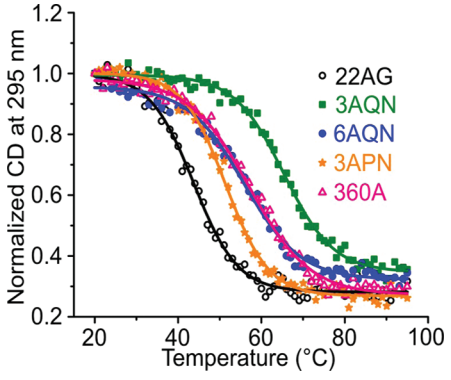

Figure 5. CD melting curves of telomeric DNA (5 μM, 10 mM NaCl, 90 mM LiCl, and 10 mM sodium cacodylate buffer pH 7.2) with 3 molar equiv of ligands (15 μM). Ligand **3AQN** provided higher stabilization than **3APN**. ΔT_m values are listed in Table 2.

3AQN enhanced telomeric DNA quadruplex stability by 21.0 °C, which is 3 °C higher than that of the reference compound **360A** (Table 2). The ΔT_m values of **6AQN** and **3APN** were 15.1 and 7.7 °C, respectively (Table 2). Furthermore, duplex DNA was monitored by CD melting studies to examine the effect of ligands on duplex stabilization. Even when increasing the ligand concentration 3-fold, only a slight increase (up to 1.6 °C) of thermal stability was observed (Figure S10A, Supporting

dx.doi.org/10.1021/jo201816g | J. Org. Chem. 2012, 77, 229−242

Table 2. Thermal Stability of Various Quadruplex DNA and Duplex DNA with Ligands Measured by CD Melting Experiments

	ΔT_m[a]				
ligands	telomeric	*c-kit1*	*c-kit2*	*c-myc*	duplex (ds17)
3AQN	21.0 ± 0.4	>20	>25	>30	1.1 ± 0.5
6AQN	15.1 ± 0.9	>20	>25	>30	1.6 ± 0.5
3APN	7.7 ± 0.4	28.9 ± 0.5	23.0 ± 1.2	21.2 ± 0.9	1.4 ± 0.4
360A	17.4 ± 0.8	>20	>25	>30	0

[a] ΔT_m represents difference in thermal melting [$\Delta T_m = T_m$ (DNA + 3 molar equiv ligand) − T_m (DNA)]. The buffer used was 10 mM sodium cacodylate buffer, pH 7.2. The T_m values are 44.5 ± 0.4 °C [telomeric DNA (5 μM) in 10 mM NaCl, 90 mM LiCl]; 46.5 ± 0.3 °C [*c-kit1* DNA (15 μM) in 20 mM KCl, 80 mM LiCl]; 54.0 ± 0.5 °C [*c-kit2* DNA (10 μM) in 5 mM KCl, 95 mM LiCl]; 47.6 ± 0.4 °C [*c-myc* DNA (5 μM) in 100 mM LiCl]; 63.3 ± 0.5 °C [ds-17 DNA (15 μM) in 100 mM NaCl]. All experiments were triplicated, and the values reported are average of 3 measurements with the estimated standard deviation. The salt concentration was adjusted such that the melting temperature of DNA without ligand is around 50 °C.[63]

Information and Table 2). These results underscore the fact that ligands selectively stabilize quadruplex DNA over duplex DNA. The ΔT_m of values of **3AQN** and **6AQN** for telomeric DNA and duplex DNA were comparable with that of reference compound **360A**.

The melting temperatures of parallel promoter quadruplex DNAs such as *c-kit1* and *c-kit2* were monitored at 263 nm. All ligands enhanced quadruplex stability similarly to reference compound **360A** (Table 2). Since very high stabilization was observed with ligands **3AQN**, **6AQN**, and **360A**, we were not able to determine accurate melting temperatures from the melting curves (Figure S10B and C, Supporting Information). Ligand **3APN** increased the T_m of *c-kit1* by 28.9 °C and *c-kit2* by 23 °C. In the case of the highly stable parallel *c-myc* quadruplex DNA, thermal denaturation experiments were performed in the absence of K^+ ions. The ligands **3AQN** and **6AQN** enhanced the stability of the *c-myc* quadruplex more than 30 °C (Table 2). Since a stable baseline curve was not achieved even above 90 °C, accurate measurement of T_m was also not possible in this case (Figure S10D, Supporting Information). T_m enhancement of **3AQN** and **6AQN** were comparable to that of **360A**. Interestingly, ligand **3APN** has enhanced the stability of *c-myc* quadruplex by 21 °C (Table 2). This is in agreement with FID studies, where it was found that **3APN** binds specifically to *c-myc* and *c-kit1* DNAs. This shows that **3APN** stabilizes promoter quadruplexes much better than human telomeric quadruplex.

Taq Polymerase Stop Assay. Quadruplex stabilization by the ligands was further tested by concentration-dependent *Taq* DNA polymerase stop assay.[64] Primer extension of DNA is inhibited by the stabilization of a quadruplex structure in the template sequence. DNA templates containing telomeric sequence and *c-myc* sequence were used in these studies. For telomeric DNA, the assay was carried out in the presence of 100 mM NaCl. Though quadruplex formation was favored in the presence of salts, primer extension was not inhibited in absence of ligands. This indicates that unstable quadruplex DNAs unfold easily and can be extended by *Taq* polymerase leading to full extension product (Figure 6A). Stabilization of quadruplex structure by ligands **3AQN**, **6AQN**, and **360A** inhibited the formation of full length products. As a result, stop products at the quadruplex forming sites were observed with increasing ligand concentration (Figure 6A). Normalized stop products in each lane was plotted against concentration of ligands, and IC_{50} values were calculated (Figure S11, Supporting Information). Ligands **3AQN** and **6AQN** have lower IC_{50} values of ∼0.8 and ∼0.7 μM, respectively, suggesting improved stabilization of quadruplex at lower ligand concentration. The IC_{50} value **360A** was slightly higher (∼1.2 μM). Ligand **3APN** did not inhibit the primer extension by *Taq* polymerase. These results are in agreement with the results of FID and CD melting experiments where bisquinolinium derivatives of naphthyridine (**3AQN** and **6AQN**) exhibit higher quadruplex binding affinity and melting temperature than the pyridinium based **3APN** ligand.

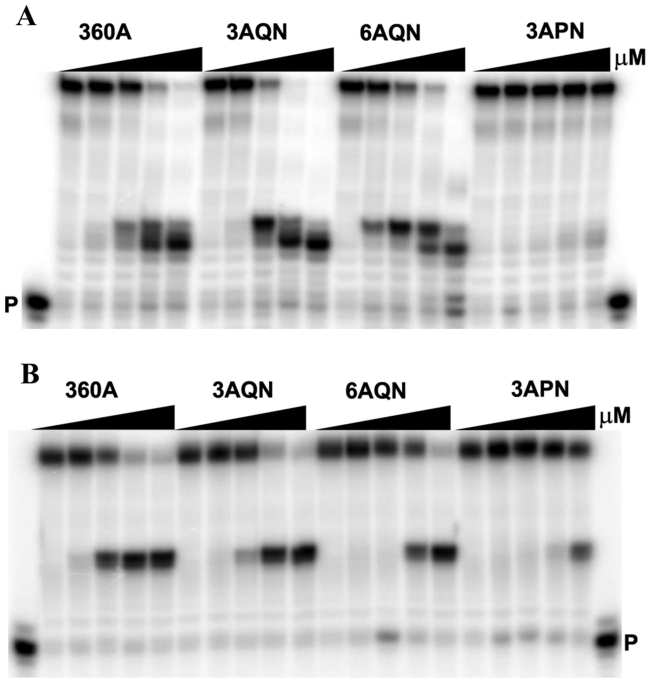

Figure 6. Denaturing PAGE for the *Taq* polymerase based primer extension stop assay in the presence of **360A**, **3AQN**, **6AQN**, and **3APN** ligands. (A) Template containing human telomeric DNA with increasing ligand concentration (0, 0.5, 1, 2, 4 μM). Primer extension reaction in the presence of 100 mM NaCl at 35 °C. (B) Template containing *c-myc* DNA with increasing ligand concentration (0, 0.25, 0.5, 1, 2 μM). Primer extension reaction at 55 °C. Conditions: 200 nM template, 50 nM primer, 0.2 mM dNTs in *Taq* polymerase buffer. P denotes primer. Formation of full length products decreases with increasing ligand concentration.

For *c-myc* DNA, the assay was carried out at 55 °C to destabilize the preformed quadruplex structures that could otherwise interfere with ligand induced stabilization.[65] A pause at quadruplex forming sites was observed for extension products in presence of all ligands (Figure 6B). The reference compound **360A** and ligands **3AQN** and **6AQN** have lower IC_{50} values of ∼0.5, ∼0.7, and ∼1.0 μM, respectively (Figure

dx.doi.org/10.1021/jo201816g | J. Org. Chem. 2012, 77, 229–242

S11B, Supporting Information). The IC_{50} value of ligand **3APN** was found to be more than 2.0 μM with *c-myc* DNA, suggesting that at high ligand concentrations, **3APN** could stabilize *c-myc* quadruplex structure.

Nondenaturing Gel Electrophoresis. Ligand-induced quadruplex formation was also studied by nondenaturing gel electrophoresis. The quadruplex structures, being more compact, move faster in gel compared to the unfolded nonquadruplex forms.[66] Telomeric DNA was titrated with ligands in the absence of any added monovalent metal cations. Interestingly, all ligands except **3APN** accelerated the mobility of telomeric DNA in the gel compared to the DNA in the absence of ligands (Figure 7). The mobility of bands was

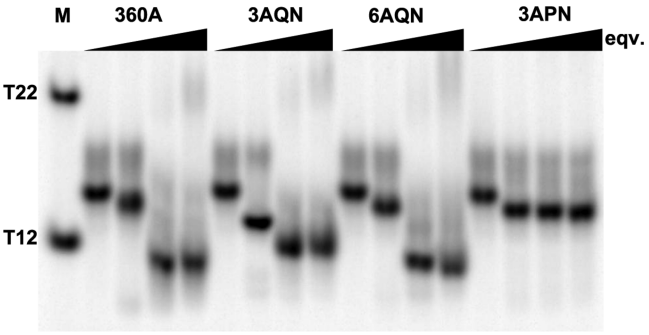

Figure 7. Nondenaturing PAGE of human telomeric DNA (5 μM) with increasing molar equivalents of ligands (0, 1, 2, and 5) in the absence of monovalent cations at 4 °C. Induction of stable compact quadruplex structure by ligands results in accelerated mobility of telomeric DNA. M denotes unstructured size markers, dT_{12} and dT_{22}, and the retarded mobilities of the markers are in agreement with the literature findings.[68]

increased with increasing ligand concentration from 1 to 2 molar equiv. However, the mobility of quadruplex DNA with 5 molar equiv was the same as with 2 molar equiv (Figure 7). This suggests that complete induction of quadruplex form might have been attained with 2 equiv of ligands. Hence, no effect was observed upon further addition of ligands. Furthermore, the electrophoretic mobilities of quadruplex structures induced by the ligands in the absence of salts were higher than the mobility of the T_{12} marker. This behavior is similar to the native gel mobility of human telomeric DNA observed in K^+ conditions.[67] These results are consistent with the observations from CD studies where ligands, in the absence of monovalent ions, were shown to induce the telomeric DNA into quadruplex form. Experiments were also performed in the presence of NaCl. The addition of ligands did not have any pronounced effect on the mobility (data not shown). This supports the fact that Na^+ induces the quadruplex structures even in the absence of added ligands. Since the promoter quadruplexes are much more stable and can be formed even in the absence of ligands, native gel titrations were not performed with those DNA sequences.

Molecular Modeling Studies. Initially the ligands were energy optimized using Hartee-Fock method (HF/6-31G*, Figures S12–S15, Supporting Information), and then they were docked to the antiparallel human telomeric G-quadruplex DNA (PDB entry 143D)[57] using Autodock.[69] As anticipated, ligands readily bound to the pseudointercalation site at the top quartet. On the basis of docking results, 20 ns MD simulations were carried out for all ligands and quadruplex DNA complex using AMBER 10.[70] The structures shown in Figure 8 are the final MD snapshot of each complex after 20 ns simulations.

Binding energies were estimated using molecular mechanics Poisson–Boltzmann surface area (MM-PBSA)[71] and nmode analysis. The binding free energy components are summarized in Table 3. The individual energy components (Table S1, Supporting Information) allowed a better understanding of the ligand–quadruplex interaction and their driving forces. For all complexes the electrostatic energy, van der Waals energy, and nonpolar solvation energy contributed favorably to the binding free energies. The electrostatic solvation energy was found to be unfavorable for all of the ligands. A direct comparison of the energy components of **3AQN** [ΔG_{bind} = −89.2 ± 7.4] and **360A** [ΔG_{bind} = −84.8 ± 7.2] (Table S1, Supporting Information) complexes enables a better understanding of the structure and activity relationship. van der Waals energy for the **3AQN** and quadruplex complex (−155.0 kcal mol^{-1}) was more than that of the **360A** and quadruplex complex (−128.2 kcal mol^{-1}) (Table S1, Supporting Information). This can be attributed to the presence of two aromatic rings in the central core of **3AQN**, which makes it a more efficient stacker on G-quartets than **360A**. nmode calculation revealed a more negative ΔS for **3AQN** (−62.2 kcal mol^{-1}) and **6AQN** (−59.3 kcal mol^{-1}) than that of **360A** (−43.6 kcal mol^{-1}) (Table S1, Supporting Information). This indicates a decrease in the rotational and translational freedom of **3AQN** and **6AQN** upon complexation with G-quadruplex when compared to those of **360A**. Although the number of aromatic rings possessed by **3AQN** and **6AQN** are the same, ligand **6AQN** shows slightly higher binding free energy (ΔG_{bind} = −80.4 ± 8.4). This indicates that minor changes in the position of methylated nitrogen in quinolone play a key role in determining the binding affinity of the ligands. The crescent-like scaffold in the **3AQN** molecule was maintained during MD simulation, enabling it to stack more effectively with the G-quartet (Figure 8A). The planar crescent-like conformation of **3AQN** is stabilized by strong intramolecular hydrogen bonds [(N–H···N) indicated as a red dotted line in Figure 8A]. However, a reorientation of the side chain of **6AQN** from the G-quartet surface to the nearby groove/backbone region was observed, which results in the loss of planarity of the compound (Figure 8B). This reorientation was not observed in **3AQN** or in **360A** (Figure S16, Supporting Information), and this indicates that the positively charged N-methyl group at the 6-amino position of the quinoline side chain is attracted by electrostatic force to the negatively charged backbone atoms (Figure 8B).

The binding free energy of **3APN** with quadruplex DNA is not reported because after 3 ns of MD simulation, **3APN** moved away from the DNA with little disruption of the quartet (Figure S17, Supporting Information). The pyridine side chains of **3APN** are positively charged and readily interact with the backbone of the diagonal loop. Also, the pyridinium side chains failed to form the stacking interaction with the quartet. The strong interaction between the diagonal loop and side chain of the ligand increases the distance between the diagonal loop and the top quartet. Because of this, dG17 moves from the plane of the quartet followed by dG18 in the middle quartet, which moves toward the top quartet. Furthermore, the K^+ ion is not precisely coordinated when one of the guanines moves away from the plane of the quartet (Figure S17, Supporting Information).

dx.doi.org/10.1021/jo201816g | J. Org. Chem. 2012, 77, 229–242

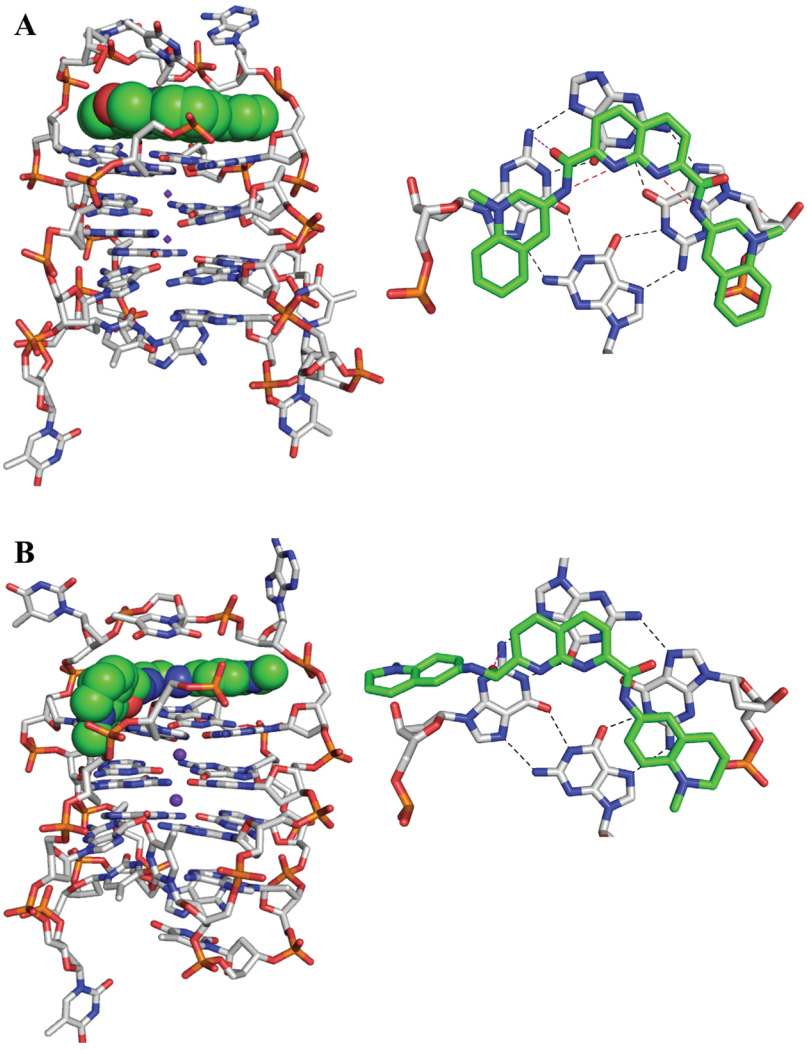

Figure 8. Final MD snapshots of the ligand-quadruplex complexes after 20 ns simulations. Side views (left side) show the ligands bound onto the top quartet of quadruplex DNA. DNA and ligands are represented as stick and sphere, respectively. The K^+ ions, present in between the two quartets, are shown as purple spheres. Axial views (right side) show the stick representation of top quartet and ligand. Hydrogen bonds present in the quartet are shown in dotted lines. (A) **3AQN**-quadruplex DNA complex. A hydrogen bond between carbonyl oxygen atom of ligand and N2 hydrogen atom of dG-10 is indicated in red dotted line. (B) **6AQN**-quadruplex DNA complex shows the reoriented side chain of the interacts with the backbone/groove of quadruplex DNA.

Table 3. Estimated Free Energy of Binding (ΔG, kcal mol^{-1}) for Quadruplex and ds DNA with Each Ligand Calculated from 20 ns MD Simulations[a]

type of DNA	3AQN	6AQN	360A
human telomeric	−89.29 ± 7.49	−80.42 ± 8.42	−84.81 ± 7.28
ds DNA	−25.76 ± 2.3	−30.10 ± 3.4	−39.34 ± 2.12

[a]The values reported from MM/PBSA and nmode analysis are the average values of three independent MD simulations of the G-quadruplex DNA and ligand complex. Different ligand conformations at the same binding mode or position from docking results were used in each MD run. As there was no significant interaction found between **3APN** and quadruplex DNA after 3 ns of MD simulation, its energy value is not reported here.

The stability of the ligand−quadruplex structures after 20 ns MD simulations is examined by measuring the root-mean-square deviation (rmsd) values of the heavy atoms of ligands and DNA and H-bond occupancies in the quartets and between ligand and DNA, and by performing single point energy calculations. rmsd values for heavy atoms in the G-quartet were monitored for all MD trajectories by comparing those with NMR structure using the ptraj module implemented in AMBER10 (Figure S18, Supporting Information). By inspecting the rmsd values, it can be concluded that the G-quartets are stable over the course of simulation with all of the ligands except **3APN**. To investigate the overall stability of quadruplex DNA, the rmsd values of backbone atoms were monitored. A sharp increase in rmsds was observed between 2 and 4 ns simulation in all complexes, which can be attributed to the backbone relaxation of the starting structure. The complexes were stabilized after 5 ns, when the rmsd values converged to a steady state (Figure S18, Supporting Information). The backbone atoms were not significantly shifted from the starting structure in three complexes. Although the average rmsd values were the same for all three, upon close examination of rmsds, we observed the least change in backbone atoms of the **3AQN**−quadruplex complex (2.5 Å) in comparison to the **360A** complex (3.5 Å) and **6AQN** complex (3.2 Å) (Table S2, Supporting Information). This is perhaps due to the additional flexibility of nucleotides in the diagonal loop in the **360A**−

dx.doi.org/10.1021/jo201816g | J. Org. Chem. 2012, 77, 229−242

quadruplex complex. To investigate this further, averaged structures (Figure S19, Supporting Information) were obtained from MD simulation snapshots that were taken from the final 10 ns of the MD trajectory with an interval of every 20 ps. The averaged structures were superimposed onto their corresponding initial equilibrated docked structures. It can be clearly seen that the **3AQN** binding to G-quartet has better backbone stability compared to the binding of **360A** (Figure S19, Supporting Information). The ligand conformational changes were also analyzed using rmsd values. Larger rmsd fluctuation was observed in **6AQN** because of the reorientation of its quinolinium side chain as mentioned earlier; rmsd values of the ligand heavy atoms show that **3AQN** has rmsd (0.81 Å) lower than those of **6AQN** (1.07 Å) and **360A** (1.04 Å) (Table S2, Supporting Information). Further, the movements of metal ions inside the quartet cavity and ions in the solvent were observed during MD simulations. The K^+ metal cation on the outermost exposed quartet was released into the solvent. However, the other two K^+ ions stayed stable during simulations (Figure S20, Supporting Information).

To study the impact of ligand binding to the G-quartet, the hydrogen bond (N_2−H···N7 and N1−H···O6) occupancies of the quartet were calculated along all MD trajectories (Table S3, Supporting Information). The inner hydrogen bond occupancies in the middle and the bottom quartets were less than that for the top ligand bound G-quartet. The average hydrogen bond occupancy of all of the three G-quartets was slightly higher for the **3AQN** complex when compared to the **6AQN** and **360A** complexes (Table S3, Supporting Information). This suggests that **3AQN** binding imparts more stability to G-quartets. Hydrogen bond interactions between the quadruplex and ligand were computed over the last 10 ns MD trajectories keeping the distance cutoff as 3.0 Å and 35° of angle deviation. There was only one stable hydrogen bond formed by the **3AQN** carbonyl oxygen atom with DNA (NH_2 atom in Guanine-10 at the top quartet) (Figure 8A). Additionally, **3AQN** and **6AQN** interact with thymine base of diagonal loop by means of $\pi-\pi$ stacking (Figure S21, Supporting Information).

Since G-quartets are stacked together by $\pi-\pi$ interactions, stacking energies between the quartets with and without ligand bound were calculated to investigate the impact of small molecules on quadruplex stabilization. All single point energies were calculated using BH&H/6-311++ G (d,p) in Gaussian03.[72] In the absence of ions, the stacking energy between G-quartets was found to be −186.7 kcal/mol, and a further decrease in stacking energy was observed upon ligand binding to the ion-free G-quadruplex DNA (Table S4, Supporting Information). It is thus clear that ligands have a strong impact on the stabilization of quadruplex DNA even in the absence of any ions. It was also evident that the quadruplex structure in the geometry of the **3AQN** complex has stronger interquartet interactions (−217.1 kcal/mol) (Table S4, Supporting Information). Quadruplexes in the **6AQN** (−209.4 kcal/mol) and **360A** (−210.6 kcal/mol) complex has approximately the same interquartet interactions (Table S4, Supporting Information). Also, no effect was observed in the interaction of the last quartet when the ligand bound to the top quartet. Along with the ligands, addition of K^+ ions resulted in considerable stabilization of quartets. In the presence of K^+ ions, **3AQN** has more effect on quartet stabilization; while **6AQN** and **360A** bound quartets have similar interquartet stacking energy (Table S4, Supporting Information).

In order to determine the selectivity of the ligands toward quadruplex DNA over duplex DNA, the interaction between the ligands and ds DNA (17 bp) was examined using 20 ns of MD simulation by employing the same protocol used for quadruplex and ligand simulations. The final MD snapshot of ds DNA and ligands, (Figure S22, Supporting Information) binding energy values (Table 3 and Table S5, Supporting Information), and rmsd graphs (Figure S23, Supporting Information) showed that, overall, the ligands neither stabilize nor destabilize the ds DNA.

CONCLUSIONS

We have synthesized three novel amide derivatives of 1,8-napthyridine and studied their interaction with various quadruplex DNAs. The FID assay indicates that naphthyridine bisquinolinium ligands **3AQN** and **6AQN** have high binding affinity and selectivity for quadruplex DNAs over duplex DNA. Moreover, the concentration-dependent *Taq* polymerase stop assay shows that ligands at low concentration stabilize the quadruplex and thus inhibit the *Taq* polymerase enzyme activity. Ligand **3APN** with pyridinium side chains does not stabilize the human telomeric quadruplex, which clearly suggests that unstable quadruplexes can be easily unwound and extended by polymerase enzymes.

CD studies show that ligands **3AQN** and **6AQN** induce and stabilize only the antiparallel quadruplex form of human telomeric DNA in both the absence and presence of monovalent cations. Though **3APN** induces the same form in the absence of cations, it does not induce the antiparallel form in the presence of K^+ ions. This result indicates that formation of the antiparallel quadruplex from the highly stable telomeric quadruplex in K^+ ions require strong stabilizing agents having quinolinium side chains. It should be noted that the highly potent quadruplex stabilizing ligand telomestatin also induces a basket-type antiparallel quadruplex form in solution in the presence of K^+ ions.[62] In fact, a recent study shows that the parallel form of telomeric quadruplex may not be biologically relevant.[73] Therefore, ligands that could induce only antiparallel quadruplex topology of human telomeric DNA may find use in the therapeutic arena. Furthermore, stabilization of quadruplex structures by ligands revealed by CD melting suggests that all ligands could only stabilize quadruplex DNA structures and not duplex DNA. More interestingly, ligand **3APN** exhibited enhanced stabilization of promoter quadruplexes (*c-myc*, *c-kit1*, and *c-kit2*) and weak stabilization of telomeric quadruplex. This underscores the importance of the side chains of ligands in quadruplex topology recognition. Ligand **3APN** could possibly be fine-tuned to impart selective recognition of promoter quadruplex topologies.

Modeling studies provide the relative stability of DNA quadruplex−ligand complexes. The rmsd, single point energy, and binding energy calculations from molecular dynamics studies suggest that the **3AQN**−quadruplex DNA complex is the most stable among the four ligand−quadruplex DNA complexes studied. It is interesting to note that the position of the positive charge in the quinoline side chains appears to play an important role in the orientation of the ligand when bound to quadruplex DNA. Ligand **3APN** contains a small pyridinium side chain, which is inefficient in forming a strong stacking interaction with the G-quartet. Instead, it is involved in electrostatic interactions with the backbone of the diagonal loop that leads to the disruption of quadruplex DNA. Ligands **3AQN** and **6AQN** with naphthyridine as the central core are

dx.doi.org/10.1021/jo201816g | J. Org. Chem. 2012, 77, 229−242

able to impart increased stability to quadruplex structures in comparison to **360A**, which has pyridine as the central moiety.

Although achieving selectivity among various quadruplex topologies is considered to be an important challenge, a recent study shows that ligands that target and stabilize more than one type of quadruplex topologies (telomeric and *c-kit*) could still impart high anticancer activity.[74] Our studies indicate that further optimization of side chains could provide discriminatory ability to ligands in targeting the loops of different quadruplex topologies. This in turn could lead to enhanced selectivity between various quadruplex structures.

In summary, this study presents an organized approach to ascertain the importance of the central aromatic core of ligands in quadruplex stabilization, which has been an important criterion for design of quadruplex stabilizing ligands. Additionally, our studies underscore the importance of side chains in recognizing loops and discriminating among various quadruplex topologies. Taken together, the results presented here clearly suggest that naphthyridine derivatives are an important class of G-quadruplex stabilizing agents with strong discrimination against duplex DNA. Moreover, strong quadruplex stabilizing agents such as the ones reported here may find applications to sequester quadruplex forming sequences *in vivo*.[42]

EXPERIMENTAL SECTION

General. Thin-layer chromatography (TLC) was performed on silica gel plates precoated with fluorescent indicator with visualization by UV light (254 nm). ^{1}H NMR (400 or 300 MHz), ^{13}C NMR (100 MHz), and ^{19}F NMR (376 MHz) were recorded on a 400 or 300 MHz instrument. The chemical shifts in parts per million were referenced to the residual proton signal of deuterium solvents (^{1}H NMR $CDCl_3$: δ 7.26 ppm; ^{13}C NMR $CDCl_3$: δ 77.2 ppm; ^{1}H NMR DMSO-d_6: δ 2.50 ppm; ^{13}C NMR DMSO-d_6: δ 39.5 ppm). Multiplicities of ^{1}H NMR spin couplings are reported as s (singlet), d (doublet), t (triplet), q (quartet), dd (doublet of doublets), or m (multiplet and overlapping spin systems). Values for apparent coupling constants (J) are reported in hertz. High resolution mass spectra (HRMS) were obtained in positive ion electrospray ionization (ESI) mode. DNA sequences were synthesized using automated synthesizer by employing standard phosphoramidite chemistry.

Preparation of 2,7-Dimethyl-1,8-naphthyridiene (2). To a solution of compound **1**[51] (4 g, 20.7 mmol) and ammonium formate (6.5 g, 103.2 mmol) in methanol (70 mL) and water (4 mL) was added a small piece of dry ice to make an oxygen-free atmosphere. To this solution was added Pd (10%)/C (1 g), and the reaction mixture was stirred for 6 h in room temperature. Then the reaction mixture was filtered through a Celite pad, and the filtrate was evaporated. The resulting residue was dissolved in DCM (200 mL) and washed with water (100 mL). The organic layer was dried over anhydrous Na_2SO_4. Solvent was removed under reduced pressure to furnish compound **2** as a yellow solid (2.8 g, 86% yield). R_f = 0.40 (5% MeOH in DCM); ^{1}H NMR (400 MHz, $CDCl_3$) δ 8.01 (d, J = 8.0 Hz, 2H), 7.31(d, J = 8.0 Hz, 2H), 2.78 (s, 6H); ^{13}C NMR (100 MHz) δ 162.7, 155.7, 136.6, 122.2, 118.7, 25.7; HRMS (ESI) calcd for $C_{10}H_{11}N_2$ (M + H) 159.0922 found 159.0919 (Δm −0.0003, error −1.8 ppm).

General Procedure for Introduction of Amide Side Chains in the Naphthyridine Core. To a stirred solution of diacid compound **3**[53,54] (1 equiv) in 8 mL dry DMF under N_2 atm were added the corresponding amine (2 equiv), EDC·HCl (2.5 equiv), HOBt (0.2 equiv), and DMAP (0.2 equiv). The mixture was stirred for 24 h at room temperature and then kept in a freezer for 6 h. The precipitate formed was filtered through a sintered funnel and washed with saturated $NaHCO_3$, water, acetone, and diethyl ether to furnish the amide.

***N,N′*-Di(quinolin-3-yl)-1,8-naphthyridine-2,7-dicarboxamide (4a).** Compound **3** (200 mg, 0.92 mmol) in 8 mL of dry DMF, 3-aminoquinoline (264 mg, 1.83 mmol), EDC·HCl (440 mg, 2.30 mmol), HOBt (25 mg, 0.18 mmol), and DMAP (22 mg, 0.18 mmol) were used (210 mg, 48% yield). R_f = 0.38 (5% MeOH in DCM); ^{1}H NMR (300 MHz, DMSO-d_6) δ 11.40 (s, 2H), 9.36 (d, J = 2.6 Hz, 2 H), 9.02 (d, J = 2.6 Hz, 2H), 8.93 (d, J = 8.4 Hz, 2 H), 8.51 (d, J = 8.4 Hz, 2 H), 8.02 (d, J = 8.4 Hz, 4H), 7.74−7.61 (m, 4H); ^{13}C NMR (100 MHz, DMSO-d_6) δ 163.4, 154.0, 152.5, 145.6, 144.7, 140.4, 132.1, 128.7, 128.5, 128, 127.7, 127.3, 125.6, 123.9, 121.5; HRMS (ESI) calcd for $C_{28}H_{19}N_6O_2$ $[M + H]^+$ 471.1569, found 471.1559 (Δm −0.0010, error −2.3 ppm).

***N,N′*-Di(quinolin-6-yl)-1,8-naphthyridine-2,7-dicarboxamide (4b).** Compound **3** (200 mg, 0.92 mmol) in 8 mL of dry DMF, 6-aminoquinoline (264 mg, 1.83 mmol), EDC·HCl (440 mg, 2.30 mmol), HOBt (25 mg, 0.18 mmol), and DMAP (22 mg, 0.18 mmol) were used (222 mg, 51% yield). R_f = 0.52 (5% MeOH in DCM); ^{1}H NMR (300 MHz, DMSO-d_6) δ 11.22 (s, 2 H), 8.92−8.85 (m, 4 H), 8.71 (s, 2 H), 8.49 (d, J = 8.4 Hz, 2 H), 8.38 (d, J = 8.1 Hz, 2 H), 8.27 (d, J = 8.4 Hz, 2 H), 8.08 (d, J = 8.8 Hz, 2 H), 7.54 (dd, J = 8.1, 4.0 Hz, 2 H); ^{13}C NMR (100 MHz, DMSO-d_6) δ 162.8, 154.1, 152.3, 149.6, 145.1, 140.3, 136.2, 135.8, 129.6, 128.3, 125.4, 124.2, 122.0, 121.3, 116.6; HRMS (ESI) calcd for $C_{28}H_{19}N_6O_2$ $[M + H]^+$ 471.1 569, found 471.1552 (Δm −0.0017, error −3.7 ppm).

***N,N′*-Di(pyridin-3-yl)-1,8-naphthyridine-2,7-dicarboxamide (4c).** Compound **3** (100 mg, 0.45 mmol) in 4 mL dry DMF, 3-aminopyridine (94 mg, 1.0 mmol), EDC·HCl (220 mg, 1.14 mmol), HOBt (12 mg, 0.08 mmol) and DMAP (22 mg, 0.18 mmol) were used (40 mg, 23%). R_f = 0.16 (5% MeOH in DCM); ^{1}H NMR (300 MHz, DMSO-d_6) δ 11.14 (s, 2 H), 9.13 (d, J = 1.8 Hz, 2 H), 8.90 (d, J = 8.4 Hz, 2 H), 8.45 (d, J = 8.4 Hz, 2 H), 8.39−8.36 (m, 4 H), 7.47 (dd, J = 8.4, 4.8 Hz, 2 H); ^{13}C NMR (100 MHz, DMSO-d_6) δ 163.2, 154.0, 152.4, 144.7, 141.7, 140.3, 135.2, 128.1, 125.5, 124.0, 121.5; HRMS (ESI) calcd for $C_{20}H_{15}N_6O_2$ $[M + H]^+$ 371.1256, found 371.1267 (Δm +0.0011, error +2.9 ppm).

General Procedure for N-Methylation of Side Chains. To a stirred solution of corresponding amine compound (1 equiv) in dry DMF (2 mL) was added methyl triflate (∼58 equiv). It was heated at 80 °C, and stirring was continued for 4 days. The reaction mixture was then cooled to room temperature followed by keeping at −20 °C for 3 h. The cooled reaction mixture was filtered through sintered funnel, and the residue was washed with cold acetone and diethyl ether to furnish the desired product.

3,3′-[1,8-Naphthyridinediyl-2,7-bis(carbonylimino)]bis(1-methylquinolinium)triflate (3AQN). Compound **4a** (50 mg, 0.106 mmol) in dry DMF (2 mL) and methyl triflate (0.7 mL, 6.19 mmol) were used (47 mg, 55% yield). ^{1}H NMR (400 MHz, DMSO-d_6) δ 11.92 (s, 2 H), 10.07 (d, J = 1.8 Hz, 2H), 9.64 (s, 2H), 9.01 (d, J = 8.5 Hz, 2H), 8.56−8.50 (m, 6H), 8.24−8.20 (m, 2H), 8.06 (t, J = 7.5 Hz, 2H), 4.74 (s, 6H); ^{13}C NMR (100 MHz, DMSO-d_6) δ 164.0, 153.4, 152.6, 145.0, 141.1, 135.9, 134.7, 134.3, 132.8, 130.6, 130.2, 129.4, 126.3, 122.0, 119.3, 46.4; ^{19}F NMR (376 MHz, DMSO-d_6) δ −77.8; HRMS m/z calcd for $C_{30}H_{24}N_6O_2$ $[M/2]^+$ 250.0980, found 250.0981 (Δm +0.0001, error +0.4 ppm).

6,6′-[1,8-Naphthyridinediyl-2,7-bis(carbonylimino)]bis(1-methylquinolinium)triflate (6AQN). Compound **4b** (50 mg, 0.106 mmol) in dry DMF (2 mL), methyl triflate (0.7 mL, 6.19 mmol) were used (44 mg, 52% yield). ^{1}H NMR (400 MHz, DMSO-d_6) δ 11.66 (s, 2H, N−H), 9.39 (d, J = 5.5 Hz, 2H), 9.30 (d, J = 8.3 Hz, 2H), 9.19 (d, J = 2.3 Hz, 2H), 8.96 (d, J = 8.3 Hz, 2H), 8.71 (dd, J = 2.3, 9.7 Hz, 2H), 8.64−8.59 (m, 2H), 8.52 (d, J = 8.3 Hz, 2H), 8.15 (dd, J = 5.8, 8.3 Hz, 2H), 4.65 (s, 6H); ^{13}C NMR (100 MHz, DMSO-d_6) δ 163.7, 153.9, 152.4, 148.6, 146.5, 140.6, 139.1, 135.4, 130.2, 129.4, 125.8, 122.5, 121.7, 120.3, 117.6, 45.3.^{19}F NMR (376 MHz, DMSO-d_6) δ −77.7; HRMS (ESI) calcd for $C_{30}H_{24}N_6O_2$ $[M/2]^+$ 250.0980, found 250.0977 (Δm −0.0003, error −1.2 ppm).

3,3′-[1,8-Naphthyridinediyl-2,7-bis(carbonylimino)]bis[1-methylpyridinium]triflate (3APN). Compound **4c** (40 mg, 0.108 mmol) in dry DMF (2 mL) and methyl triflate (0.7 mL, 6.19 mmol) were used (43 mg, 57% yield). ^{1}H NMR (400 MHz, DMSO-d_6) δ 11.89 (s, 2H, N−H), 9.66 (s, 2H), 8.98 (d, J = 8.5 Hz, 2H), 8.89 (d, J = 8.5 Hz, 2H), 8.81 (d, J = 5.8 Hz, 2H), 8.50 (d, J = 8.5 Hz, 2H), 8.19 (dd, J = 5.9, 8.7 Hz, 2H), 4.45 (s, 6H); ^{13}C NMR (DMSO-d_6, 100

dx.doi.org/10.1021/jo201816g | J. Org. Chem. 2012, 77, 229−242

MHz) δ 163.9, 153.3, 152.4, 141.0, 140.8, 138.4, 136.9, 135.2, 128.0, 126.1, 122.3, 121.9, 48.7; ^{19}F NMR (DMSO-d_6, 376 MHz) δ −77.7; HRMS (ESI) calcd for $C_{22}H_{20}N_6O_2$ $[M/2]^+$ 200.0824, found 200.0816 (Δm −0.0008, error −4.1 ppm).

3,3′-[2,6-Pyridinediylbis(carbonylimino)]bis[1-methylquinolinium]triflate (360A). The *N*,*N*′-bis(3-quilonyl)-pyridine-2,6-dicarboxamide[75] (0.05 g, 0.119 mmol) in dry DMF (2 mL) and methyl triflate (0.8 mL, 7.07 mmol) were used (51 mg, 57% yield). R_f = 0.35 (7% MeOH in DCM). ^{1}H NMR (400 MHz, DMSO-d_6) δ 11.89 (s, 2H), 10.10 (s, 2H), 9.65 (s, 2H), 8.59−8.47 (m, 7H), 8.24 (t, J = 8.0 Hz, 2H), 8.09 (t, J = 8.0 Hz, 2H), 4.78 (s, 6H); ^{13}C NMR (100 MHz, DMSO-d_6) δ 162.5, 147. 5, 144.7, 141.2, 135.9, 134.5, 134.2, 132.3, 130.5, 130.0,129.3, 126.5, 122.3, 119.3, 49.2; ^{19}F NMR (DMSO-d_6, 376 MHz) δ −77.77; HRMS (ESI) calcd for $C_{27}H_{23}N_5O_2$ $[M]^+$ 449.1852, found 449.1854 (Δm +0.0002, error +0.5 ppm).

Oligonucleotides. The following oligonucleotide sequences were used for FID and CD and native gel experiments: human telomeric DNA sequence (22AG: 5′-AGGGTTAGGGTTAGGGTTAGGG-3′); self-complementary duplex sequence (ds26: 5′-CAATCGGATC-GAATTCGATCCGATTG-3′); duplex sequence (ds17: 5′-CCAGTTCGTAGTAACCC-3′and its complementary sequence 5′-GGGTTACTA CGAACTGG-3′) and promoter DNA sequences (*c-kit1*: 5′-GGGAGGGCGCTGGGAGGAGGG-3′; *c-kit2*: 5′-GGGCGGGCGCGAGGGAGGGG-3′; *c-myc*: 5′-TGAGGGTGGG-TAGGGTGGGTAA-3′). For *Taq* polymerase stop assay, primer sequence (5′-ACGACTCACTATAGCAATTGCG-3′), template containing telomeric DNA sequence (5′-**AGGGTTAGGGTTAGGGT-TAGGG**GCCACCGCAATTGCTATAGTGAGTCGT-3′, where bold letters indicate quadruplex forming region) and template containing *c-myc* sequence (5′-**TGAGGGTGGGTAGGGTGGGTAA**GCCACCG-CAATTGCTATAGTGAGTCGT -3′, where bold letters indicate quadruplex forming region) were used. All sequences were synthesized on 0.2 μmol scale with appropriate controlled pore glass (CPG) beads used as 3′ solid support. All oligonucleotides were deprotected and PAGE (20%, 7 M urea) purified employing standard protocols. The concentration of all oligonucleotides was measured at 260 nm in UV−vis spectrophotometer using appropriate molar extinction coefficients (ε). The integrity of oligonucleotides was confirmed by negative mode of ESI-MS analysis.

Fluorescence Intercalator Displacement Assay. The FID assay was carried out as described by Teulade-Fichou and co-workers.[76] The quadruplex forming DNA (0.25 μM) in KCl (100 mM) or NaCl (100 mM) and sodium cacodylate buffer (10 mM, pH 7.2) were annealed by heating at 95 °C for 5 min and cooling in ice for 10 min. Two molar equivalents of thiazole orange (TO, 0.5 μM for quadruplex DNA) or 3 molar equiv (0.75 μM for duplex DNA) was added. After TO addition, 2−3 h equilibration time was provided. Experiments were performed at 20 °C by using thermostatted cell holders. The excitation and emission wavelength used were 501 and 510−750 nm, respectively, and the slit width was 5 nm. Ligands stock solution were made (500 μM) in DMSO. Each addition of ligand (from 0 to 10 equiv, i.e., 0, 0.1, 0.2, 0.3, 0.4, 0.5, 0.6, 0.8, 1.0, 1.25, 1.5, 2.0, and 2.5 μM) was followed by 3−4 min equilibration period. Each curve was integrated using Origin 8.0 software to get the fluorescence area. The fluorescence area was converted into percentage of displacement (PD) by using the following equation. PD = 100 − [(FA/FA$_0$) × 100]; FA$_0$ is fluorescence area of DNA−TO complex alone (without ligand), and FA is fluorescence area in the presence of added ligand. FID curves were obtained by plotting percentage of displacement versus concentration of ligand used.

5′-End Radiolabeling of Oligonucleotides. Labeling of oligonucleotide was carried out for stop assay and native gel. The DNA (10 pmol) was mixed with T4 polynucleotide kinase (PNK) enzyme (5 U) and [γ-^{32}P] ATP (3000 Ci/mmol) in 1 x PNK buffer (50 mM Tris-HCl (pH 7.6), 10 mM $MgCl_2$, 5 mM DTT, 0.1 mM each spermidine and EDTA) in a total volume of 10 μL. The reaction mixture was incubated at 37 °C for 1 h followed by deactivation of enzyme by heating at 70 °C for 3 min. The end labeled DNA was then purified using a QIAquick nucleotide removal kit protocol provided by Qiagen.

DNA Polymerase Stop Assay. This assay was done as reported previously with slight modifications.[64] Appropriate amount of labeled primer oligonucleotide [∼15,000 counts per minute (CPM)] was mixed with cold primer (50 nM) and template (200 nM). They were annealed using an annealing buffer (5 mM Tris pH 7.5, 115 mM NaCl, 0.1 mM EDTA) by heating at 90 °C for 5 min followed by gradual cooling to room temperature over 4−5 h. For *c-myc* stop assay, corresponding primer−template duplex was annealed in the absence of 15 mM NaCl (5 mM Tris (pH 7.5), 0.1 mM EDTA). The annealed primer−template was mixed with polymerase buffer [50 mM Tris, 0.5 mM DTT, 0.1 mM EDTA, 10 mM NaCl, 5 mM MgCl, 1 μg/μL BSA] and dNTP (0.2 mM). The ligands in appropriate concentration were added to the reaction mixture (10 μL total volume) and incubated for 30 min at room temperature. The primer extension reaction was initiated by the addition of *Taq* DNA polymerase (0.5 U), and the reactions were incubated at 35 and 55 °C for 30 min for telomeric and *c-myc* DNA, respectively. The extension reaction was stopped by adding 10 μL of 2× stop buffer (10 mM EDTA, 10 mM NaOH, 0.1% each bromophenol blue (w/v) and xylene cyanole (w/v) in formamide). The products were analyzed in 15% denaturing PAGE (7 M urea) in which 1× TBE (89 mM of each Tris and boric acid and 2 mM of EDTA, pH 8.3) was used as running buffer. Autoradiograms were generated and bands were quantified by ImageQuantTL software provided by GE healthcare.

Nondenaturing Gel Electrophoresis. Appropriate amount of labeled oligonucleotides (∼14,000 CPM) was mixed with corresponding cold oligonucleotides (5 μM in 10 mM Tris pH 7.2). Various amounts (1−5 equiv) of ligands were incubated with DNA at 4 °C for overnight. The total volume was 10 μL. Prior to loading the reaction mixture onto the gel, 1 μL of 10× glycerol dye [60% glycerol (v/v), 0.1% each bromophenol blue and xylene cyanol (w/v)] was added. Analysis was carried out in 15% native PAGE at 4 °C in which 1× TB (89 mM of each Tris and boric acid, pH 8.3) was used as running buffer.

CD Titrations and Melting. CD spectra were measured in the wavelength range of 225−330 nm using a quartz cuvette with 1.0 mm path length. The scanning speed of the instrument was set to 100 nm/min, and response time used was 2 s. The strand concentration of oligonucleotide used was 12.5 μM, and ligand stock solution used was 1 mM in water. The quadruplex DNA solutions were annealed by heating corresponding quadruplex forming DNA (12.5 μM) with NaCl (100 mM) or KCl (100 mM) in Tris (50 mM, pH 7.2) buffer at 95 °C for 5 min and cooling in ice for 10 min. For the studies without salt, DNA (12.5 μM) in Tris (50 mM, pH 7.2) buffer was used. Each spectrum was an average of 3 measurements at 25 °C. All spectra were baseline corrected and analyzed using Origin 8.0 software.

For melting studies, 5−15 μM strand concentration of oligonucleotide in 10 mM sodium cacodylate (pH 7.2), required amount of monovalent salts such as LiCl, KCl, or NaCl, and 3 molar equiv of ligands (15−45 μM) were used. Telomeric DNA (5 μM DNA in 10 mM NaCl and 90 mM LiCl), *c-kit1* (15 μM DNA in 20 mM KCl and 80 mM LiCl), *c-kit2* (10 μM DNA in 5 mM KCl, and 95 mM LiCl), *c-myc* quadruplex (5 μM in 100 mM LiCl), and duplex DNA (15 μM ds17 in 100 mM NaCl) were annealed by heating at 95 °C for 5 min followed by gradual cooling to room temperature. Thermal melting was monitored at 295, 263, and 274 nm for telomeric, promoter and duplex DNAs, respectively, at the heating rate of 1 °C/min. The melting temperatures were determined from curve fit of melting profiles using two state transition model implemented in KaleidaGraph.[77]

Molecular Modeling Studies. The binding mode and interaction of ligand−G-quadruplex DNA complexes were studied by performing docking, molecular dynamics, and binding energy evaluation by following the protocol reported by Haider and Neidle.[78] The coordinates were derived from PDB code 143D, which is a 6 solution NMR structure of human telomeric unimolecular antiparallel basket-type G-quadruplex.[57] The single point energies were calculated for all of the 6 models in NMR structures using AMBER force-field FF03.[79]

The structure with the lowest energy was taken as our study model. The pseudointercalation binding site[78] was created between the diagonal loop (TTA) and the top G-Quartet using Biopolymer building module implemented in Discovery Studio 2.5 from Accelrys Inc.[80] Ligand structures were constructed and optimized with Gaussian 03[72] using Hartree−Fock method with 6-31G* as the basis set.

Docking studies were performed with Autodock4.0 program.[69] Auto dock-tools (ADT) was used to merge the nonpolar hydrogens of the quadruplex DNA to their corresponding carbons. Following this partial atomic charges were assigned. Similarly for the ligands, ADT was used to merge nonpolar hydrogens and assign rotatable bonds. Grid maps were generated for each atom type in the ligand using Auto grid. An active site box was created and centered at the quadruplex DNA with a grid spacing of 0.375 Å. Docking calculations were performed using Lamarckian genetic algorithm. A population of random individuals (size 150) was used with a maximum number of 25,000,000 energy evaluations, a maximum number of 27,000 generations and a mutation rate of 0.02. For each ligand, 200 independent dockings were carried out. The resulting positions were subsequently clustered according to a root-mean-square criterion of 0.5 Å.

On the basis of the structures derived from docking studies, MD studies were carried out for the complexes with the SANDER module in AMBER 10 with FF03 force field for DNA. Generalized AMBER force field (GAFF) parameters were used for the ligand molecule.[81] Partial atomic charges obtained with the restrained electrostatic potential (RESP)[82] were calculated using the Gaussian03 program at HF/6-31G* level. The charges were assigned to the atoms using the Antechamber program in AMBER 10. For MD simulations, G-quadruplex DNA and ligands were solvated by a truncated octahedron TIP3P water box extending to a distance of 10 Å from any solute atom, which yielded 4500−4900 water molecules. K^+ ions were added to neutralize the DNA backbone charges, and three K^+ ions were manually added in the core of the G-quartets. The solvated structures were subjected to two stages of minimization by using the well-defined parameters.[78] Subsequently, constant pressure MD simulation of 20 ns was then performed in an NPT ensemble at 1 atm and 300 K. The hydrogen bonds were constrained using SHAKE algorithm. For the nonbonded interaction the residue based cutoff of 10 Å was used. The output and trajectory files were saved for every 0.1 and 1 ps respectively for the subsequent analysis. All trajectory analysis was done with the ptraj module in the AMBER 10 suite and examined visually using the Visual Molecular Dynamics (VMD).[83]

In MM/PBSA[71] calculations, all of the ions and water molecules were removed except the ions present in the core of the G-quadruplex. Independent free energy estimates for the complex formed by G-quadruplex and ligands were calculated from the collected snapshots using the MM/PBSA energy analysis in AMBER 10.[70] The solute entropic contribution ($T\Delta S$) was estimated with the nmode module. The Poisson−Boltzmann polar solvation free energy (ΔG_{PB}) was obtained with a built-in PBSA module in AMBER 10. The nonpolar solvation free energy (ΔG_{np}), calculated by MOLSURF, was directly related to the solvent-accessible surface area (SASA).[84] To study the impact of the ligand binding to the stability of the G-quartet, the hydrogen bond occupancies of the G-quartet were calculated along all MD trajectories.

Single point energy calculations[85] were carried out to study $\pi-\pi$ stacking with the Becke's half-and-half functional (BH&H/6-311++G (d, p)) method in Gaussian. In these calculations the G-quadruplex structures emerged from 20 ns MD simulations were studied after removing the ligands. The G-quadruplex DNA is excised to the central core of 12 guanine bases containing two K^+ ions. Dangling bonds on the guanines were terminated with hydrogen atoms leaving a total of 194 atoms. To compare the ligand impact on quartet stabilization, stacking energy of G-quartets in the starting NMR structure was also computed.

Molecular modeling studies of the interactions between ligand and duplex DNA were performed following the same procedures and parameters described for quadruplex-ligand complexes. A double stranded duplex DNA (17 bp) was built using nucgen implemented in AMBER 10. All of the structures were visualized and the figures were generated using PyMOL v0.99 (http://www.pymol.org).

■ ASSOCIATED CONTENT

Ⓢ Supporting Information

Additional experimental data from FID assays, CD titrations, polymerase stop assay, molecular modeling studies, ESI-MS data of oligonucleotides, and copies of NMR spectra of all of the compounds. This material is available free of charge via the Internet at http://pubs.acs.org.

■ AUTHOR INFORMATION

Corresponding Author

*E-mail: pradeep@chem.iitb.ac.in.

Present Addresses

[§]Department of Chemistry, University of Illinois at Urbana−Champaign, Illinois, USA.

[‡]Department of Chemistry, University of Konstanz, Germany.

■ ACKNOWLEDGMENTS

We are thankful to Computer Center, IIT Bombay and BRAF-CDAC, Pune for providing computing facility and SAIF-IIT Bombay for NMR spectra. We are also thankful to Dr. Claudia Hobartner and Benjamin Brandsen for critical reading of the manuscript; Prof. David A. Case for waiving of the licensing fee for AMBER 10; Dr. Ashok K. Varma for providing access to Discovery Studio; Prof. Raghavan B. Sunoj, Sudarshan Wadkar, and Rajeev, R. for giving valuable suggestions and their help in performing single point energy calculations; Dr. Ruchi Anand for providing access to her laboratory facilities; Prof. Marie-Paule Teulade-Fichou and Eric Largy for their advice on FID assay; and Prof. Philip C. Bevilacqua and Betsy Whitman for their assistance in melting curve analysis using Kaleidagraph. This work was financially supported by grants from Council of Scientific and Industrial Research (CSIR, 01-2233/08/EMR-II)-Government of India; IRCC-IIT Bombay; Department of Biotechnology (DBT)-Government of India (BT/PR10693/AGR/36/586/2008); and Department of Science and Technology (DST)-Government of India (FAST track scheme, SR/FT/LS-133/2008). P.I.P is a recipient of Max-Planck India Fellowship (MPG-DST scheme). V.D thanks CSIR for the fellowship.

■ REFERENCES

(1) Burge, S.; Parkinson, G. N.; Hazel, P.; Todd, A. K.; Neidle, S. *Nucleic Acids Res.* **2006**, *34*, 5402−5415.

(2) Patel, D. J.; Phan, A. T.; Kuryavyi, V. *Nucleic Acids Res.* **2007**, *35*, 7429−7455.

(3) Wright, W. E.; Tesmer, V. M.; Huffman, K. E.; Levene, S. D.; Shay, J. W. *Genes Dev.* **1997**, *11*, 2801−2809.

(4) Huppert, J. L.; Balasubramanian, S. *Nucleic Acids Res.* **2007**, *35*, 406−413.

(5) Rankin, S.; Reszka, A. P.; Huppert, J.; Zloh, M.; Parkinson, G. N.; Todd, A. K.; Ladame, S.; Balasubramanian, S.; Neidle, S. *J. Am. Chem. Soc.* **2005**, *127*, 10584−10589.

(6) Agarwal, T.; Roy, S.; Chakraborty, T. K.; Maiti, S. *Biochemistry* **2010**, *49*, 8388−8397.

(7) Balasubramanian, S.; Hurley, L. H.; Neidle, S. *Nat. Rev. Drug Discovery* **2011**, *10*, 261−275.

(8) Eddy, J.; Maizels, N. *Nucleic Acids Res.* **2008**, *36*, 1321−1333.

(9) Huppert, J. L.; Bugaut, A.; Kumari, S.; Balasubramanian, S. *Nucleic Acids Res.* **2008**, *36*, 6260−6268.

(10) Zahler, A. M.; Williamson, J. R.; Cech, T. R.; Prescott, D. M. *Nature* **1991**, *350*, 718−720.

(11) Halder, K.; Wieland, M.; Hartig, J. S. *Nucleic Acids Res.* **2009**, *37*, 6811−6817.
(12) Arora, A.; Dutkiewicz, M.; Scaria, V.; Hariharan, M.; Maiti, S.; Kurreck, J. *RNA* **2008**, *14*, 1290−1296.
(13) Kumari, S.; Bugaut, A.; Huppert, J. L.; Balasubramanian, S. *Nat. Chem. Biol.* **2007**, *3*, 218−221.
(14) Azzalin, C. M.; Reichenbach, P.; Khoriauli, L.; Giulotto, E.; Lingner, J. *Science* **2007**, *318*, 798−801.
(15) Paeschke, K.; Capra, J. A.; Zakian, V. A. *Cell* **2011**, *145*, 678−691.
(16) Lipps, H. J.; Rhodes, D. *Trends Cell Biol.* **2009**, *8*, 414−422.
(17) Ribeyre, C.; Lopes, J.; Boule, J.-B.; Piazza, A.; Guedin, A.; Zakian, V. A.; Mergny, J.-L.; Nicolas, A. *PLoS Genet.* **2009**, *5*, e1000475.
(18) Lopes, J.; Piazza, A.; Bermejo, R.; Kriegsman, B.; Colosio, A.; Teulade-Fichou, M.-P.; Foiani, M.; Nicolas, A. *EMBO J.* **2011**, *30*, 4033−4046.
(19) Dai, J.; Carver, M.; Yang, D. *Biochimie* **2008**, *8*, 1172−1183.
(20) Lim, K. W.; Amrane, S.; Bouaziz, S.; Xu, W.; Mu, Y.; Patel, D. J.; Luu, K. N.; Phan, A. N. *J. Am. Chem. Soc.* **2009**, *131*, 4301−4309.
(21) Huppert, J. L. *Chem. Soc. Rev.* **2008**, *37*, 1375−1384.
(22) Cevec, M.; Plavec, J. *Biochemistry* **2005**, *44*, 15238−15246.
(23) Risitano, A.; Fox, K. R. *Nucleic Acids Res.* **2004**, *32*, 2598−2606.
(24) Chaires, J. B. *FEBS J.* **2010**, *277*, 1098−1106.
(25) Campbell, N. H.; Patel, M.; Tofa, A. B.; Ghosh, R.; Parkinson, G. N.; Neidle, S. *Biochemistry* **2009**, *48*, 1675−1680.
(26) Haider, S. M.; Neidle, S.; Parkinson, G. N. *Biochimie* **2011**, *93*, 1239−1251.
(27) Xue, L.; Ranjan, N.; Arya, D. P. *Biochemistry* **2011**, *50*, 2838−2849.
(28) Neidle, S. *FEBS. J.* **2010**, *127*, 1118−1125.
(29) Balasubramanian, S.; Neidle, S. *Curr. Opin. Chem. Biol.* **2009**, *13*, 345−353.
(30) Sun, D.; Thompson, B.; Cathers, B. E.; Salazar, M.; Kerwin, S. M.; Trent, J. O.; Jenkins, T. C.; Neidle, S.; Hurley, L. H. *J. Med. Chem.* **1997**, *40*, 2113−2116.
(31) Monchaud, D.; Teulade-Fichou, M. P. *Org. Biomol. Chem.* **2008**, *6*, 627−636.
(32) Ou, T.; Lu, Y.; Tan, J.; Huang, Z.; Wong, K.; Gu, L. *Chem. Med. Chem.* **2008**, *3*, 690−713.
(33) De Cian, A.; Cristofari, G.; Reichenbach, P.; Lemos, E. L.; Monchaud, D.; Teulade-Fichou, M. P.; Shin-ya, K.; Lacroix, L.; Lingner, J.; Mergny, J. L. *Proc. Natl. Acad. Sci. U.S.A.* **2007**, *104*, 17347−17352.
(34) Burger, A. M.; Dai, F.; Schultes, C. M.; Reszka, A. P.; Moore, M. J.; Double, J. A.; Neidle, S. *Cancer Res.* **2005**, *65*, 1489−1496.
(35) Phatak, P.; Cookson, J. C.; Dai, F.; Smith, V.; Gartenhaus, R. B.; Stevens, M. F.; Burger, A. M. *Br. J. Cancer* **2007**, *96*, 1223−1233.
(36) Granotier, C.; Pennarun, G.; Riou, L.; Hoffschir, F.; Gauthier, L. R.; De Cian, A.; Gomez, D.; Mandine, E.; Riou, J. F.; Mergny, J. L.; Mailliet, P.; Dutrillaux, B.; Boussin, F. D. *Nucleic Acids Res.* **2005**, *33*, 4182−4190.
(37) Izbicka, E.; Wheelhouse, R. T.; Raymond, E.; Davidson, K. K.; Lawrence, R. A.; Sun, D.; Windle, B. E.; Hurley, L. H.; Von Hoff, D. D. *Cancer Res.* **1999**, *59*, 639−644.
(38) Tauchi, T.; Shin-Ya, K.; Sashida, G.; Sumi, M.; Okabe, S.; Ohyashiki, J. H.; Ohyashiki, K. *Oncogene* **2006**, *25*, 5719−5725.
(39) Sparapani, S.; Haider, S. M.; Doria, F.; Gunaratnam, M.; Neidle, S. *J. Am. Chem. Soc.* **2010**, *132*, 12263−12272.
(40) Dash, J.; Shirude, P. S.; Hsu, S. D.; Balasubramanian, S. *J. Am. Chem. Soc.* **2008**, *130*, 15950−15956.
(41) Huang, Y. U.; Cheng, A. K. H.; Yu, H.; Sen, D. *Biochemistry* **2009**, *48*, 6794−804.
(42) Müller, S.; Kumari, S.; Rodriguez, R.; Balasubramanian, S. *Nat. Chem.* **2010**, *12*, 1095−1098.
(43) Nakatani, K.; Hagihara, S.; Sando, S.; Sakamoto, S.; Yamaguchi, K.; Maesawa, C.; Saito, I. *J. Am. Chem. Soc.* **2003**, *125*, 662−666.
(44) Monchaud, D.; Yang, P.; Lacroix, L.; Teulade-Fichou, M. P.; Mergny, J. L. *Angew. Chem.* **2008**, *47*, 4858−4861.
(45) Campbell, N. H.; Parkinson, G. N.; Reszka, A. P.; Neidle, S. *J. Am. Chem. Soc.* **2008**, *130*, 6722−6724.
(46) Riou, J. F.; Guittat, L.; Mailliet, P.; Laoui, A.; Renou, E.; Petitgenet, O.; Mégnin-Chanet, F.; Hélène, C.; Mergny, J. L. *Proc. Natl. Acad. Sci. U.S.A.* **2002**, *99*, 2672−2677.
(47) Pennarun, G.; Granotier, C.; Gauthier, L. R.; Gomez, D.; Hoffschir, F.; Mandine, E.; Riou, J. F.; Mergny, J. L.; Mailliet, P.; Boussin, F. D. *Oncogene* **2005**, *24*, 2917−2928.
(48) De Cian, A.; DeLemos, E.; Mergny, J. L.; Teulade-Fichou, M. P.; Monchaud, D. *J. Am. Chem. Soc.* **2007**, *129*, 1856−1857.
(49) Rodriguez, R.; Müller, S.; Yeoman, J. A.; Trentesaux, C.; Riou, J.-F.; Balasubramanian, S. *J. Am. Chem. Soc.* **2008**, *130*, 15758−15759.
(50) Bugaut, A.; Rodriguez, R.; Kumari, S.; Hsu, S. D.; Balasubramanian, S. *Org. Biomol. Chem.* **2010**, *8*, 2771−2776.
(51) Chandler, C. J.; Deady, L. W.; Reiss, J. A.; Tzimos, V. *J. Heterocycl. Chem.* **1982**, *19*, 1017−1019.
(52) He, C.; Lippard, S. J. *Tetrahedron* **2000**, *56*, 8245−8252.
(53) Goswami, S.; Mukherjee, R.; Mukherjee, R.; Jana, S.; Maity, A. C.; Adak, A. K. *Molecules* **2005**, *10*, 929−936.
(54) Fahrni, C. J.; Pfaltz, A. *Helv. Chim. Acta* **1998**, *81*, 491−506.
(55) Anwer, M. K.; Sherman, B. D.; Roney, J. G.; Spatola, A. F. *J. Org. Chem.* **1989**, *54*, 1284−1289.
(56) Monchaud, D.; Allain, C.; Bertrand, H.; Smargiasso, N.; Rosu, F.; Gabelica, V.; De Cian, A.; Mergny, J. L.; Teulade-Fichou, M. P. *Biochimie* **2008**, *90*, 1207−1223.
(57) Wang, Y.; Patel, D. J. *Structure* **1993**, *1*, 263−282.
(58) Paramasivan, S.; Rujan, I.; Bolton, P. H. *Methods* **2007**, *43*, 324−331.
(59) Ambrus, A.; Chen, D.; Dai, J.; Bialis, T.; Jones, R. A.; Yang, D. *Nucleic Acids Res.* **2006**, *34*, 2723−2735.
(60) Dailey, M. M.; Miller, M. C.; Bates, P. J.; Lane, A. N.; Trent, J. O. *Nucleic Acids Res.* **2010**, *38*, 4877−4888.
(61) Gaynutdinov, T. I.; Neumann, R. D.; Panyutin, I. G. *Nucleic Acids Res.* **2008**, *36*, 4079−4087.
(62) Rezler, E. M.; Seenisamy, J.; Bashyam, S.; Mu-Yong, K.; White, E.; Wilson, W. D.; Hurley, L. H. *J. Am. Chem. Soc.* **2005**, *127*, 9439−9447.
(63) Guedin, A.; Lacroix, L.; Mergny, J. L. *Methods Mol. Biol.* **2010**, *613*, 25−35.
(64) Sun, D.; Hurley, L. H. *Methods Mol. Biol.* **2010**, *608*, 65−79.
(65) Seenisamy, J.; Bashyam, S.; Gokhale, V.; Vankayalpati, H.; Grand, C. L.; Siddiqui-Jain, A.; Streiner, N.; Wilson, W. D.; Hurley, L. H. *J. Am. Chem. Soc.* **2005**, *127*, 2944−2959.
(66) Kim, M. Y.; Vankayalapati, H.; Kazuo, S.; Wierzba, K.; Hurley, L. H. *J. Am. Chem. Soc.* **2002**, *124*, 2098−2099.
(67) Balagurumoorthy, P.; Brahmachari, S. K. *J. Biol. Chem.* **1994**, *269*, 21858−21869.
(68) Kejnovska, I.; Kypr, J.; Vorlickova, M. *Biochem. Biophys. Res. Commun.* **2007**, *353*, 776−779.
(69) Morris, G. M.; Goodsell, D. S.; Halliday, R. S.; Huey, R.; Hart, W. E.; Belew, R. K.; Olson, A. J. *J. Comput. Chem.* **1998**, *19*, 1639−1662.
(70) Case, D. A. *AMBER 10*; University of California: San Francis co, CA, 2008.
(71) Kollman, P. A.; Massova, I.; Reyes, C.; Kuhn, B.; Huo, S.; Chong, L.; Lee, M.; Lee, T.; Duan, Y.; Wang, W.; Donini, O.; Cieplak, P.; Srinivasan, J.; Case, D. A.; Cheatham, T. E. *Acc. Chem. Res.* **2000**, *33*, 889−897.
(72) Frisch, M. J. et al. *Gaussian 03, Revisions C.02 E. 01*; Gaussian, Inc.: Wallingford, CT, 2004.
(73) Hansel, R.; Lohr, F.; Foldynova-Trantirkova, S.; Bamberg, E.; Trantirek, L.; Dotsch, V. *Nucleic Acids Res.* **2011**, *39*, 5768−5775.
(74) Gunaratnam, M.; Swank, S.; Haider, S. M.; Galesa, K.; Reszka, A. P.; Beltran, M.; Cuenca, F.; Fletcher, J. A.; Neidle, S.; Gunaratnam, M. *J. Med. Chem.* **2009**, *52*, 3774−3783.
(75) Dorazco-Gonzalez, A.; Hopfl, H.; Medrano, F.; Yatsimirsky, A. K. *J. Org. Chem.* **2010**, *75*, 2259−2273.
(76) Monchaud, D.; Teulade-Fichou, M. P. *Methods Mol. Biol.* **2010**, *608*, 257−271.

(77) Siegfried, N. A.; Bevilacqua, P. C. *Methods Enzymol.* **2009**, *455*, 365−393.
(78) Haider, S.; Neidle, S. *Methods Mol. Biol.* **2010**, *608*, 17−37.
(79) Yang, L.; Tan, C. H.; Hsieh, M. J.; Wang, J.; Duan, Y.; Cieplak, P.; Caldwell, J.; Kollman, P. A.; Luo, R. *J. Phys. Chem. B* **2006**, *110*, 13166−13176.
(80) *Accelrys; Discovery Studio, version 2.0*; Accelrys Inc.: San Diego, CA, 2007.
(81) Wang, J.; Wolf, R. M.; Caldwell, J. W.; Kollman, P. A.; Case, D. A. *J. Comput. Chem.* **2004**, *25*, 1157−1174.
(82) Fox, T.; Kollman, P. A *J. Phys. Chem. B* **1998**, *102*, 8070−8079.
(83) Humphrey, W.; Dalke, A.; Schulten, K. *J. Mol. Graphics* **1996**, *14*, 33−38.
(84) Sitkoff, D.; Sharp, K. A.; Honig, B. *Biophys. Chem.* **1994**, *51*, 397−409.
(85) Clay, E. H.; Gould, I. R. *J. Mol. Graphics Model.* **2005**, *24*, 138−146.

dx.doi.org/10.1021/jo201816g | *J. Org. Chem.* 2012, 77, 229−242

Supporting Information

Selective G-quadruplex DNA Stabilizing Agents Based on Bisquinolinium and Bispyridinium Derivatives of 1, 8-Naphthyridine

V. Dhamodharan, S. Harikrishna, C. Jagadeeswaran, K. Halder & P.I. Pradeepkumar*

Department of Chemistry, Indian Institute of Technology Bombay, Powai, Mumbai 400076, India

TABLE OF CONTENTS

FID assay plots of promoter DNAs

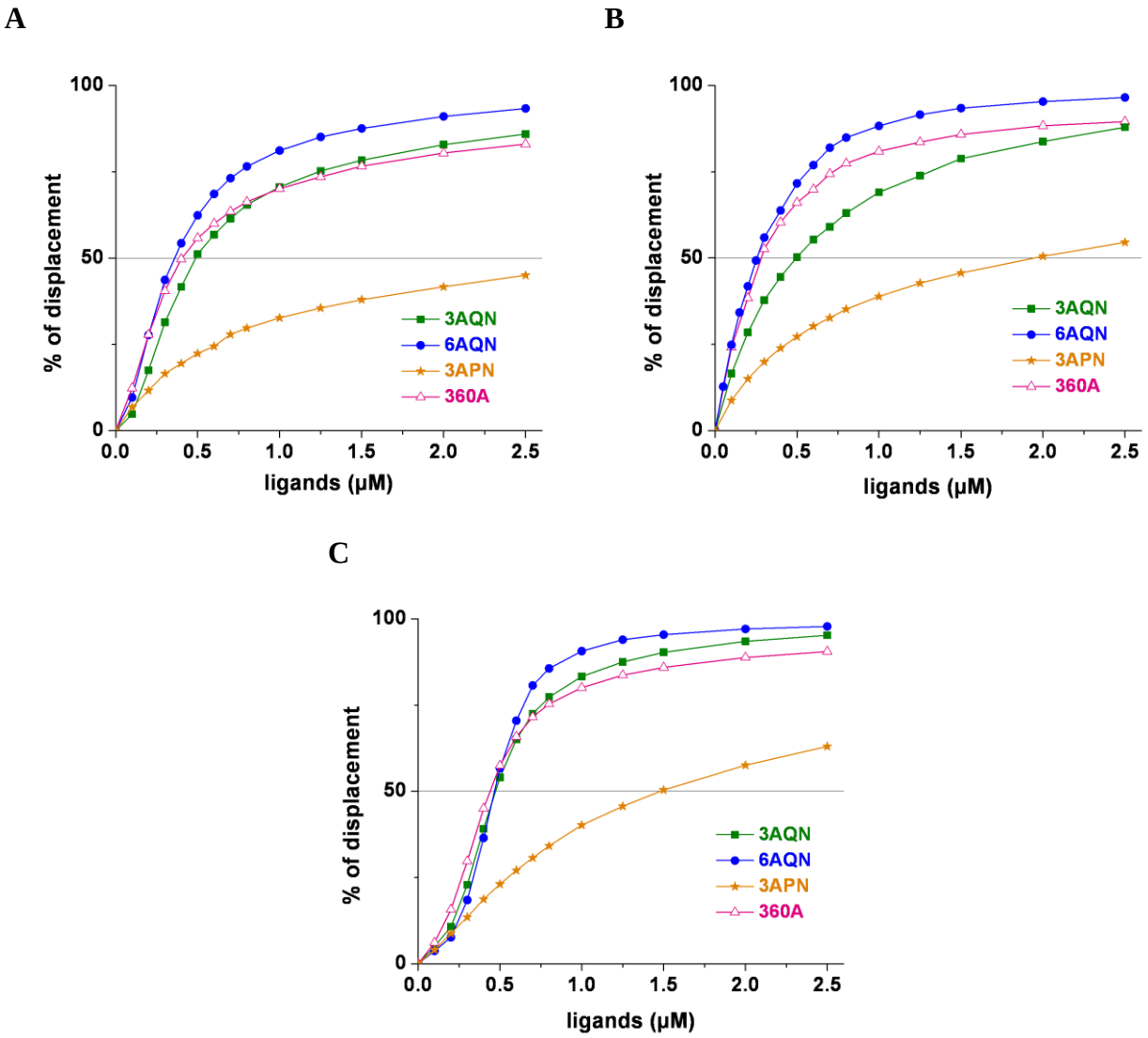

Figure S1. FID assay plots of promoter DNAs (0.25 μM in 100 mM KCl, 10 mM sodium cacodylate buffer, pH 7.2 and 0.5 μM TO) with ligands (0 to 10 molar equivalents) at 20 °C: (A) *c-kit1* DNA; (B) *c-kit2* DNA; (C) *c-myc* DNA.

CD titration spectra of telomeric DNA with ligands

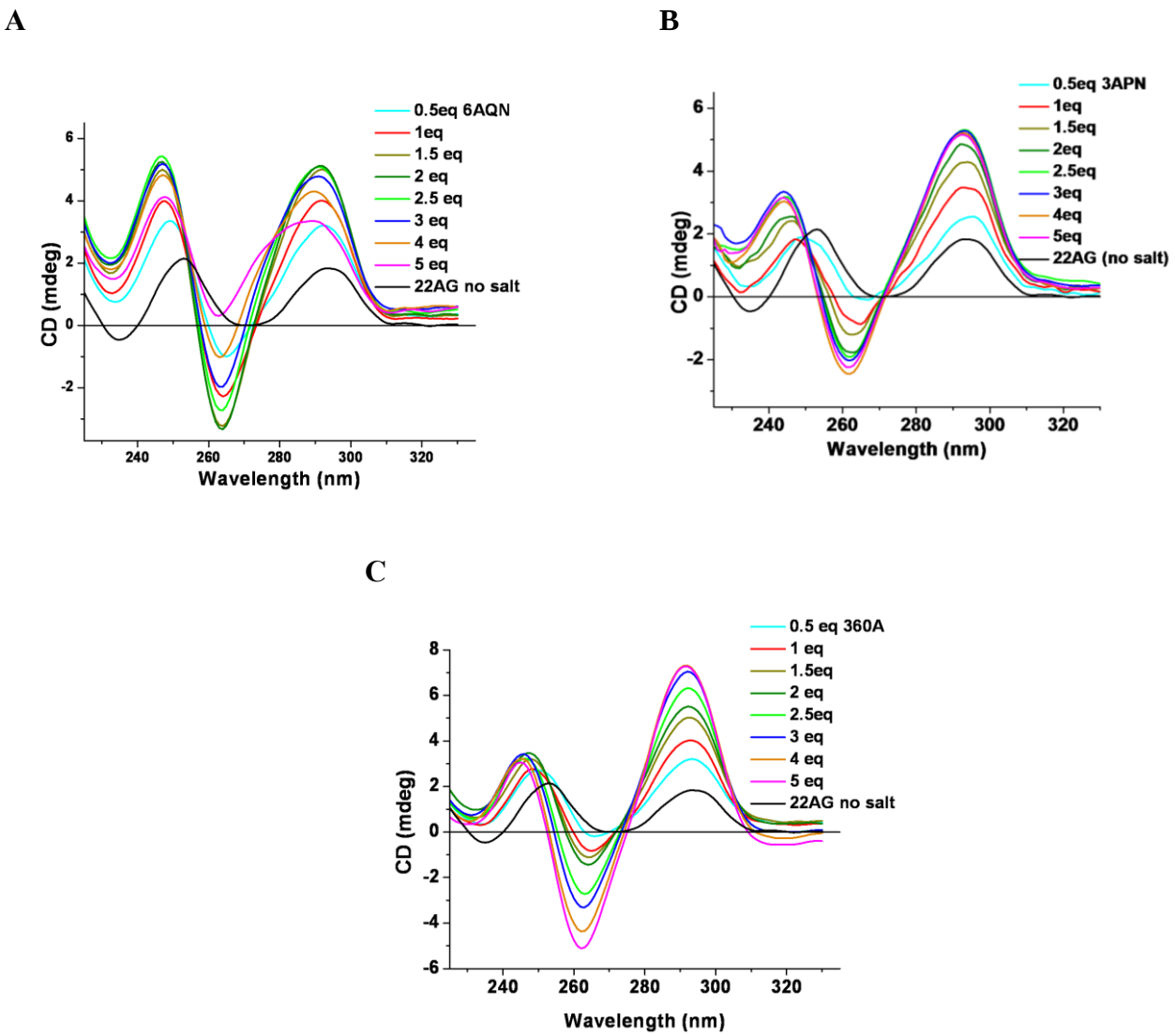

Figure S2. CD titration spectra of telomeric DNA (12.5 µM in 50 mM Tris, pH 7.2) with (A) **6AQN,** (B) **3APN** and (C) **360A** in the absence of salts.

CD titration spectra of telomeric DNA with ligands in presence of K^+/Na^+ ions

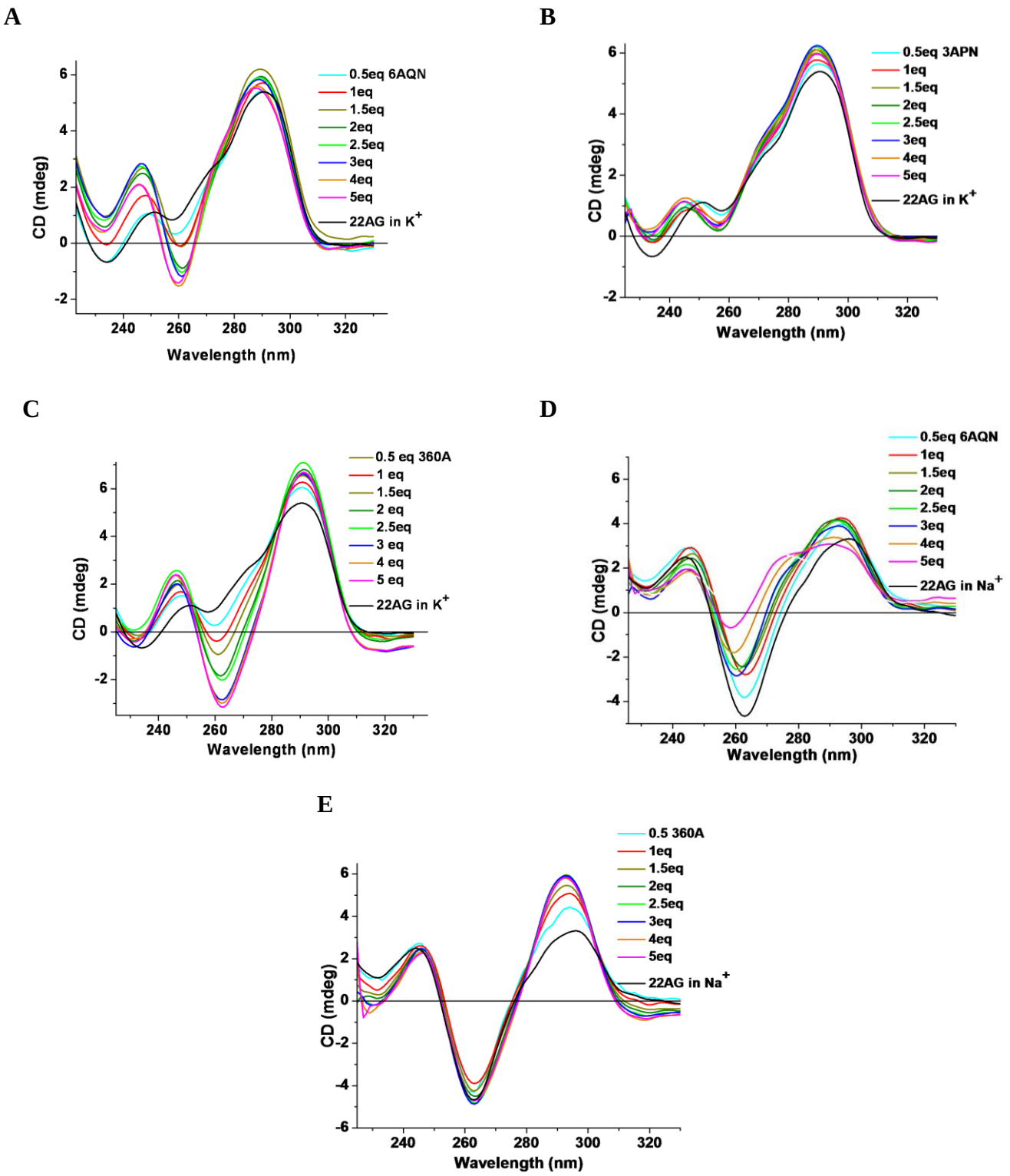

Figure S3. CD titration spectra of telomeric DNA (12.5 µM in 50 mM Tris, pH 7.2) with (A) **6AQN** in the presence of 100 mM KCl, (B) **3APN** in the presence of 100 mM KCl, (C) **360A** in the presence of 100 mM KCl, (D) **6AQN** in the presence of 100 mM NaCl, (E) **360A** in the presence of 100 mM NaCl.

CD titration spectra of *c-kit1* DNA with ligands

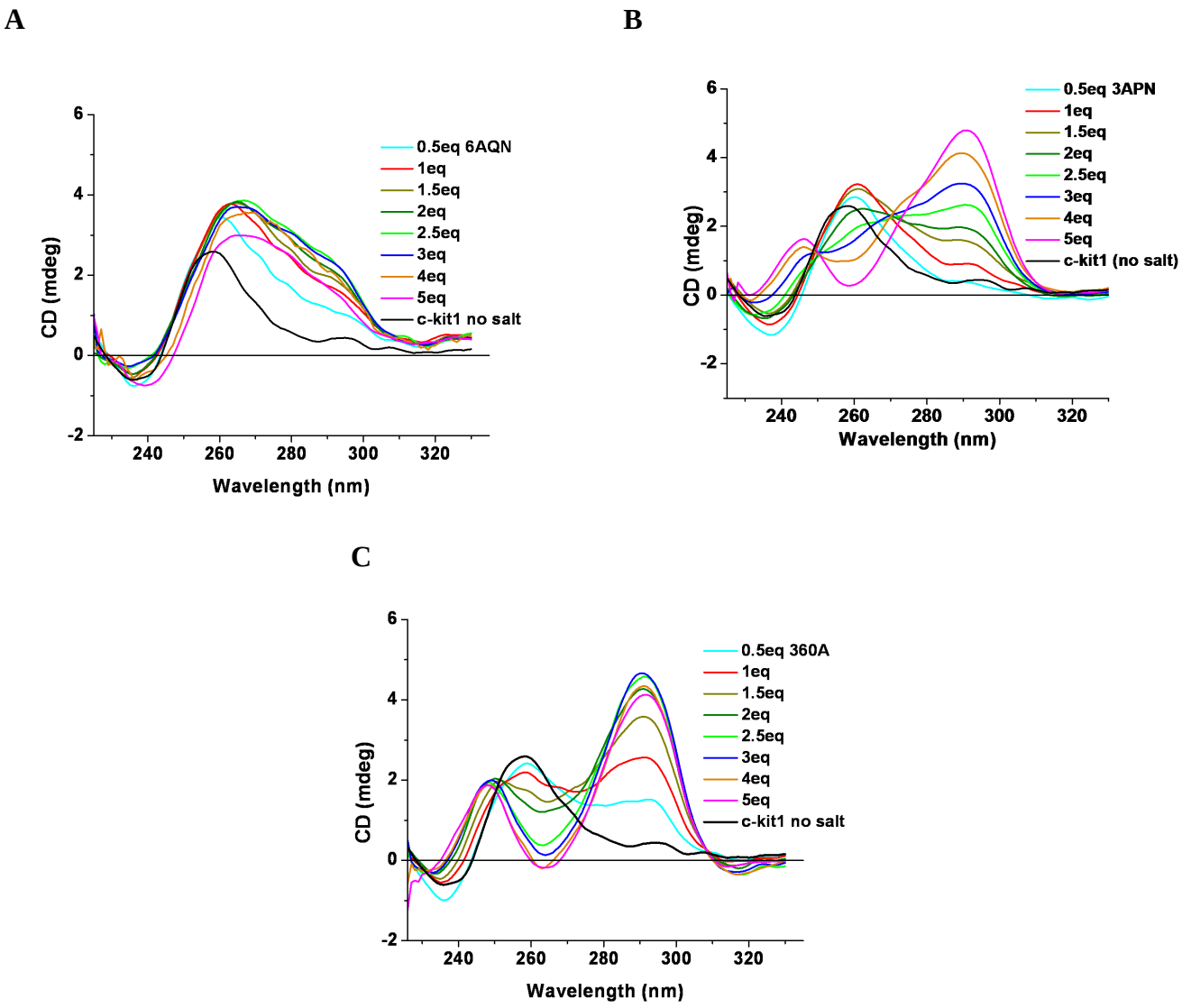

Figure S4. CD titration spectra of *c-kit1* DNA (12.5 µM in 50 mM Tris, pH 7.2) with (A) **6AQN**, (B) **3APN** and (C) **360A** in absence of monovalent cations.

CD titration spectra of *c-kit1* DNA with ligands in the presence of K^+ ions

A

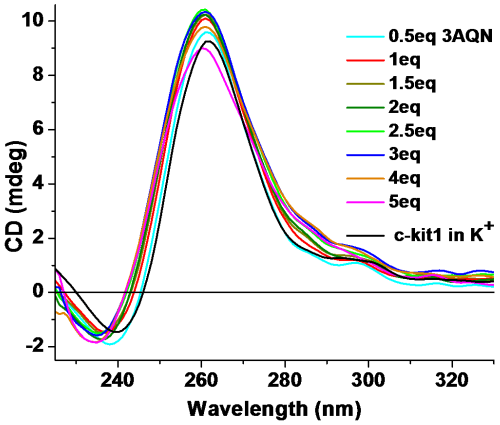

B

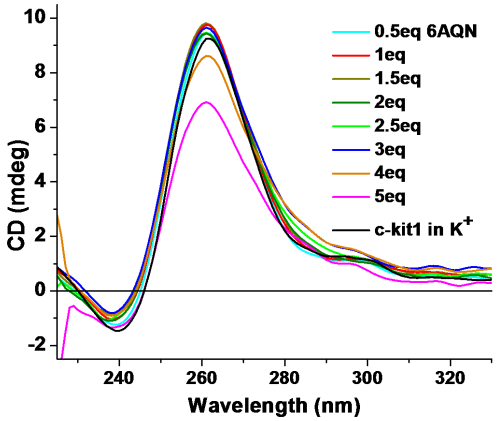

C

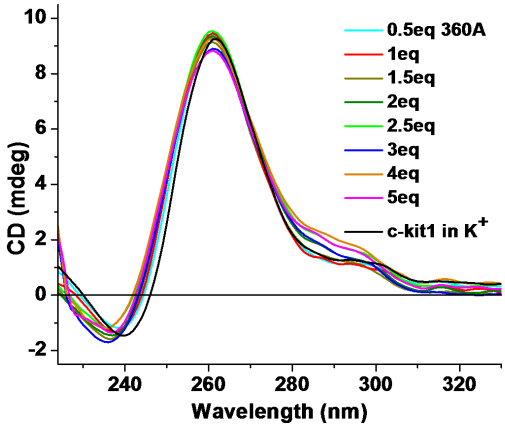

Figure S5. CD titration spectra of *c-kit1* DNA (12.5 µM in 50 mM Tris, pH 7.2, 100 mM KCl) with (A) **3AQN**, (B) **6AQN** and (C) **360A**.

CD titration spectra of *c-kit2* DNA with ligands

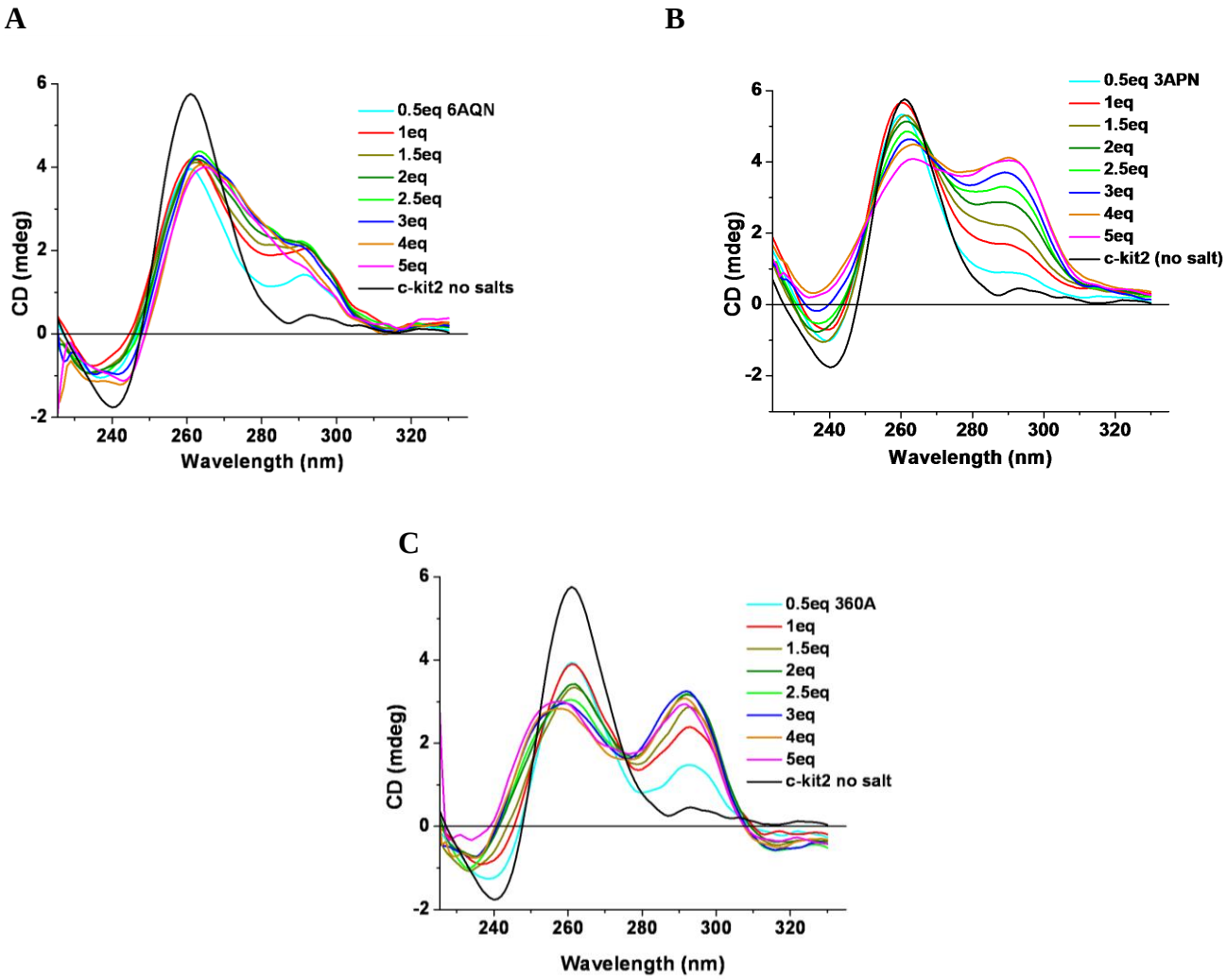

Figure S6. CD titration spectra of *c-kit2* DNA (12.5 µM in 50 mM Tris, pH 7.2) with (A) **6AQN**, (B) **3APN** and (C) **360A** in absence of monovalent cations.

CD titration spectra of *c-kit2* DNA with ligands in the presence of K^+ ions

A

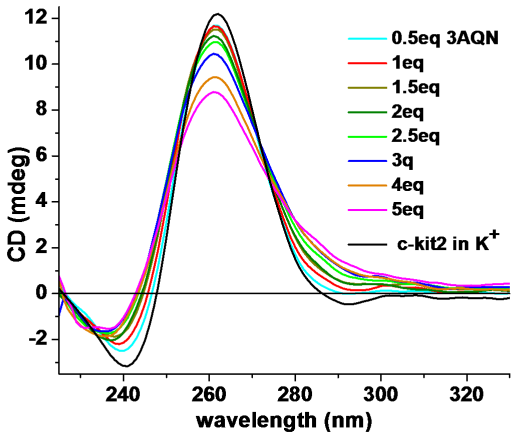

B

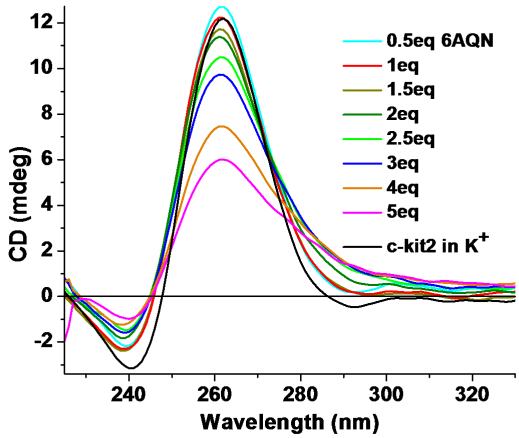

C

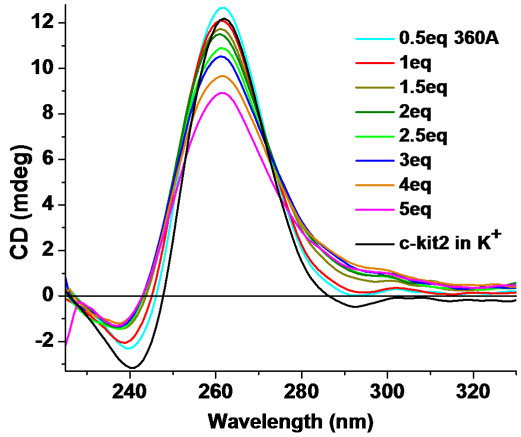

Figure S7. CD titration spectra of *c-kit2* DNA (12.5 µM in 50 mM Tris, pH 7.2, 100 mM KCl) with **(**A) **3AQN**, (B) **6AQN** and (C) **360A**.

CD titration spectra of *c-myc* DNA with ligands

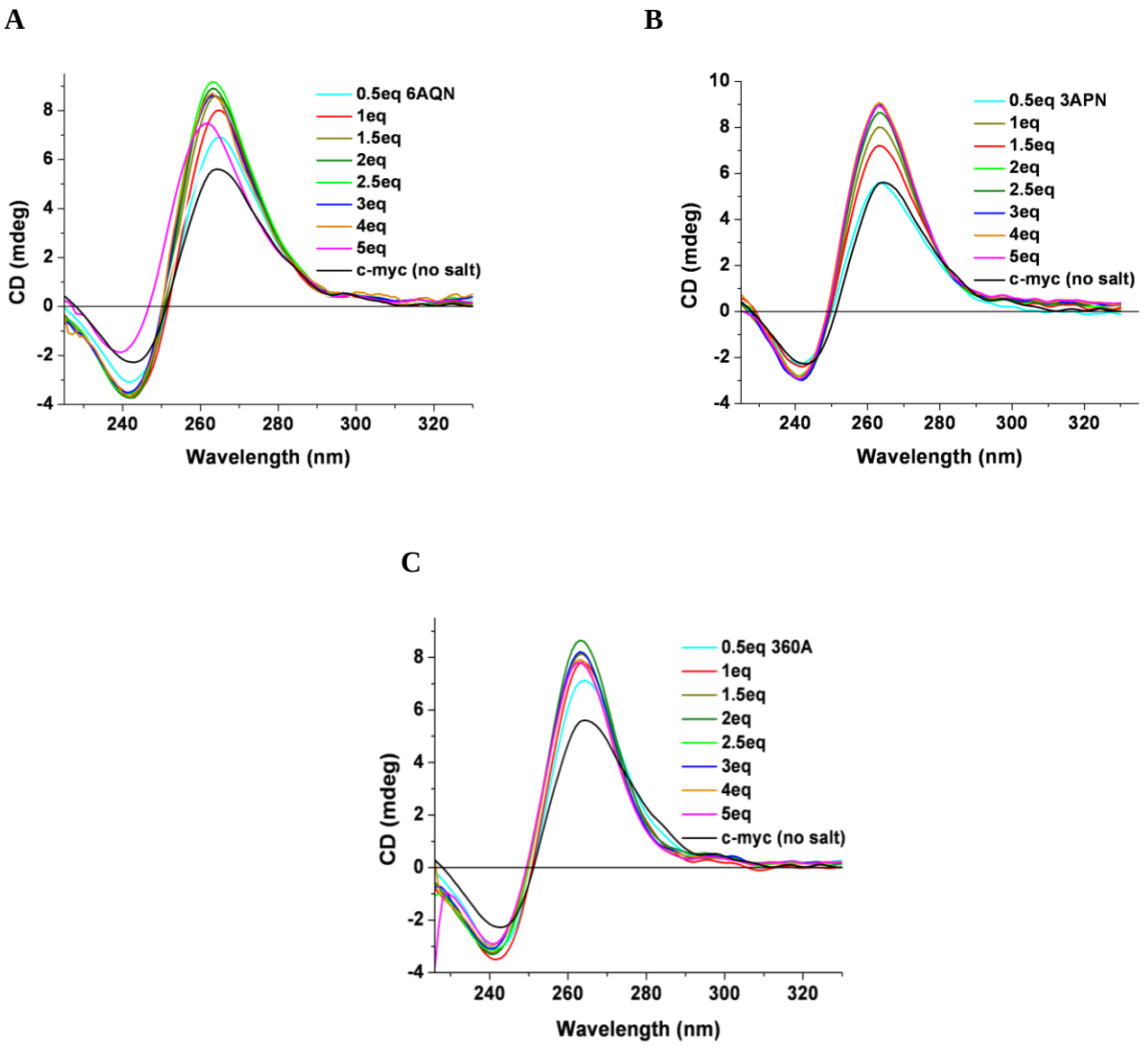

Figure S8. CD titration spectra of *c-myc* DNA (12.5 µM in 50 mM Tris, pH 7.2) with (A) **6AQN**, (B) **3APN** and (C) **360A** in absence of monovalent cations.

CD titration spectra of *c-myc* DNA with ligands in the presence of K^+ ions

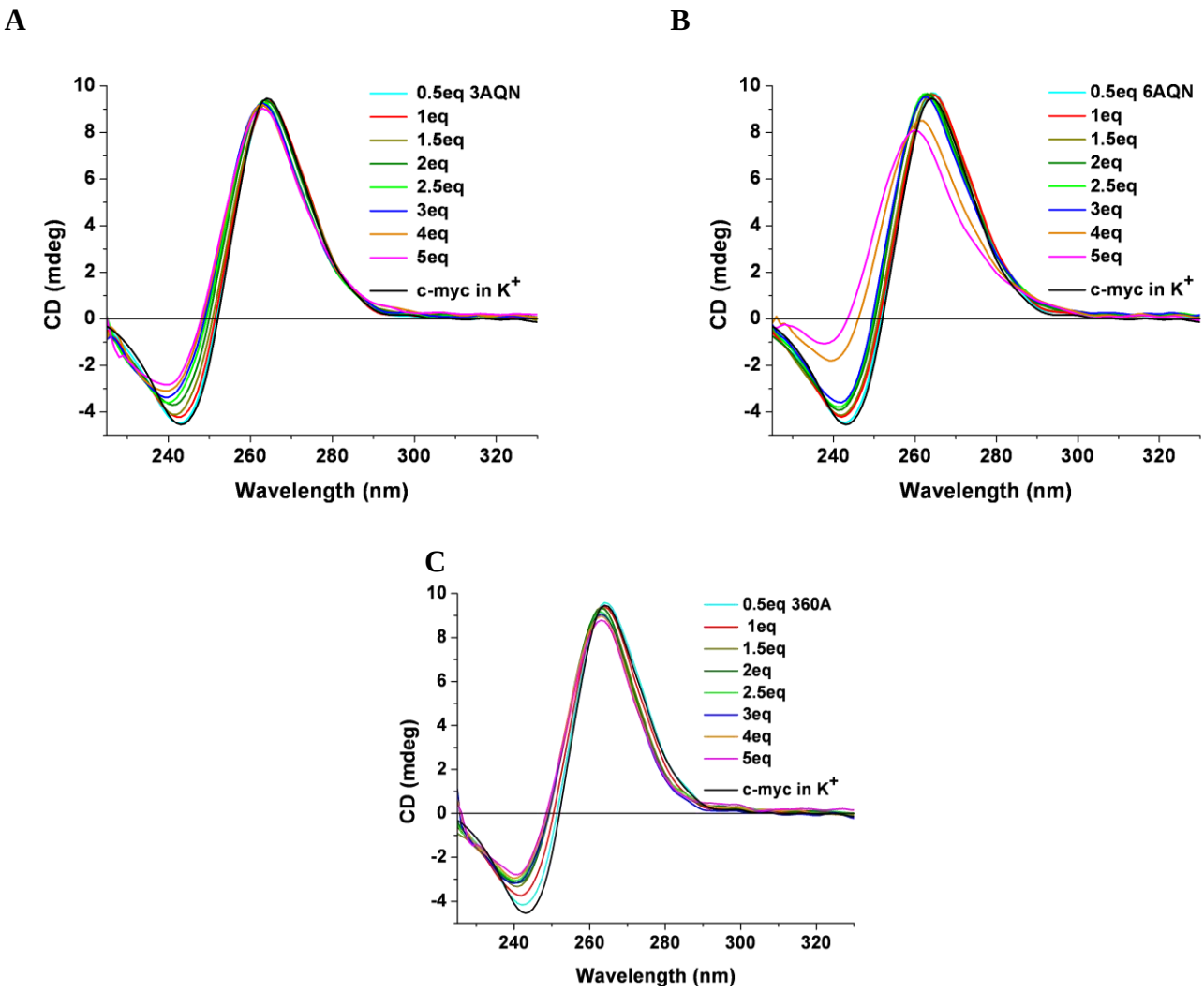

Figure S9. CD titration spectra of *c-myc* DNA (12.5 µM in 100 mM KCl and 50 mM Tris, pH 7.2) with (A) **3AQN**, (B) **6AQN** and (C) ligand **360A**.

CD melting curves of duplex and promoter quadruplex DNAs

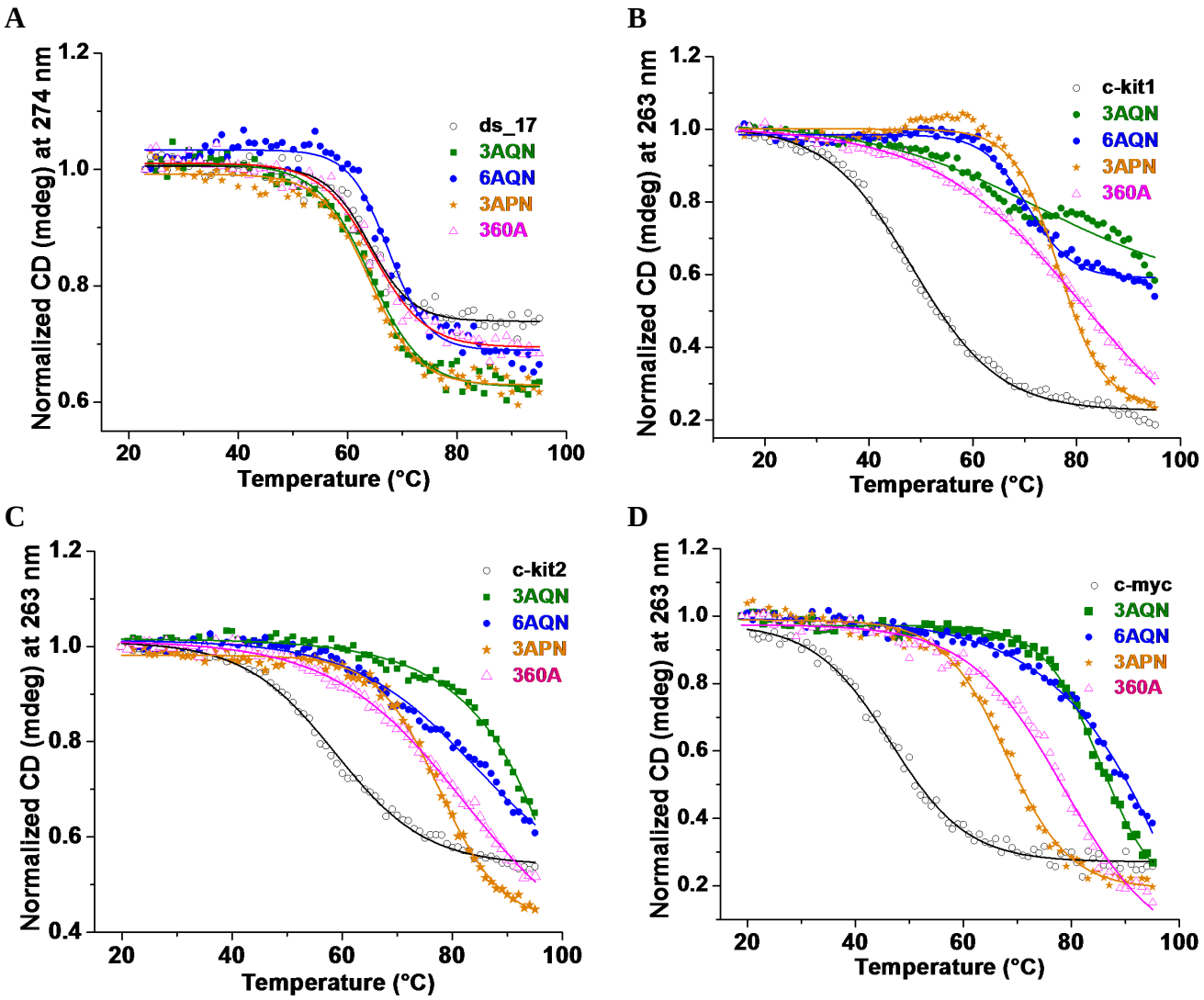

Figure S10. CD Melting curves of duplex and promoter quadruplex DNAs in the absence and in the presence of ligands. (A) Duplex DNA (15μM in 10 mM sodium cacodylate buffer pH 7.2 and 100 mM NaCl) and with 3 molar equivalent of ligands ; (B) *c-kit1* DNA (15 μM in 10 mM sodium cacodylate buffer pH 7.2, 20 mM KCl and 80 mM LiCl) and with 3 molar equivalent of ligands; (C) *c-kit2* DNA (10 μM in 10 mM sodium cacodylate buffer pH 7.2, 5 mM KCl and 95 mM LiCl) and with 3 molar equivalent of ligands; (D) *c-myc* DNA (5 μM in 10 mM sodium cacodylate buffer pH 7.2 and 100 mM LiCl) with 3 molar equivalent of ligands.

Plot of Taq polymerase stop products versus ligand concentration

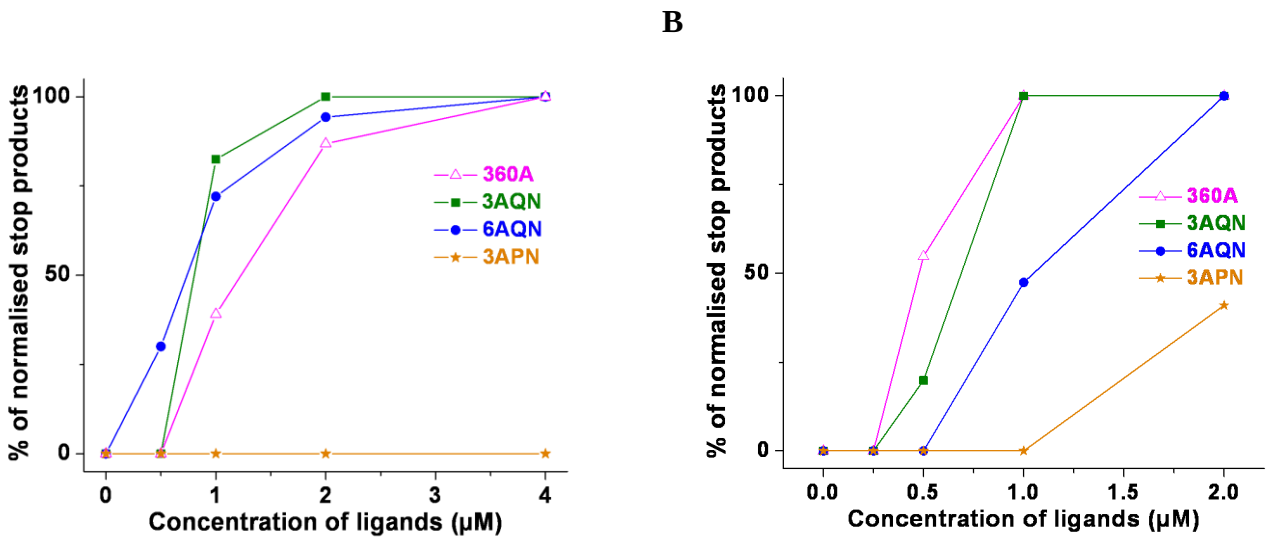

Figure S11. Normalized percentage of Taq polymerase stop products in each lane was plotted against concentration of ligand used. (A) Template containing telomeric DNA sequence; B) Template containing *c-myc* DNA sequence.

Energy optimized geometry and calculated charges for 3AQN

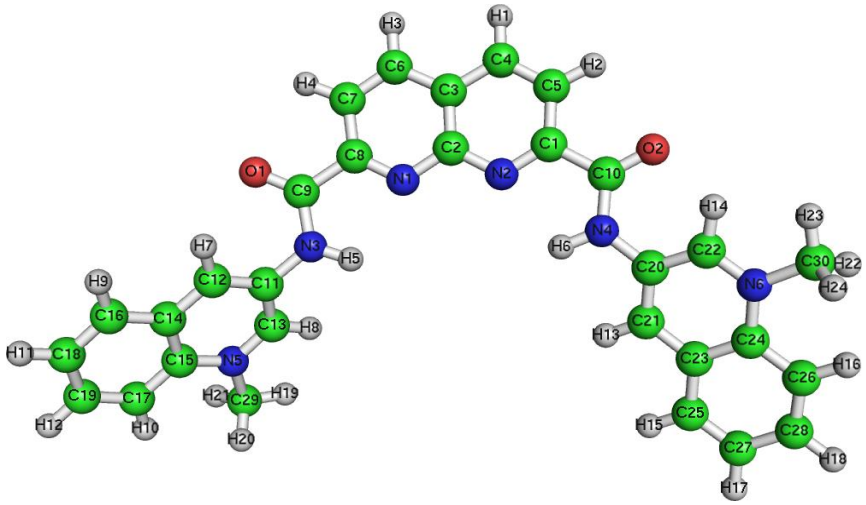

A.No	Charge	A.No	Charge	A.No	Charge	A.No	Charge
C1	0.257040	H9	0.174146	H14	0.184755	N4	-0.501953
C2	0.908469	C19	-0.020023	C24	0.232435	H13	0.220641
C3	-0.236971	H10	0.190976	C25	-0.161870	H5	0.295204
C4	-0.003096	H11	0.176823	C26	-0.293114	C23	0.044075
C5	-0.285842	H12	0.172034	C27	-0.121252	H24	0.148124
C6	-0.003096	H6	0.295204	H15	0.174146	N3	-0.501953
H1	0.173179	C11	0.156109	C28	-0.020023	C22	0.019187
H2	0.179497	C12	-0.141842	H17	0.176823	H23	0.148124
C7	-0.285842	C13	0.019187	H18	0.172034	O2	-0.519341
C8	0.257040	C14	0.044075	N5	0.010766	C21	-0.141842
H3	0.173179	H7	0.220641	H16	0.190976	H22	0.148124
H4	0.179497	H8	0.184755	N6	0.010766	O1	-0.519341
N1	-0.659942	C15	0.232435	C29	-0.231717	C20	0.156109
N2	-0.659942	C16	-0.161870	H19	0.148124	C30	-0.231717
C9	0.673005	C17	-0.293114	H20	0.148124	H21	0.148124
C10	0.673005	C18	-0.121252	H22	0.139117	H23	0.139117
H24	0.139117						

Figure S12. Energy optimized geometry and calculated charges for **3AQN** using HF/6-31G* basis set in Gaussian03.

Energy optimized geometry and calculated charges for 6AQN

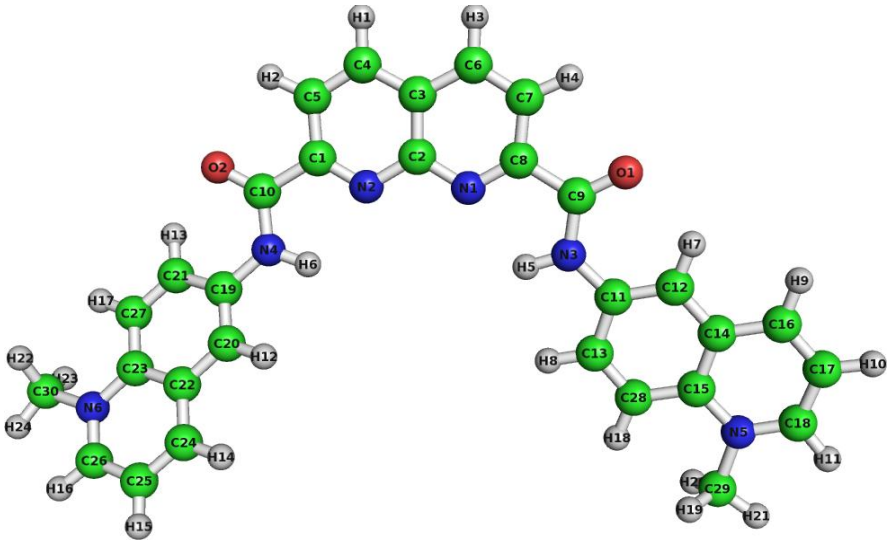

A.No	Charge	A.No	Charge	A.No	Charge	A.No	Charge
C1	0.484425	C2	1.003928	C3	-0.391687	C4	0.127820
C5	-0.524733	C6	0.127820	H1	0.146874	H2	0.231595
C7	-0.524733	C8	0.484425	H3	0.146874	H4	0.231595
N1	-0.725639	N2	-0.725639	C9	0.709603	C10	0.709603
O1	-0.516688	O2	-0.516688	N3	-0.819909	H5	0.437093
N4	-0.819909	H6	0.437093	C11	0.430028	C12	-0.411161
C13	-0.098115	C14	0.073250	H7	0.217725	H8	0.174863
C15	0.316058	C16	0.070960	C17	-0.344687	H9	0.187675
C18	0.197831	H10	0.220299	H11	0.194524	C19	0.430028
C20	-0.411161	C21	-0.098115	C22	0.073250	H12	0.217725
H13	0.174863	C23	0.316058	C24	0.070960	C25	-0.344687
H14	0.187675	C26	0.197831	H15	0.220299	H16	0.194524
N5	-0.159578	N6	-0.159578	C27	-0.451122	H17	0.288882
C28	-0.451122	H18	0.288882	C29	-0.206962	H19	0.147656
H20	0.147656	H21	0.147656	C30	-0.206962	H22	0.147656
H23	0.147656	H24	0.147656				

Figure S13. Energy optimized geometry and calculated charges for **6AQN** using HF/6-31G* basis set in Gaussian03.

Energy optimized geometry and calculated charges for 3APN

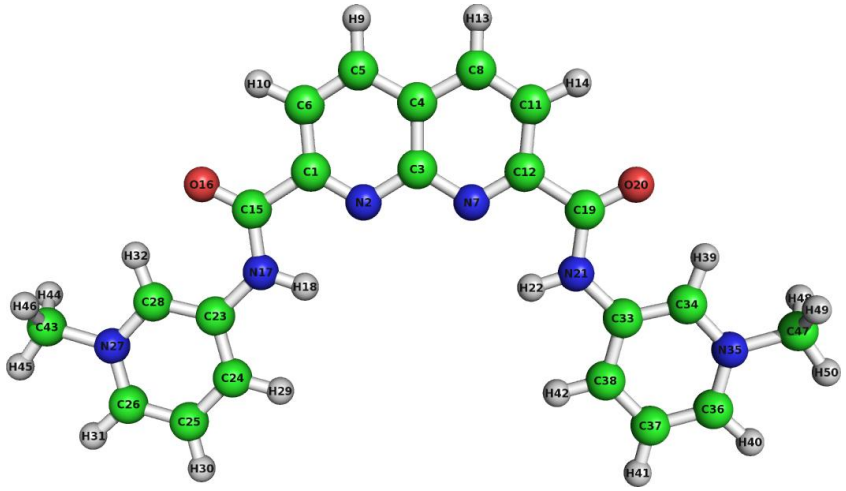

A.No	Charge	A.No	Charge	A.No	Charge	A.No	Charge
C1	0.222044	N2	-0.670319	C3	0.555923	C4	-0.067298
C5	-0.121991	C6	-0.217408	N7	-0.670320	C8	-0.121991
H9	0.271523	H10	0.290563	C11	-0.217409	C12	0.222044
H13	0.271523	H14	0.290563	C15	0.824892	O16	-0.587199
N17	-0.954604	H18	0.451686	C19	0.824890	O20	-0.587193
N21	-0.954607	H22	0.451687	C23	0.310227	C24	-0.134705
C25	-0.270417	C26	0.149384	N27	-0.587681	C28	0.144947
H29	0.272001	H30	0.291655	H9	0.301014	H10	0.353920
C16	0.310232	C17	0.144948	N18	-0.587680	C19	0.149385
C20	-0.270416	C21	-0.134708	H22	0.353913	H23	0.301014
H24	0.291655	H25	0.272001	C26	-0.333612	H27	0.254404
H28	0.240938	H29	0.254427	C30	-0.333613	H31	0.254422
H32	0.254411	H33	0.24093				

Figure S14. Energy optimized geometry and calculated charges for **3APN** using HF/6-31G* basis set in Gaussian03.

Energy optimized geometry and calculated charges for 360A

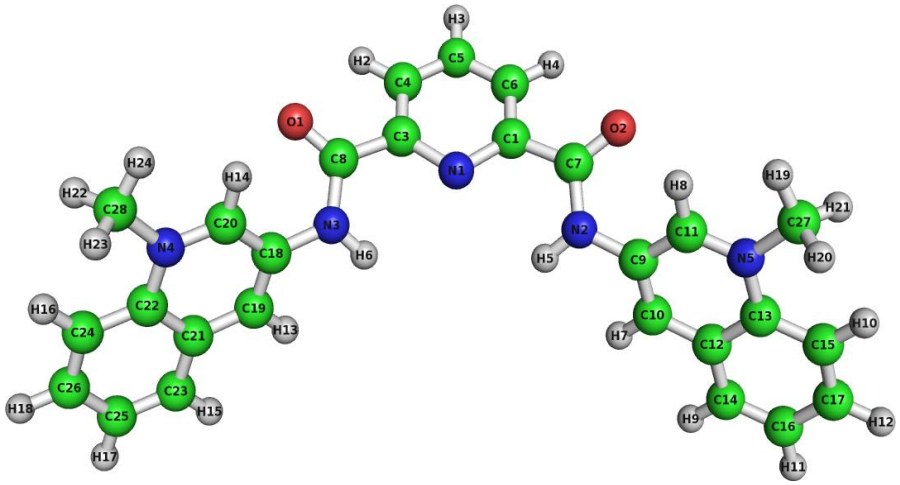

A.No	Charge	A.No	Charge	A.No	Charge	A.No	Charge
C1	0.193983	N1	-0.520210	N2	-0.866299	O1	-0.533398
N3	-0.865756	O2	-0.520101	C2	0.192954	N4	-0.717096
C3	-0.236013	N5	-0.724525	C4	-0.117653	C5	-0.235160
C6	0.717537	C7	0.716907	C8	0.168652	C9	-0.014584
C10	0.211356	C11	-0.085548	C12	0.420757	C13	-0.173260
C14	-0.236270	C15	-0.198385	C16	-0.168244	C17	0.160757
C18	-0.044089	C19	0.245058	C20	-0.079393	C21	0.407442
C22	-0.176293	C23	-0.223041	C24	-0.197634	C25	-0.169405
C26	-0.324228	C27	-0.334884	H1	0.406927	H2	0.414423
H3	0.237503	H4	0.260786	H5	0.235904	H6	0.297279
H7	0.286356	H8	0.264264	H9	0.268806	H10	0.268707
H11	0.272288	H12	0.288067	H13	0.302604	H14	0.259998
H15	0.263582	H16	0.267814	H17	0.271296	H18	0.238160
H19	0.245961	H20	0.241683	H21	0.238816	H22	0.250320
H23	0.244520	H23	0.242110				

Figure S15. Energy optimized geometry and calculated charges for **360A**using HF/6-31G* basis set in Gaussian03.

MD snapshot of 360A with quadruplex DNA

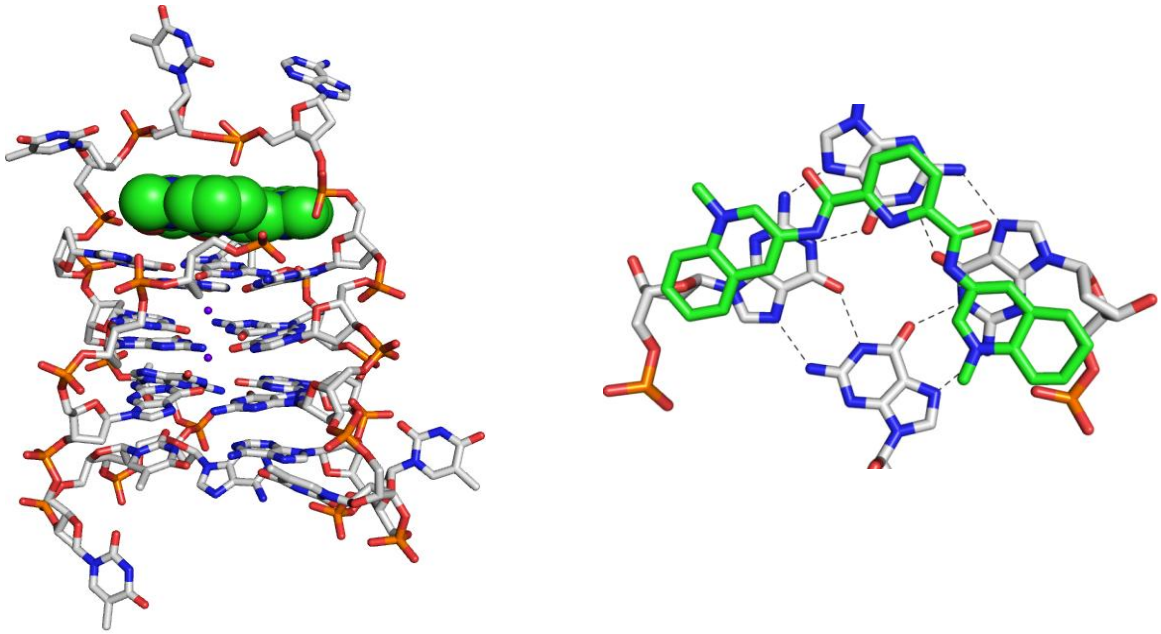

Figure S16. Final MD snapshots of the ligand-quadruplex complexes taken after 20 ns simulations. Side view of the ligand-quadruplex complex (left side), ligand (sphere) and quadruplex DNA (stick), colored by atom type, K^+ ion in the middle as purple spheres. Top view (right side) shows only ligand and top quartet represented in stick format. Hydrogen bonds within the quartets are shown in black dotted lines. **360A** and quadruplex DNA shows that there are no loop interactions with the ligand side chains. Top quartet and ligand interaction shows the partial stacking of the side chains with the quartet.

MD snapshot of 3APN with quadruplex DNA

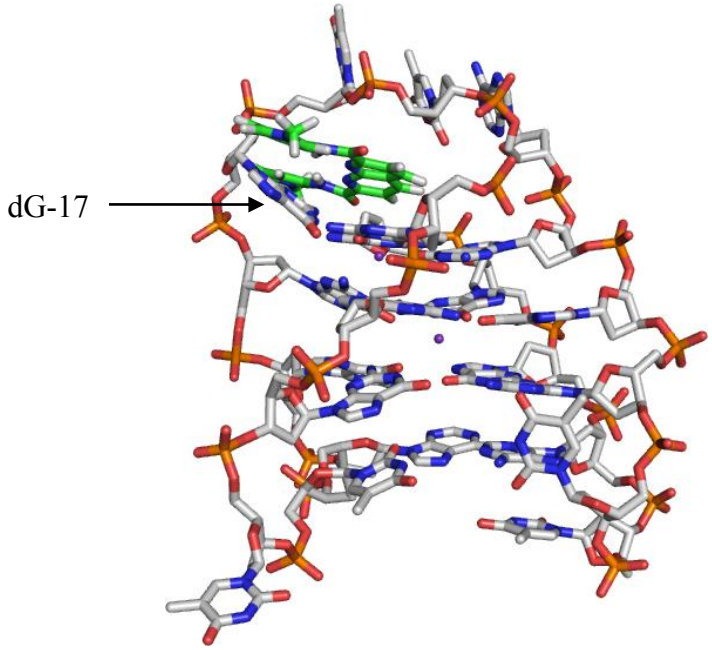

Figure S17. MD snapshot (3ns) of quadruplex DNA and **3APN** ligand. This figure shows that the top quartet is disturbed by the ligand with the movement of dG-17 (highlighted by an arrow). The K^+ ion present in between the first and second quartet cavity is not precisely coordinated.

Time dependence RMSD graphs of quadruplex DNA and ligands

A

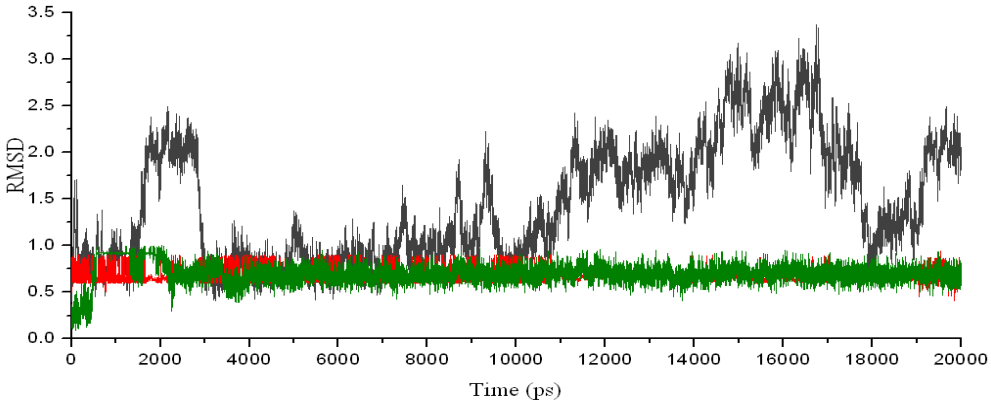

B

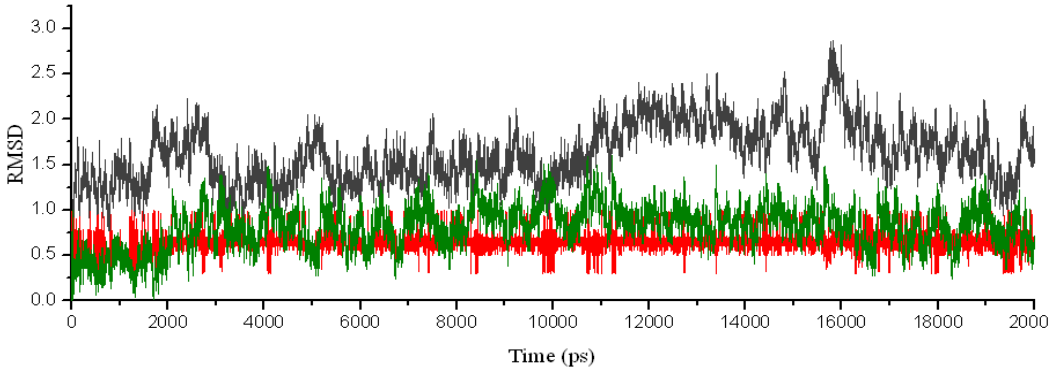

C

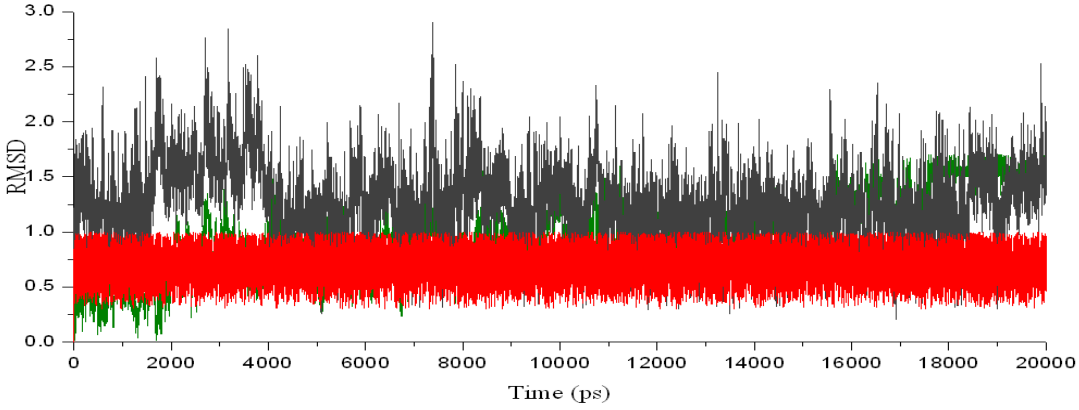

Figure S18. Time dependence of the RMSDs (Å) of G-quartet heavy atoms (green), ligand heavy atom (red) and quadruplex DNA backbone atoms (gray). (A) **3AQN** complex; (B) **6AQN** complex; and (C) **360A** complex.

Averaged structure from MD simulation superimposed with initial equilibrated structure

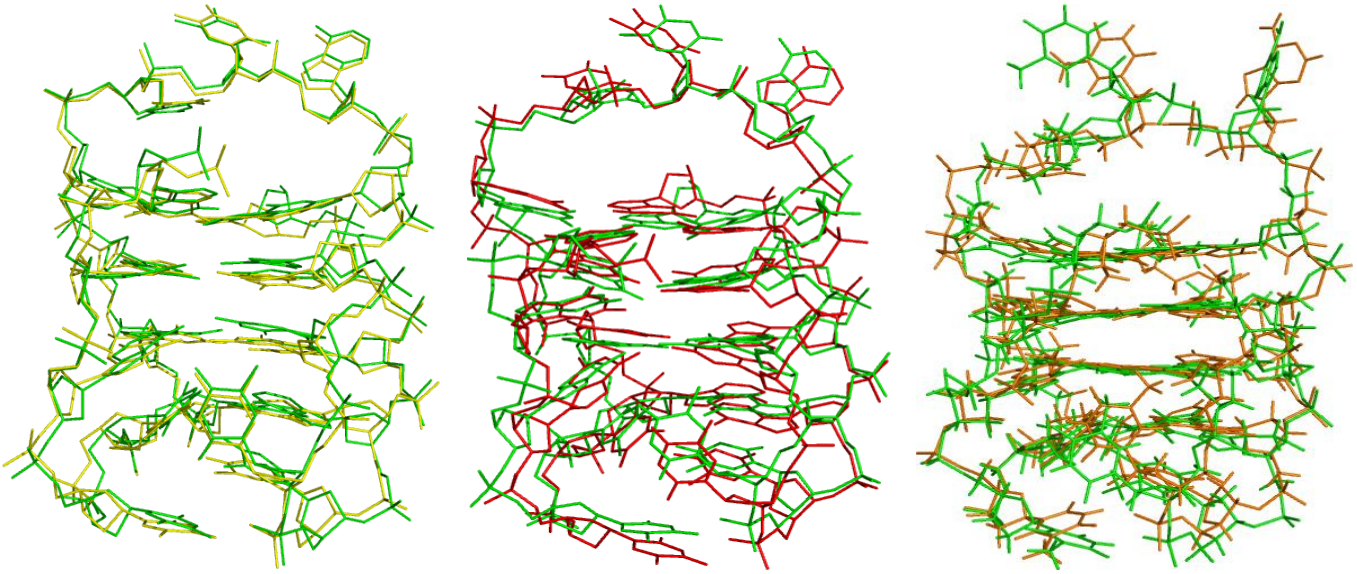

Figure S19. Averaged structure from final 10ns MD trajectories superimposed with their corresponding initial or equilibrated structure. Ligands are not shown. Green–initial equilibrated structure before MD simulations; Yellow–**3AQN** complex; Red–**6AQN** complex; Orange–**360A** complex.

Behavior of ions in G-quadruplex and ligand dynamics

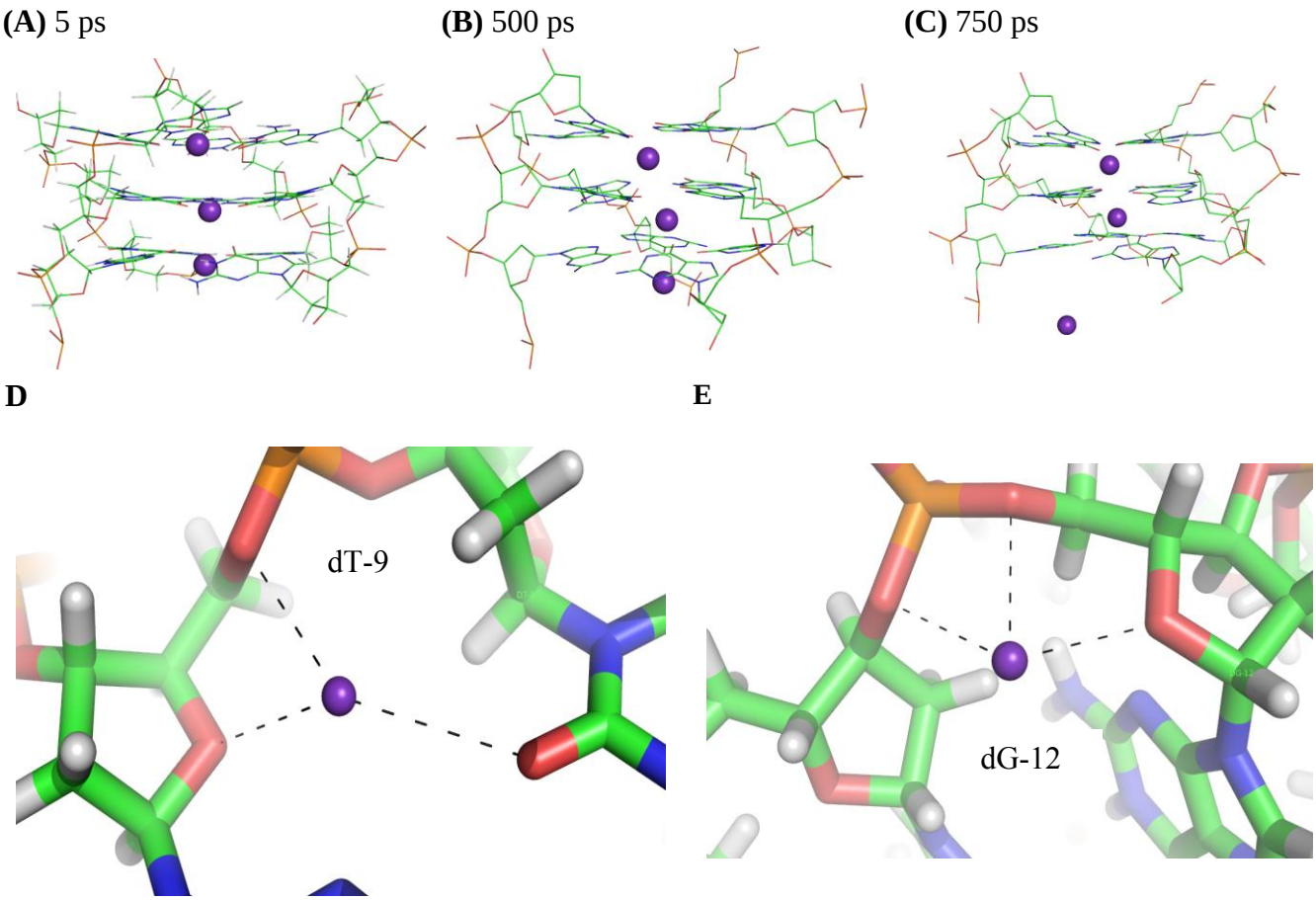

Figure S20. The role of metal ion in the stabilization of quadruplex DNA revealed from MD simulations. (A) In the beginning of the MD simulations three K^+ ions were added to the each plane of the G-quartet; (B) At 50 ps the position of the third ion in the last quartet and (C) After 750 ps the third K^+ ion which is far away from the ligand left the G-plane to the solvent. The path of the movement of K^+ ion is shown. The other two ions moved to the midway of G-quartet and stayed stable. Similar ion movement was also observed by N. Spackova et al. in a simulation of G-quadruplex DNA with sodium ions.[1] Ions present in the solvent interact with DNA other than in quartet cavities. dG-12 (D) and dT-8 (E) bases have strong interaction with K^+ ions.

3AQN and quadruplex DNA interaction

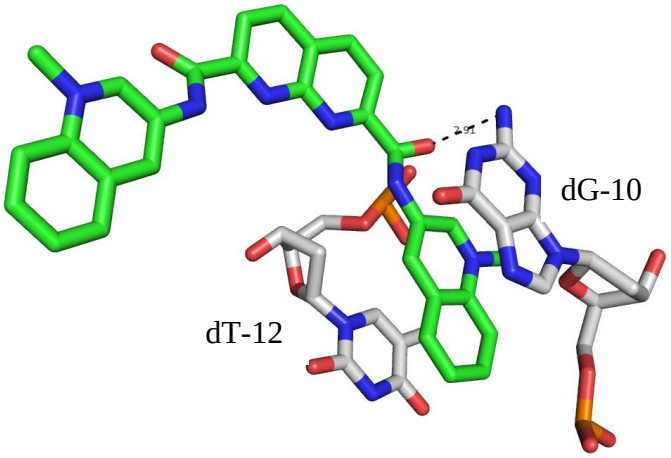

Figure S21. Strong π - π interaction between the **3AQN** and thymine base at the center of G-quadruplex (dT-12) in the diagonal loop, and the top quartet in the anti-parallel quadruplex DNA. Hydrogen bonding between carbonyl oxygen atom of the **3AQN** and the hydrogen atom (NH_2) of the dG-10 in the top quartet is also shown in dotted lines. Average distance between the two atoms (NH_2 and carbonyl oxygen atom) is 2.7 Å.

Final MD snapshot of duplex DNA and ligands

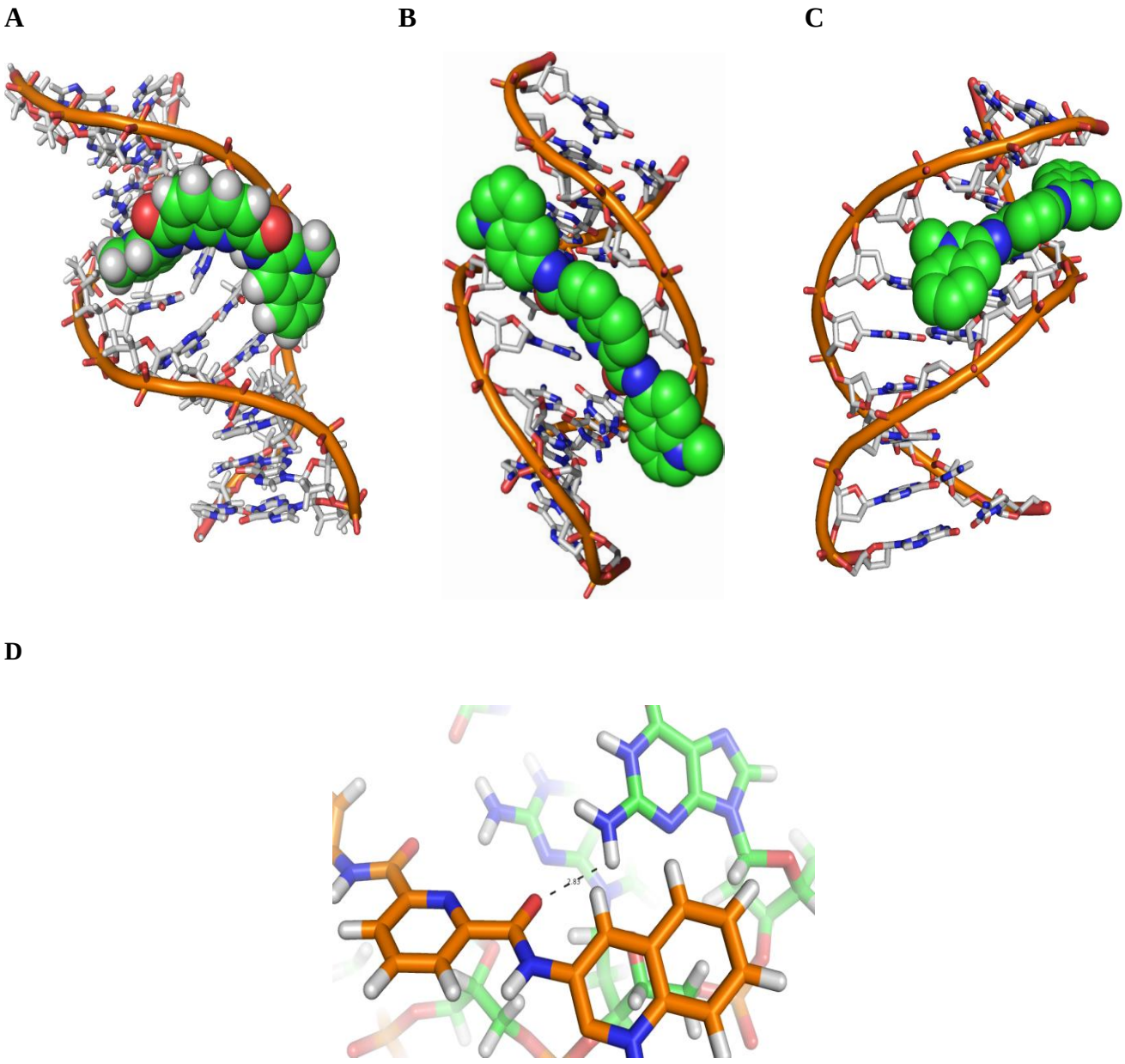

Figure S22. Final MD snapshot (20ns) of dsDNA and ligands. (A) **3AQN** and ds DNA complex; (B) **360A** and ds DNA complex; (C) **6AQN** and ds DNA complex. (D) A stable hydrogen bond between **360A** carbonyl oxygen atom and hydrogen atom (NH_2) of dG-13 of ds DNA. The distance between the two atoms is 2.03 Å

Time dependence RMSD graph of ds DNA and ligand complexes

A

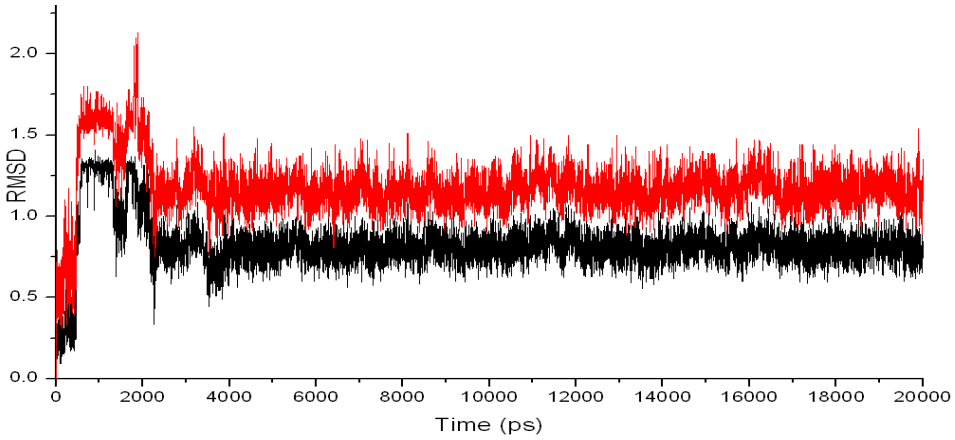

B

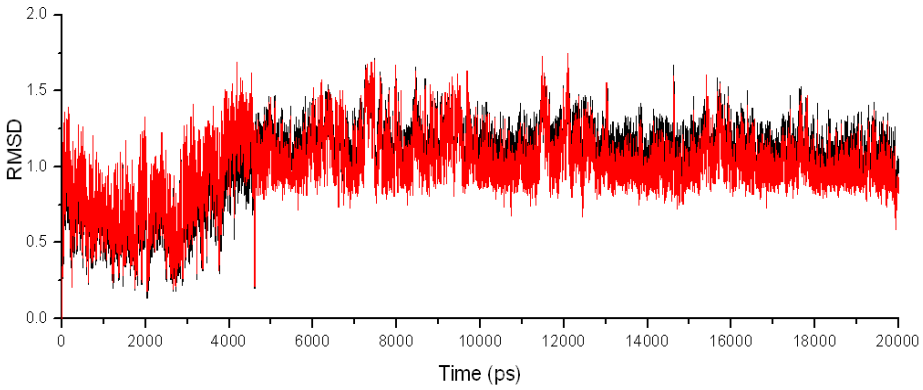

C

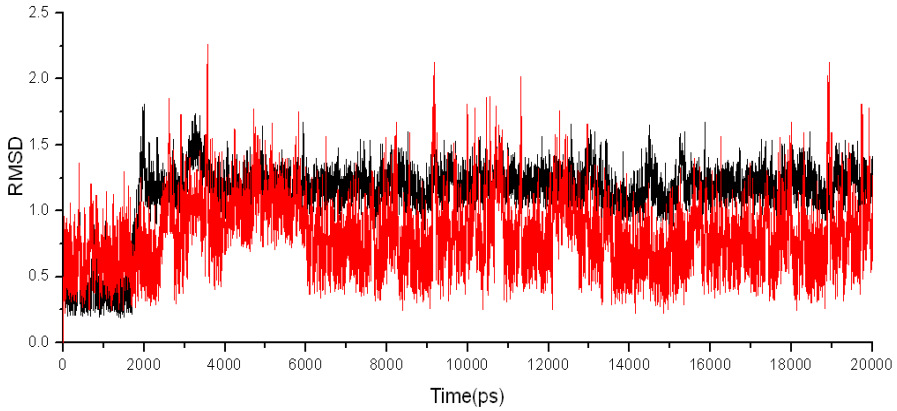

Figure S23. Time dependence of the RMSD of ds DNA heavy atoms (black), ligand heavy atoms (red). (A) **3AQN** complex; (B) **6AQN** complex and (C) **360A** complex.

Binding free energy components of G-quadruplex DNA and ligands

Average of 3 MD Simulations (20ns)	Anti-parallel human telomeric G-quadruplex DNA PDB Entry:*143D*		
	3AQN	**6AQN**	**360A**
ΔE_{elec}	−4093.81 ± 12.16	−3989.23 ± 10.54	−3903.89 ± 12.16
ΔE_{VDW}	−156.603 ± 4.55	−149.33 ± 6.17	−130.81 ± 6.33
$\Delta E_{mm}(\Delta E_{Elec}+\Delta E_{VDW})$	−4251.22 ± 15.5	−4138.56 ± 16.71	−4034.70 ± 18.49
ΔG_{np}	−17.04 ± 1.08	−15.56 ± 1.40	−11.86 ± 1.15
ΔG_{PB}	4116.49 ± 27.78	3996.78 ± 16.22	3920.18 ± 13.79
ΔGsolv ($\Delta G_{np}+\Delta G_{pb}$)	4100.61 ± 29.86	−4012.34 ± 17.61	3908.32 ± 14.94
ΔGtot ($\Delta E_{mm}+\Delta G_{sol}$)	−155.086 ± 8.57	−141.78 ± 6.49	−128.27 ± 6.01
-TΔS	−62.28 ± 8.71	−59.31 ± 1.96	−43.64 ± 1.24
ΔG_{bind} (ΔG_{tot}-TΔS)	**−89.29 ± 7.49**	**−80.42 ± 8.42**	**−84.81 ± 7.28**

Table S1. ΔEelec is the electrostatic interaction calculated by the MM force field. ΔEvdw is the Vander Waals contribution from MM. ΔEini is the internal energy which is zero for all the 3 ligands. ΔEmm is the total molecular-mechanical energy (ΔEele + ΔEvdw + ΔEini). ΔGnp is the nonpolar contribution to the solvation energy. ΔGPB is the electrostatic contribution to the solvation energy calculated by the PB approach. ΔGsolv is the total solvation energy (ΔGnp + ΔGPB). ΔGtot is the total energy without solute entropic contribution (ΔEmm + ΔGsolv). -TΔS is solute entropic contribution, where T = temperature and S = sum of translational, rotational, and vibrational entropies. ΔGbind is the total energy with solute entropic contribution (ΔGtot – TΔS).

$\Delta Gnp = \gamma\ SASA + b$

Where $\gamma = 0.0054$ kcal/(mol. Å) b=0.92 kcal/mol

Solute entropy contributions for the G-quadruplex and ligands binding were obtained by estimating the entropy for G-quadruplex DNA with ligand as a complex, then G-quadruplex DNA and ligand separately. The calculations used a subset of snapshots collected during the MD simulations, including the two explicitly bonded K^+ ions. The entropy calculations were based on normal modes and standard formulas at 300 K. The structures were first minimized in AMBER 10, using the generalized born model for solvation, followed by in vacuo minimization with a distance-dependent dielectric function. Up to 30,000 steps were performed, unless the RMS gradient dropped below 10^{-3}. The entropic estimates based on gas phase minimization of taken structures relatively represent the dynamic fluctuations. Here the values reported for MM/PBSA results are the average values of three MD simulations of the G-Quadruplex DNA and ligand complex, with different ligand conformations in each run obtained from docking results, at the same binding mode or position. All the values are reported in kcal/mol unit.

Average RMSD values of quadruplex DNA and ligands

Model	Heavy atoms of backbone	Heavy atoms of theG-quartet	Heavy atoms of the ligand
143D and **3AQN**	1.62	0.63	0.81
143D and **6AQN**	1.59	0.77	1.07
143D and **360A**	1.64	0.84	1.04

Table S2. Average RMSD values (Å) of the heavy atoms in the G-Quartet and the average mass-weighted RMSD values of the ligands of all atoms calculated from the MD simulations

Hoogsteen H-bond occupancy in G-Quartet DNA during molecular dynamics

	3AQN and **143D**	**6AQN** and **143D**	**360A** and **143D**
G-Quartet 1	99%	98.5%	98.5%
G-Quartet 2	97.7%	92%	92%
G-Quartet 3	95%	90%	90.8%

Table S3. The percentage occupancy of Hoogsteen hydrogen bonding between the guanine bases in each quartet over the course of 20ns simulation. These occupancies are calculated using ptraj module implemented in AMBER 10

Single point energy calculations

Atoms considered	Single point energy calculation using BH&H/6-311++ G (d,p)) (kcal/mol)			
	Initial structure	**3AQN bound**	**6AQN bound**	**360A bound**
Top pair without ions	−119.72	−124.86	−120.74	−120.59
Bottom pair without ions	−69.17	−72.51	−69.95	−70.21
Top pair with K^+ ion	−122.02	−149.509	−131.56	−139.785
Bottom pair with K^+ ion	−77.52	−78.93	−76.58	−77.67
Quartet with K^+ ion	−204.45	−217.112	−209.43	−210.69
Quartet without ions	−186.77	−202.19	−191.69	−195.33

Table S4. Single point energy of quadruplex DNA in the geometry of complex state with 3 ligands was tabulated. The quartet structure used is the one after 20ns of MD simulation. To understand the impact of ligand on quartet stabilization, the single point energy of quartet in the initial geometry from the minimized PDB structure is calculated and compared to the ligand stabilized G-quartets. During calculation the only guanine base contributing the quartet are considered.

Binding free energy component of ds DNA and ligands

Simulations (20ns)	Ds DNA (17 nt) with all the four ligands (kcal/mol)		
	3AQN	**6AQN**	**360A**
ΔE_{elec}	−989.5 ± 6.34	−997.4 ± 6.87	−1017.61 ± 6.84
ΔE_{VDW}	−45.7 ± 3.79	−47.96 ± 4.56	−46.97 ± 6.11
$\Delta E_{mm}(\Delta E_{Elec}+\Delta E_{VDW})$	−1035.2 ± 10.13	−1045.36 ± 10.43	−1064.58 ± 12.95
ΔG_{np}	−5.3 ± 0.57	−5.9 ± 0.65	−5.5 ± 0.55
ΔG_{PB}	1002.46 ± 11.61	1007.65 ± 10.97	1003.77 ± 10.59
ΔG_{solv} $(\Delta G_{np}+\Delta G_{pb})$	997.16 ± 12.18	1001.75 ± 11.52	1008.27 ± 11.04
ΔG_{tot} $(\Delta E_{mm}+\Delta G_{sol})$	−37.84 ± 2.05	−43.61 ± 1.91	−54.31 ± 1.99
-TΔS	−12.097 ± 0.3	−13.513 ± 1.5	−14.97 ± 0.22
ΔG_{bind} $(\Delta G_{tot}$-TΔS)	**−25.76 ± 2.3**	**−30.10 ± 3.4**	**−39.34 ± 2.12**

Table S5. The protocol used for the calculation of binding energy for ligands and duplex DNA is similar to what was employed for quadruplex DNA calculations. The double stranded nucleotide sequence used in this study is d[CCGTACCTTATAGCAGT/GGCATGGAATATCGTCA].

^{1}H NMR of compound 2

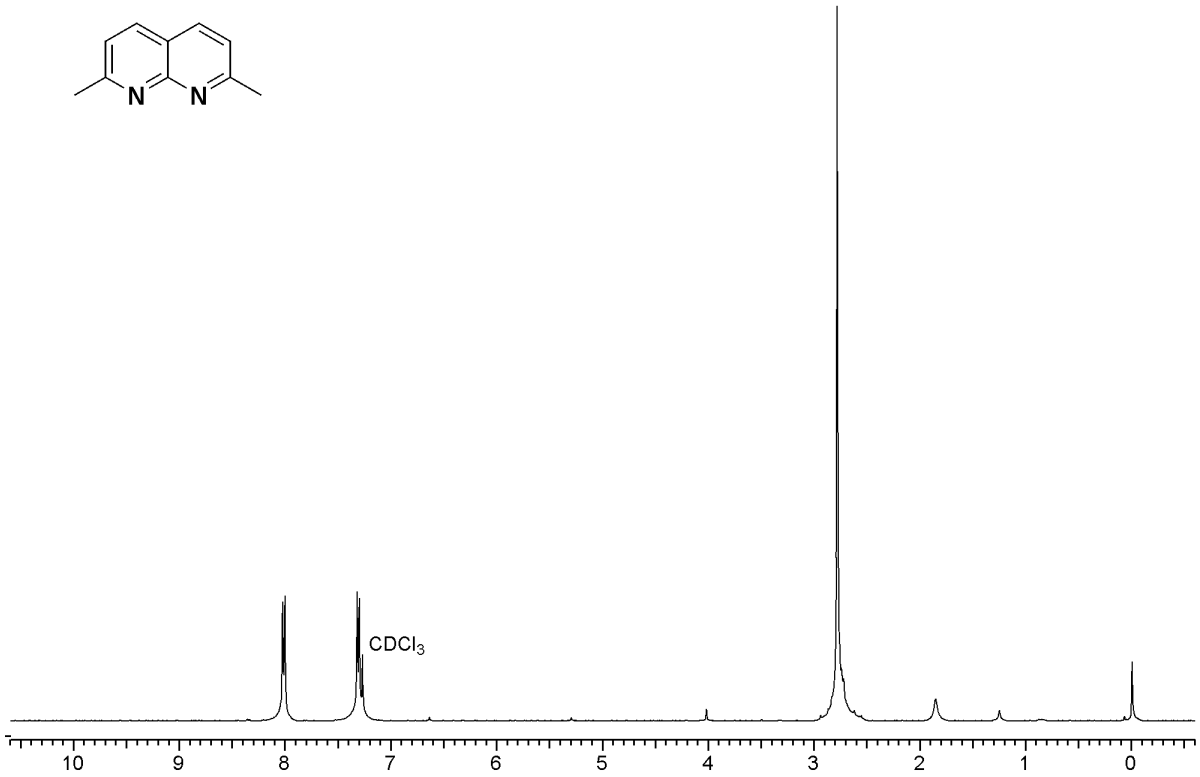

^{13}C NMR of compound 2

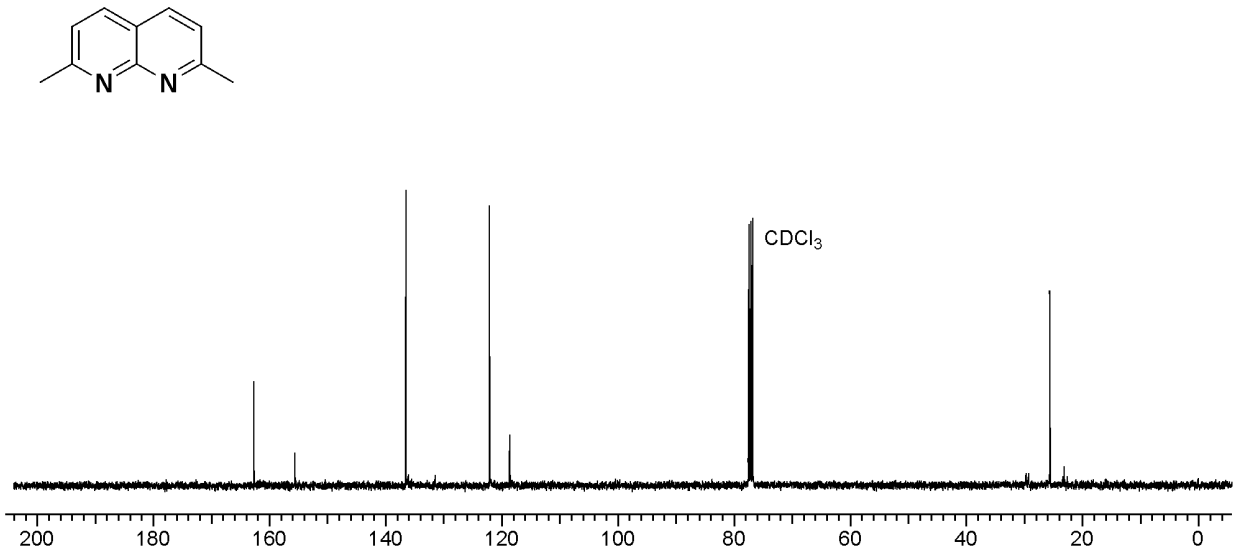

^{1}H NMR of compound 4a

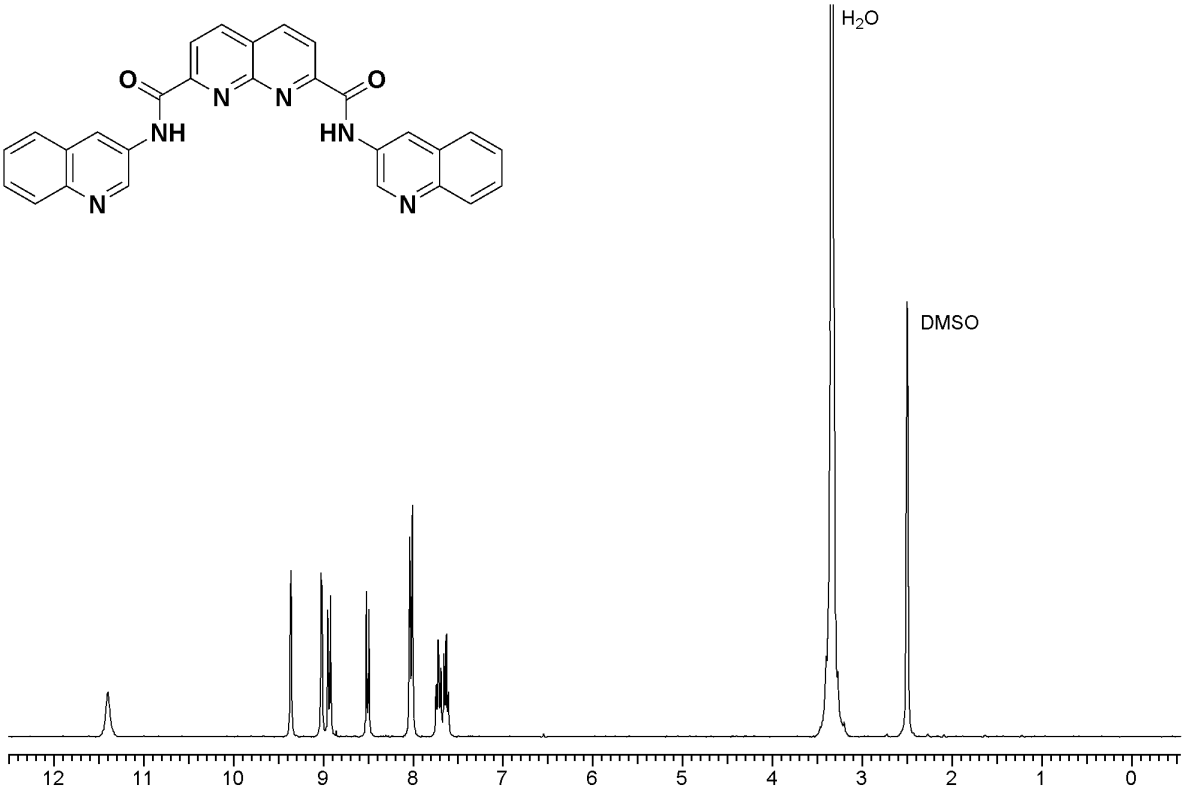

^{13}C NMR of compound 4a

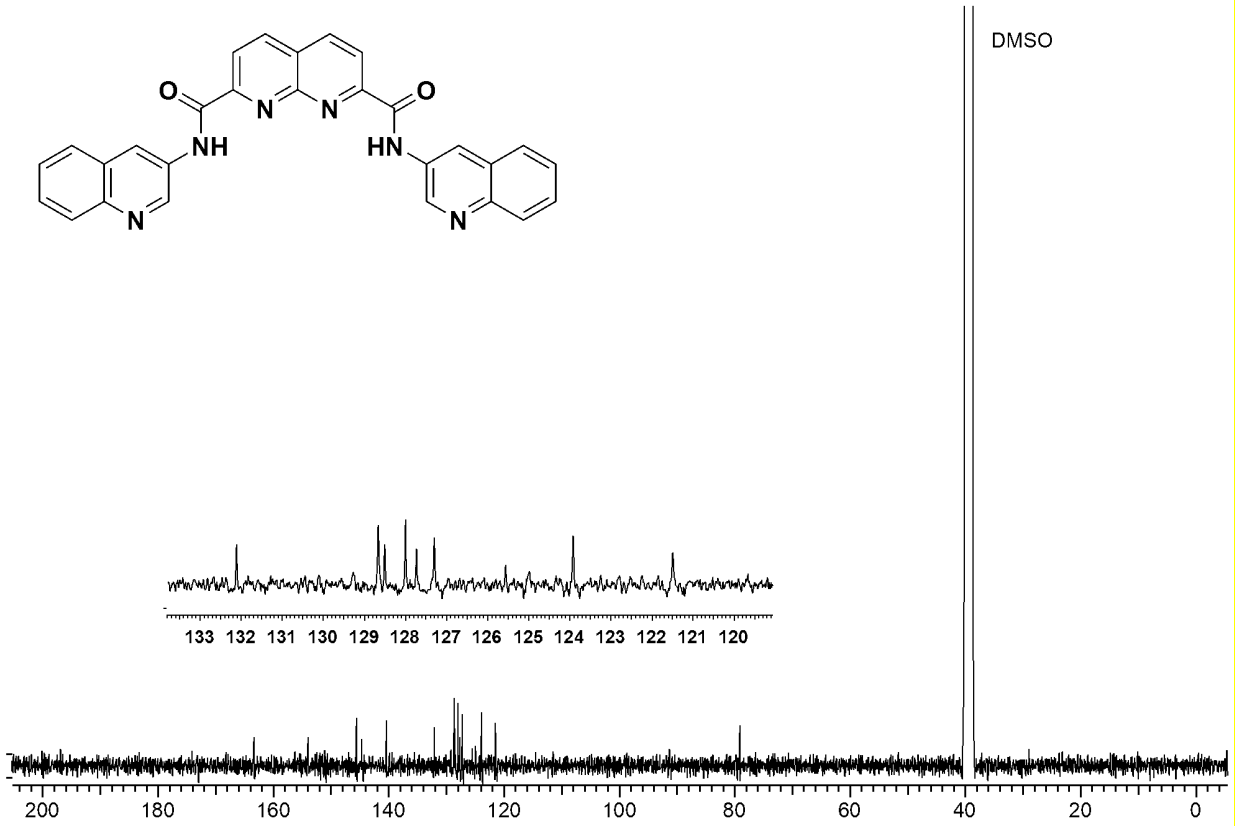

^{1}H NMR of compound 4b

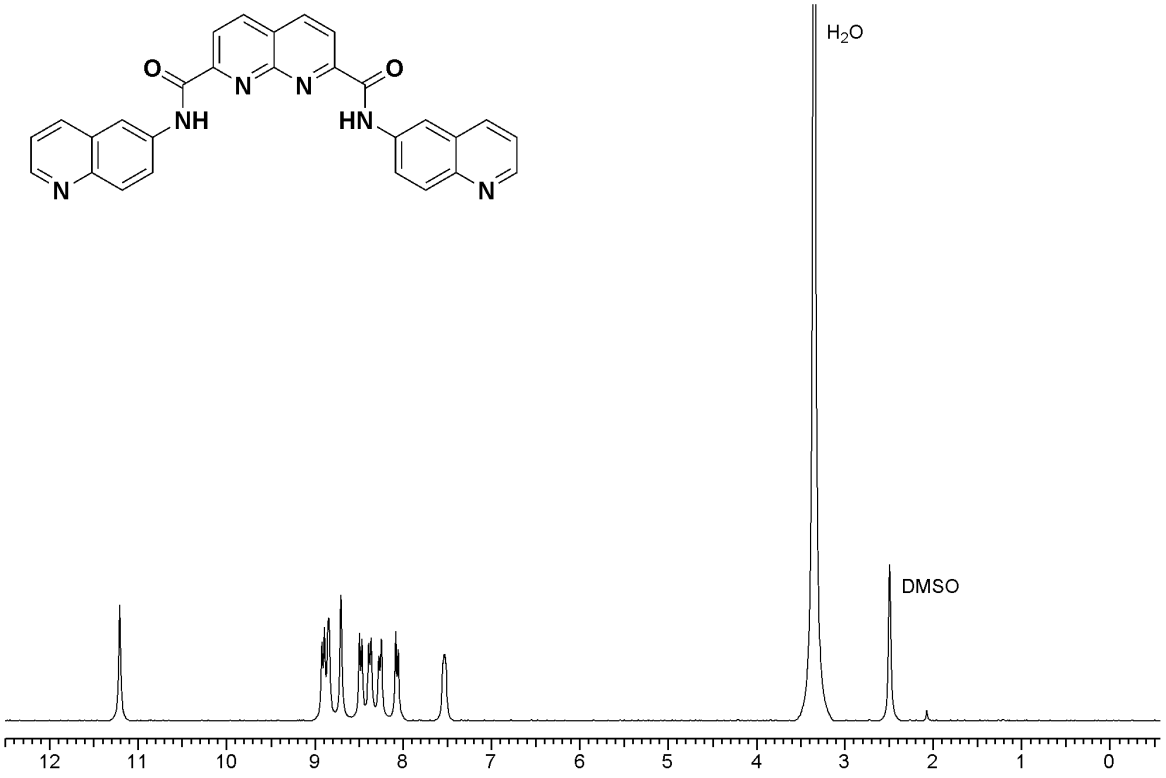

^{13}C NMR of compound 4b

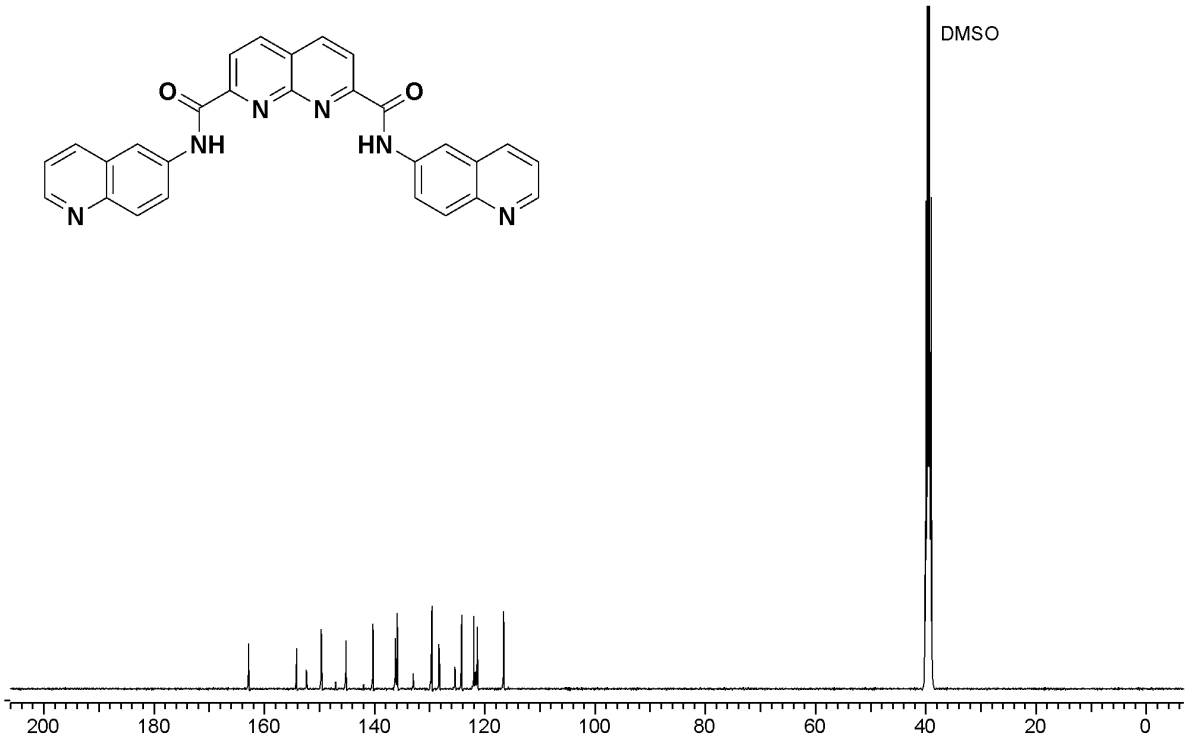

^{1}H NMR of compound 4c

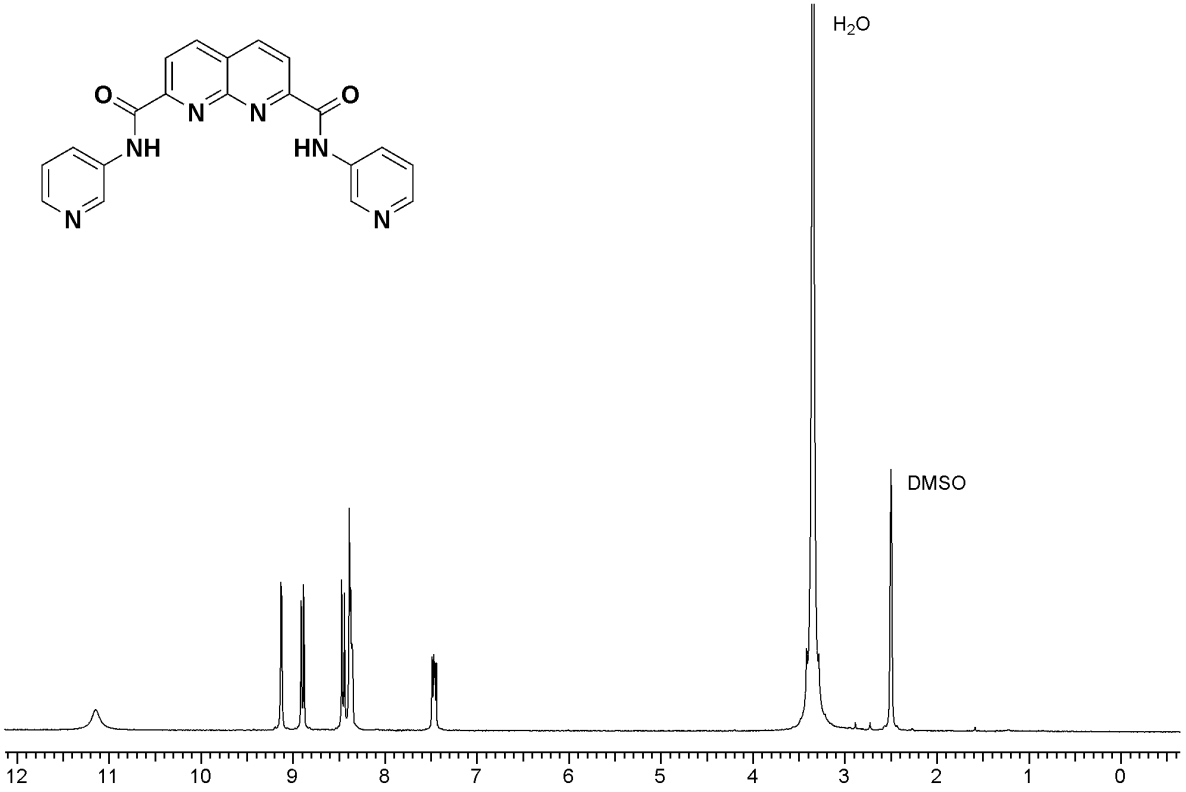

^{13}C NMR of compound 4c

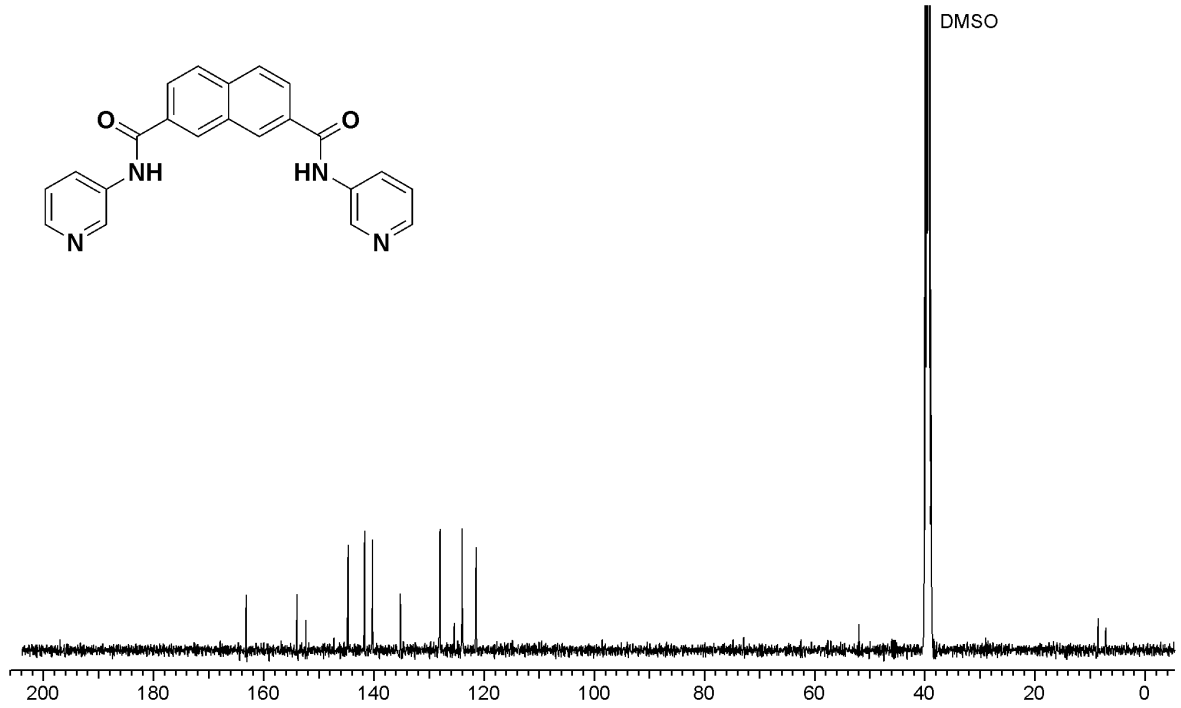

^{1}H NMR of ligand 3AQN

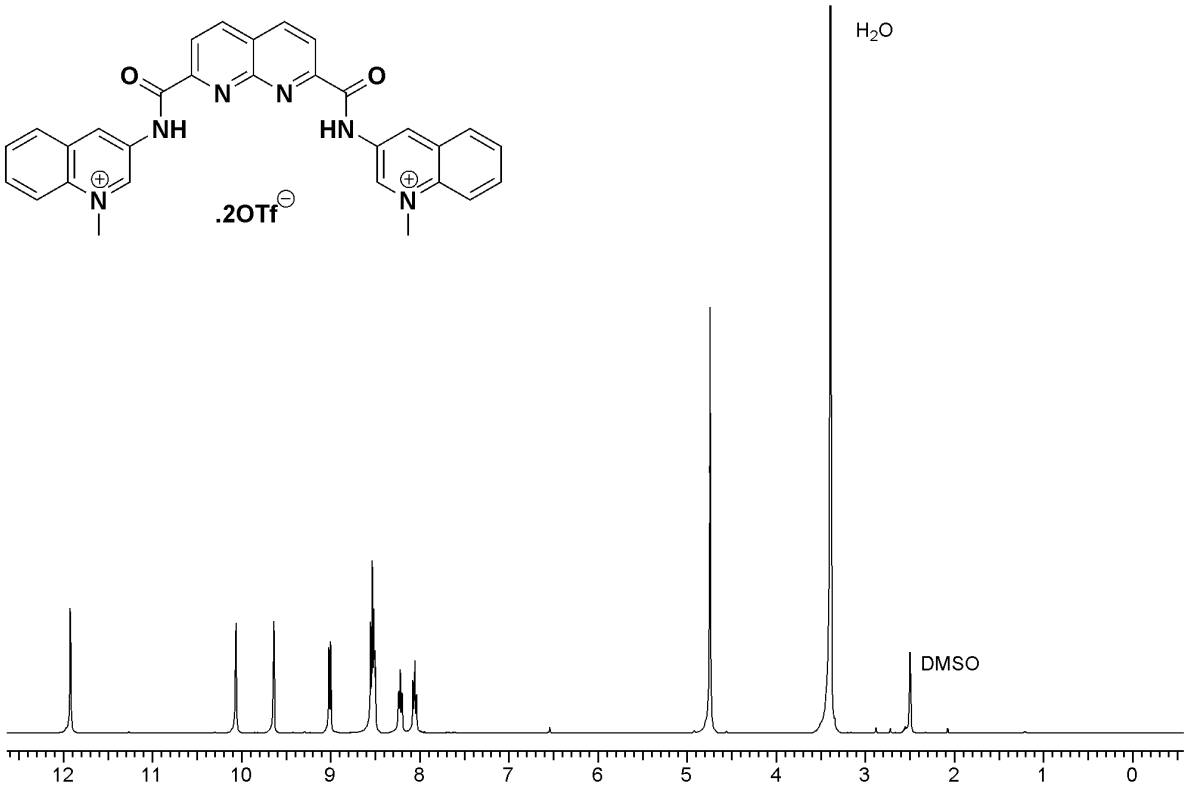

^{13}C NMR of ligand 3AQN

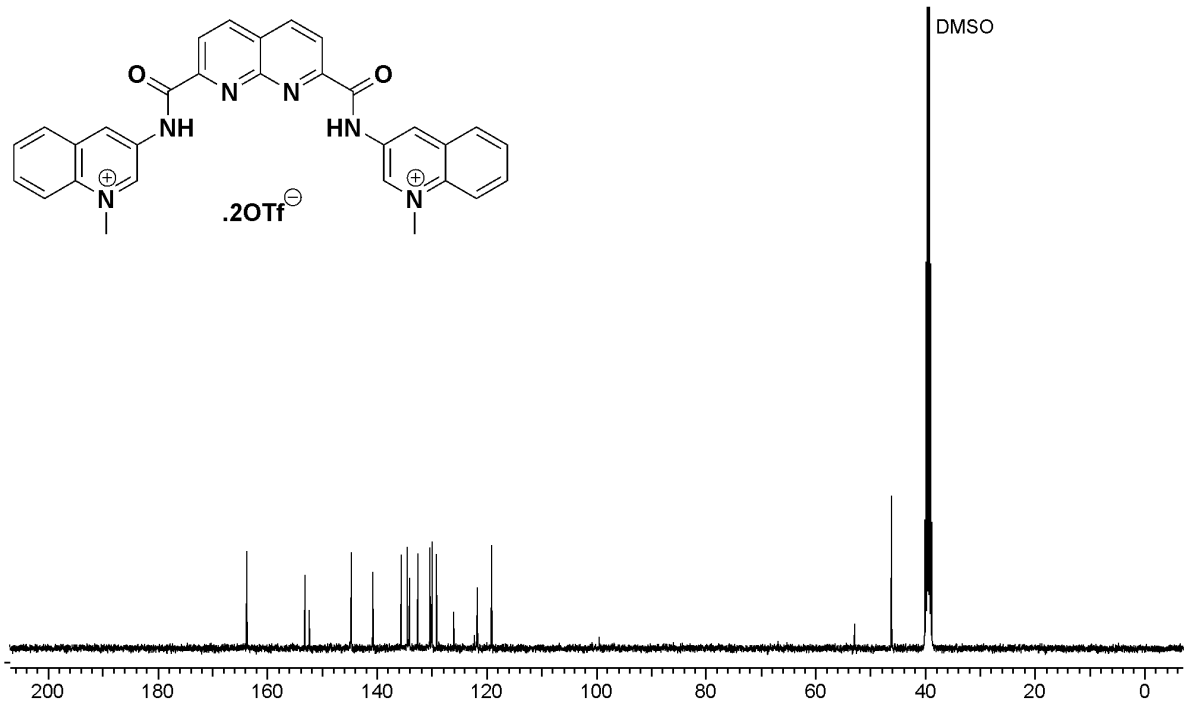

^{1}H NMR of compound 6AQN

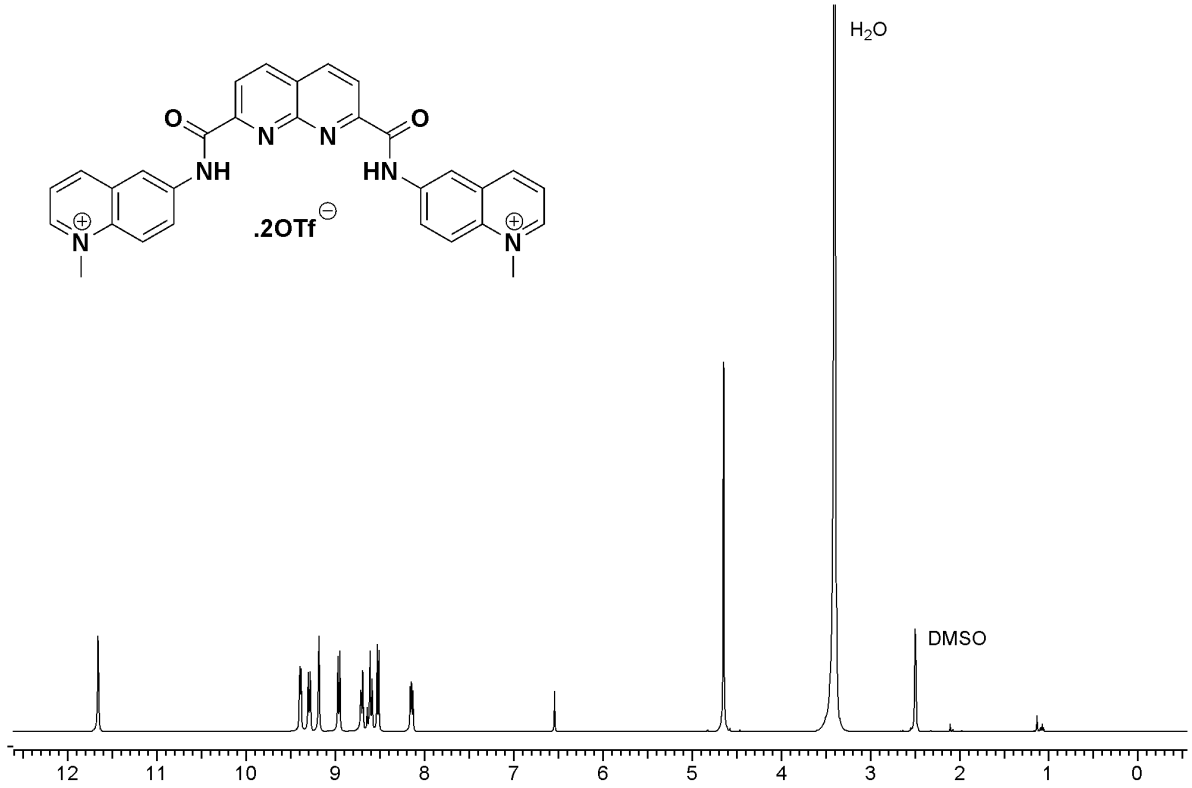

^{13}C NMR of compound 6AQN

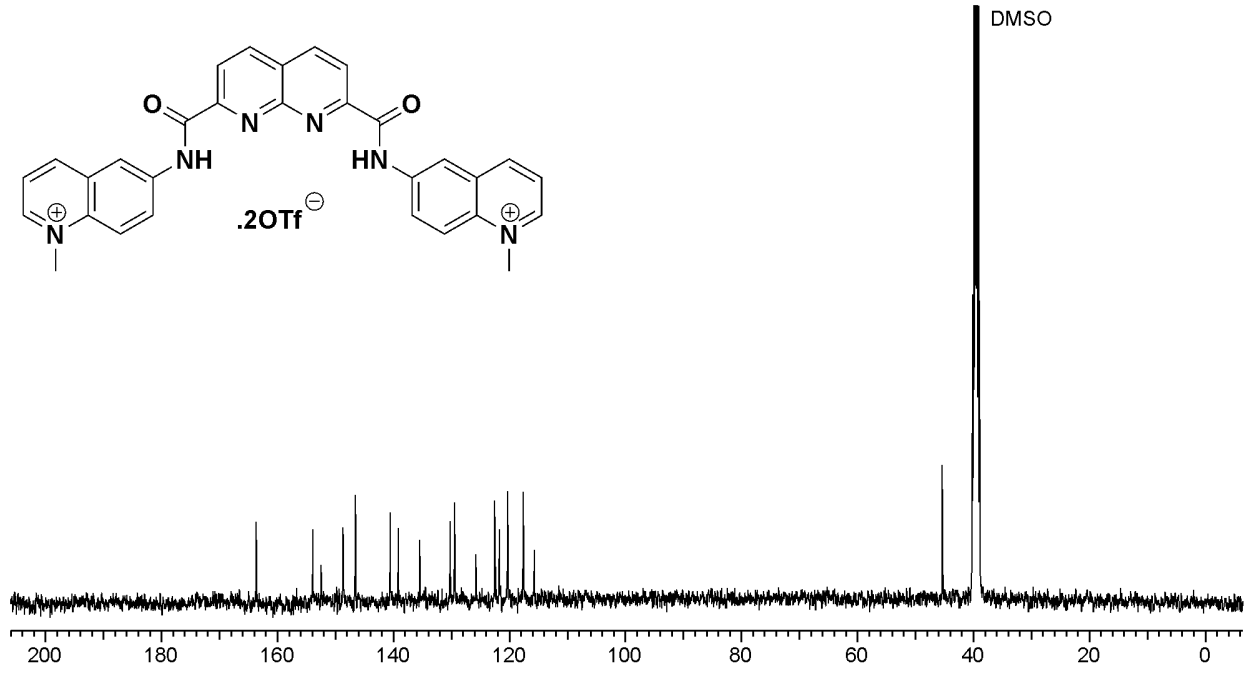

^{1}H NMR of compound 3APN

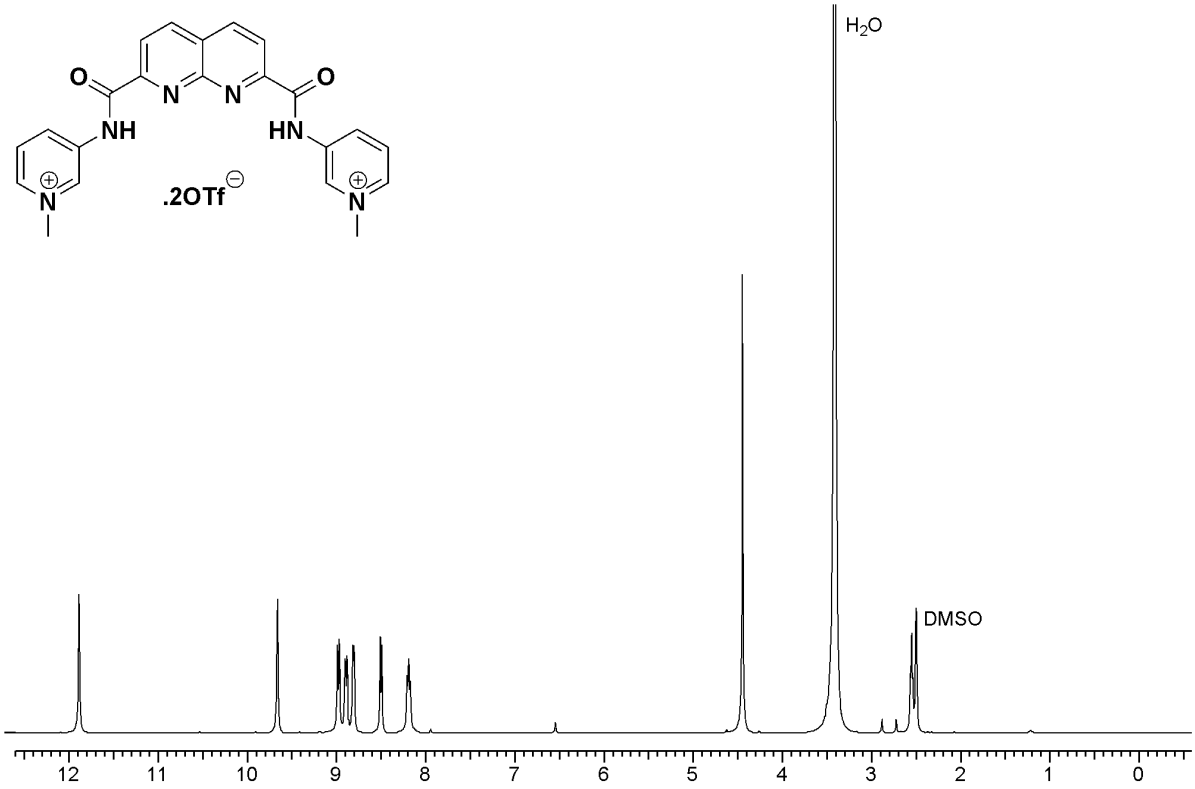

^{13}C NMR of compound 3APN

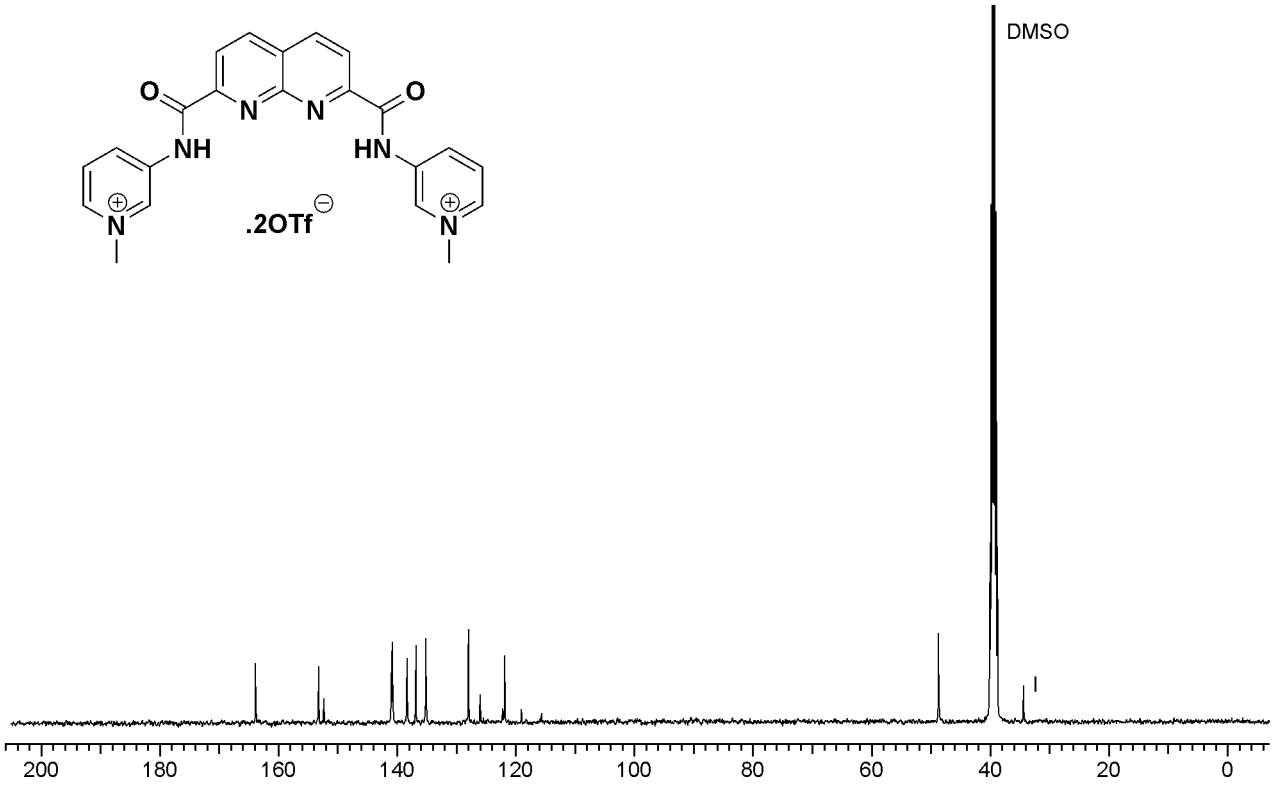

^{1}H NMR of 360A

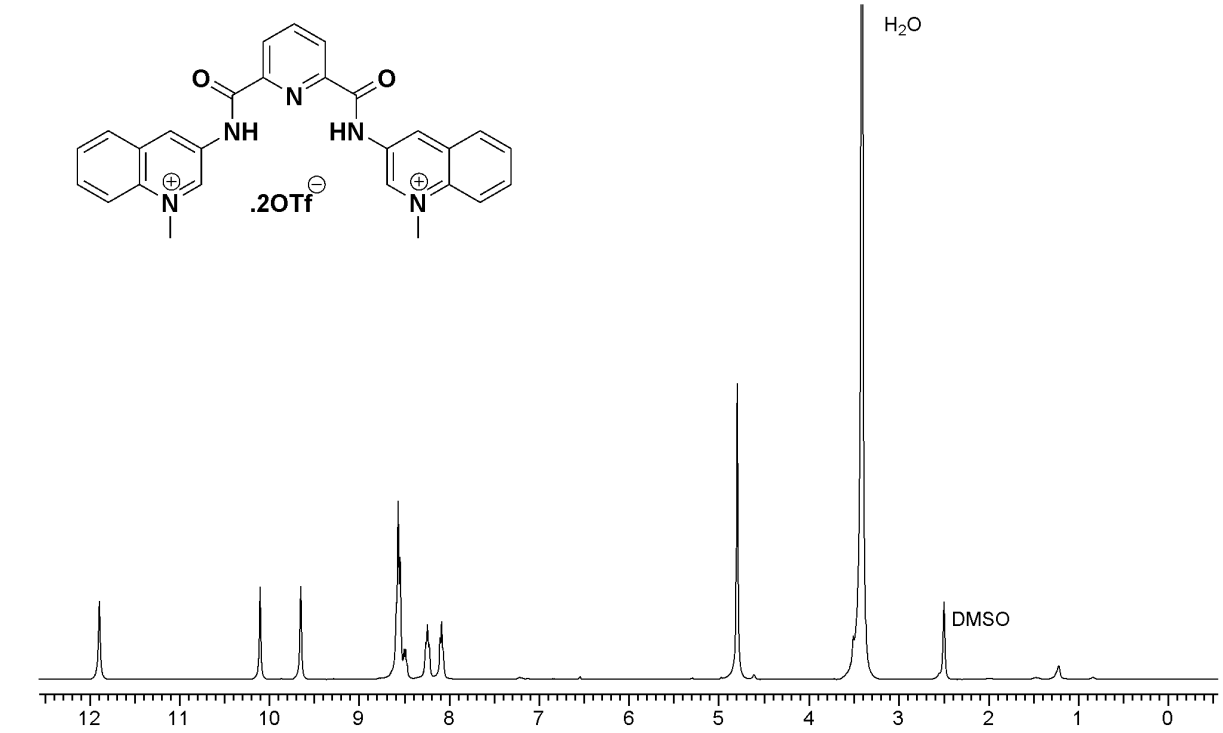

^{13}C NMR of 360A

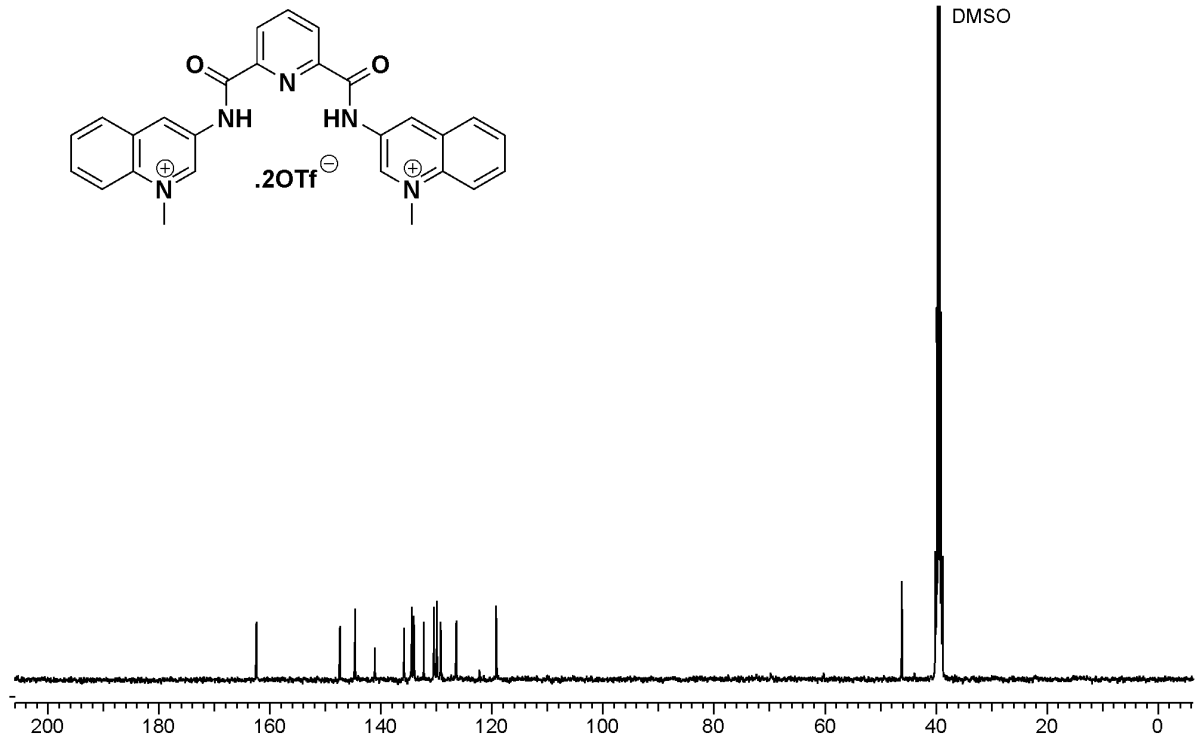

Reference

1. Spackova, N.; Berger, I.; Sponer, J. *J. Am. Chem. Soc.,* **1999**, *121*, 5519–5534.